FINAL SUMMARY REPORT
CR-121074
Project A-852

INVESTIGATION OF TECHNIQUES FOR IMPROVING SATURN V RF TRACKING AND RANGING SYSTEMS

J. R. WALSH, JR., AND R. D. WETHERINGTON

CONTRACT NAS8-20054

19 NOVEMBER 1971

Prepared for
NATIONAL AERONAUTICS & SPACE ADMINISTRATION
GEORGE C. MARSHALL SPACE FLIGHT CENTER
MARSHALL SPACE FLIGHT CENTER, ALABAMA

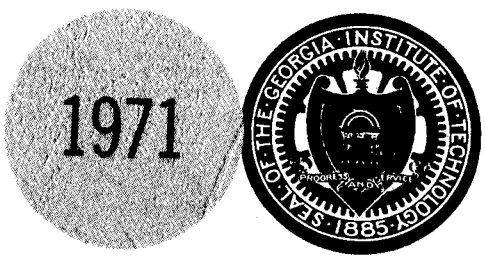

Engineering Experiment Station
GEORGIA INSTITUTE OF TECHNOLOGY
Atlanta, Georgia

N72-14673 (NASA-CR-121074) INVESTIGATION OF TECHNIQUES FOR IMPROVING SATURN 5 RF TRACKING AND RANGING SYSTEMS Final Summary
Unclas 11979 J.R. Walsh, Jr., et al (Georgia Inst. of Tech.) 19 Nov. 1971 111 p CSCL 17G G3/21
FACILITY CR-121074 (NASA CR OR TMX OR AD NUMBER) (CODE) 2 (CATEGORY)
Reproduced by NATIONAL TECHNICAL INFORMATION SERVICE Springfield, Va. 22151

GEORGIA INSTITUTE OF TECHNOLOGY
Engineering Experiment Station
Atlanta, Georgia

FINAL SUMMARY REPORT

Project A-852

INVESTIGATION OF TECHNIQUES FOR IMPROVING SATURN V RF TRACKING AND RANGING SYSTEMS

By

J. R. WALSH, JR., AND R. D. WETHERINGTON

CONTRACT NAS8-20054

19 NOVEMBER 1971

Prepared for

NATIONAL AERONAUTICS AND SPACE ADMINISTRATION
GEORGE C. MARSHALL SPACE FLIGHT CENTER
MARSHALL SPACE FLIGHT CENTER, ALABAMA

ABSTRACT

This report summarizes the investigations performed under Contract NAS8-20054. Twelve specific tasks were conducted during the six and one-half year contract performance period. Most of the details of the work have been omitted in this summary; for those interested, reference is made to the specific task reports where details are discussed. The tasks discussed include: (1) investigation of techniques for improving the Saturn radar altimeter, (2) analysis of the performance of the phase lock loop of the ODOP transponder during short term signal fades, (3) design of signal processing equipment for an orbital altitude radar return experiment, (4) spectral studies of signals present in the Command and Communications System (CCS) up-link transmitter, (5) study of intermodulation considerations in the CCS down-link data demodulators, (6) investigation of the error-rate performance of the CCS transponder command demodulator, (7) analysis of flame attenuation effects on telemetry transmissions during Saturn launches, (8) design of a digital television system which converts a standard monochrome television picture to a slow scan picture for transmission on a binary telemetry channel, (9) investigation of methods of obtaining an additional CCS 72 kilobit per second telemetry channel, (10) computation of the CCS S-band down-link spectra produced by various baseband telemetry subcarrier signals, (11) modeling in the frequency domain and on a block basis certain portions of communications systems, and (12) modeling on a circuit detail basis a telemetry transmitter. Results of the theoretical analyses of these problems are presented and, in those cases where experimental data could be obtained, comparisons of the theoretical and experimental results are given.

TABLE OF CONTENTS

TABLE OF CONTENTS (Continued)

TABLE OF CONTENTS (Concluded)

PRECEDING PAGE BLANK NOT FILMED

LIST OF FIGURES

LIST OF FIGURES (Continued)

LIST OF FIGURES (Concluded)

I. INTRODUCTION

This Final Summary Report presents a summary of the technical programs conducted under Contract NAS8-20054. The objective of the overall program was to investigate techniques for improving Saturn V RF tracking and ranging systems. This contract was initiated on 19 April 1965 and completed on 19 November 1971.

Twelve areas of investigation are summarized in this report. These are: (1) investigation of techniques for improving the Saturn radar altimeter, (2) analysis of the performance of the phase lock loop of the ODOP transponder during short term signal fades, (3) design of signal processing equipment for an orbital altitude radar return experiment, (4) spectral studies of signals present in the Command and Communications System (CCS) up-link transmitter, (5) study of intermodulation considerations in the CCS down-link data demodulators, (6) investigation of the error-rate performance of the CCS transponder command demodulator, (7) analysis of flame attenuation effects on telemetry transmissions during Saturn launches, (8) design of a digital television system which converts a standard monochrome television picture to a slow scan picture for transmission on a binary telemetry channel, (9) investigation of methods of obtaining an additional CCS 72 kilobit per second telemetry channel, (10) computation of the CCS S-band down-link spectra produced by various baseband telemetry subcarrier signals, (11) modeling in the frequency domain and on a block basis certain portions of communications systems, and (12) modeling on a circuit detail basis a telemetry transmitter. The details of this work are covered in Technical Notes Nos. 1 and 2 and in Technical Reports Nos. 1 through 10. It is the purpose of this report to summarize the results of these studies and to make available in one volume the more important results without discussion of the rather involved details.

Each of the major areas of investigation mentioned above is covered in a separate section of this report. Individual introductions to each section describe the technical problem discussed in that section. Reference is made to the individual technical report from which the summary was derived in each section.

PRECEDING PAGE BLANK NOT FILMED

II. RADAR ALTIMETER ANALYSIS

A. Introduction

The technical objective of the first task of the program was to investigate various difficulties which had been experienced with the Saturn I radar altimeter (Ryan Model 520). Among these difficulties were excessive jitter in the altitude data and amplitude jitter on the simulated video return pulse.

The approach consisted of theoretical and experimental investigations directed toward (1) the establishment of expected performance characteristics, and (2) the recommendation of changes in the altimeter for obtaining as near optimum performance as practical.

The major area of investigation was the range tracking servo system. This system was analyzed under tracking conditions since the altitude readout jitter occurred in this mode of operation.

Several portions of the altimeter system were found to be contributing to the video pulse noise, and investigation in these areas was pursued to the extent necessary to determine the source of the noise and to establish possible corrective techniques. Items investigated in this connection were (1) interference from signals originating in the timer of the altimeter, (2) difficulties with the frequency spectrum of the receiver's local oscillator, and (3) distribution of intermediate frequency gain and video gain in the altimeter.

B. Range Tracking Servo System Analysis

1. Range Tracking Servo System

The analysis of the range tracking servo system was limited to the track mode operation. Search mode analysis was not considered since the main objective of this phase of the program was the reduction of altitude readout jitter. A block diagram of the servo system in the track mode of operation is given in Figure 1.

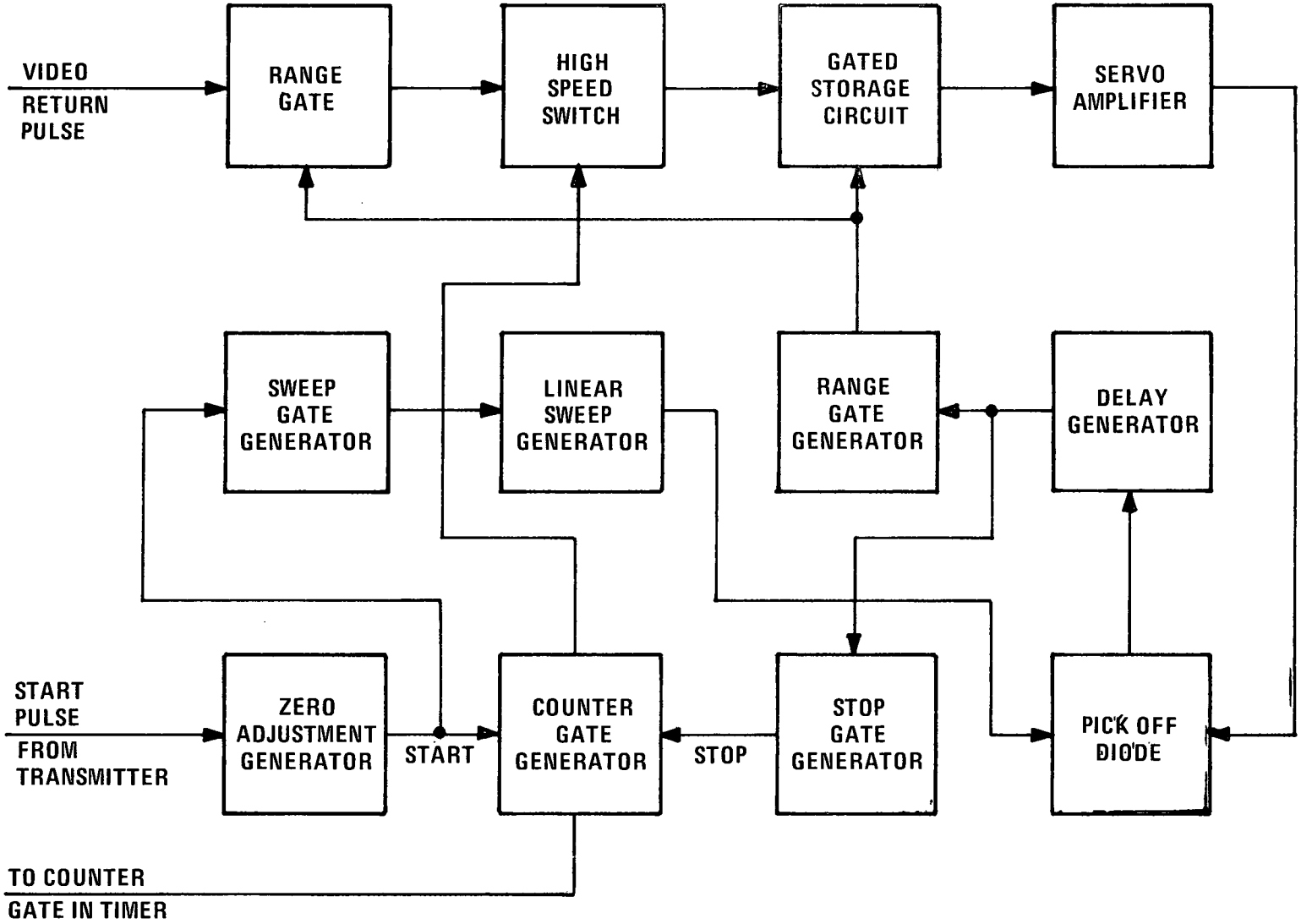

Figure 1. Block Diagram of Range Tracking Servo System in the Track Mode of Operation.

This system is essentially a range-tracking pulse radar and uses techniques common to many automatic range-tracking systems. The video signal consisting of the return pulse is passed through a range gate (positioned by the servo system) and high speed switch to a storage circuit. At the center of the gate, the high speed switch is triggered and inverts the polarity of the video. Thus, for the first half of the time that the storage circuit is gated on, it receives a video signal of one polarity, and for the second half of the gate time, it receives a video signal of the opposite polarity. If the pulse is symmetrical and exactly centered in the gate, the contribution of the two halves of the gate cancel and the net charge added to the storage circuit is zero. If the pulse is not centered in the gate, a net charge is added to the storage circuit. This charge changes the voltage on the storage capacitor; the sense of the change will depend on whether the return pulse is early or late in the gate.

The output of the storage circuit serves as the input to the servo amplifier. The servo amplifier contains two vacuum tube stages and one transistorized stage of gain. Each vacuum tube stage provides a weighted integration through use of an RC feedback network. Additional integration is provided in the transistorized stage by means of capacitive feedback.

When tracking at a fixed range, the output of the servo amplifier is linearly related to the input voltage, and this voltage is used to position the range gate. When the range is changing, the amplifier integration provides "anticipation" of the next pulse position (velocity information) so that the gate can be more precisely positioned.

For a more detailed description of the system and its operation, see the system description manual.[1]

2. Analysis and Results

Analysis of the range tracking servo system was carried out by first deriving the equation for the closed loop transfer

function of the range tracking circuit. Derivation of this equation required determining the open-loop transfer function of various subsections of the altimeter circuitry, including the summation circuit, the sample-and-hold circuit, the servo amplifier integrators, and the pick-off diode circuit. The final equation expressed the indicated output altitude as a function of the system parameters and the input forcing function. One forcing function of particular interest was a step in the input altitude.

A digital computer program for a B-5500 computer was constructed to evaluate the system response. The program starts from the basic system parameters, constructs the time function for a step input to the system, and then evaluates the time function at chosen time intervals for any selected range of time.

The computer program was used to study the theoretical response of the servo system for a number of cases. These predicted responses were compared with actual responses measured in the laboratory in most cases. The (normalized) predicted and measured response for an altitude step of 371 feet is shown in Figure 2. Comparison of these two curves shows that the ringing frequency of the actual circuit is slightly greater than the predicted frequency. This small discrepancy is to be expected in view of the many uncertainties in exact values of components that entered into the predicted values.

Additional study of the system was made with the objective of modifying the system to provide additional damping in the servo loop. A review of the equations indicated that the damping should be strongly dependent on a capacitor and resistor at the output of the sample and hold circuit. (For exact values and circuit locations of these components see Technical Report No. 1, page 35.) An estimate of the change in value of these two components was made to obtain an increase in damping sufficient to reduce the overshoot to 5 or 10 percent. By inserting these values into the computer program, the response of the modified system (Called Mod. I) was computed. The computed response to the step function is shown in Figure 3, along with that for the unmodified system.

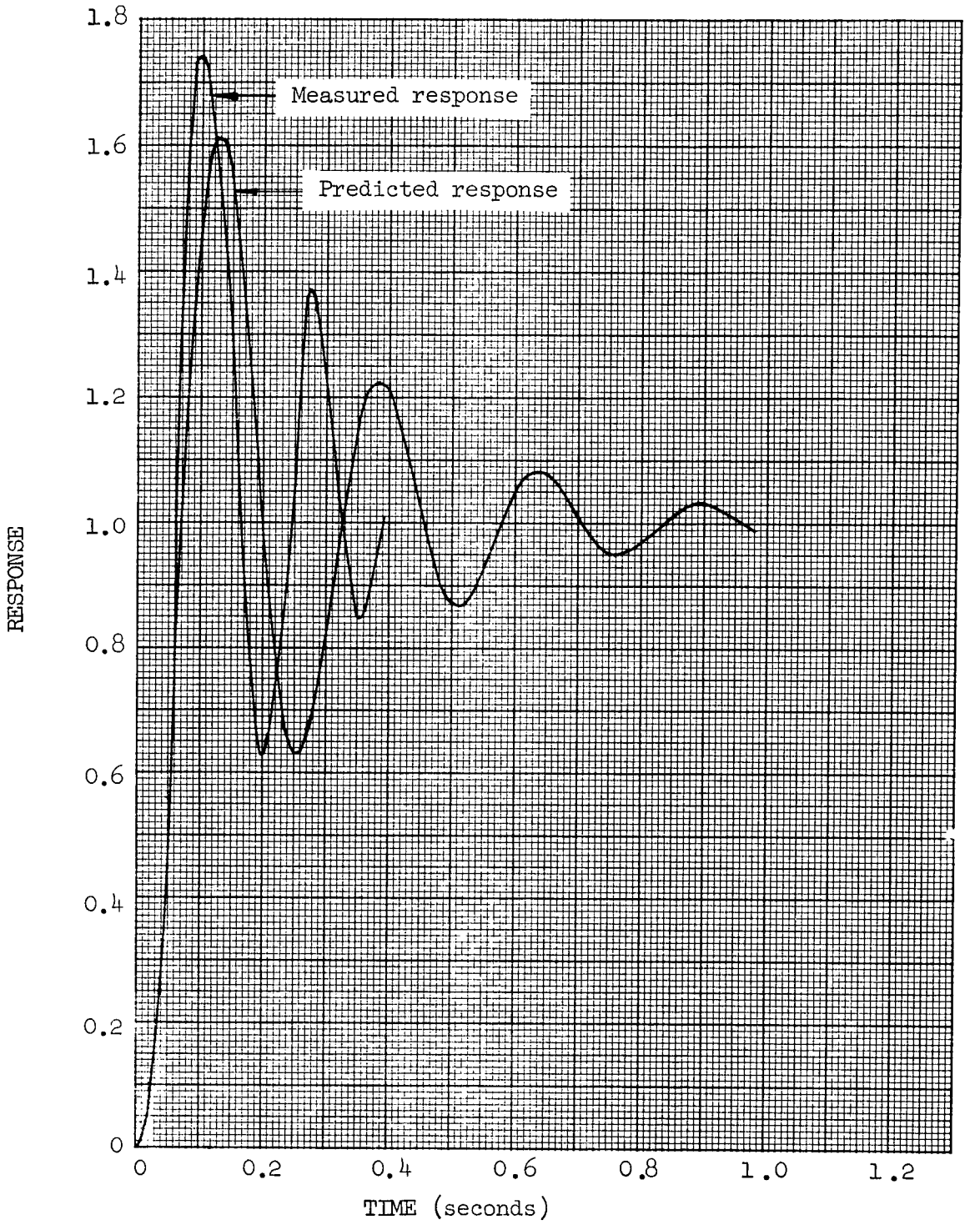

Figure 2. Measured Response vs Predicted Response of Range Tracking Servo System to a Step of Altitude.

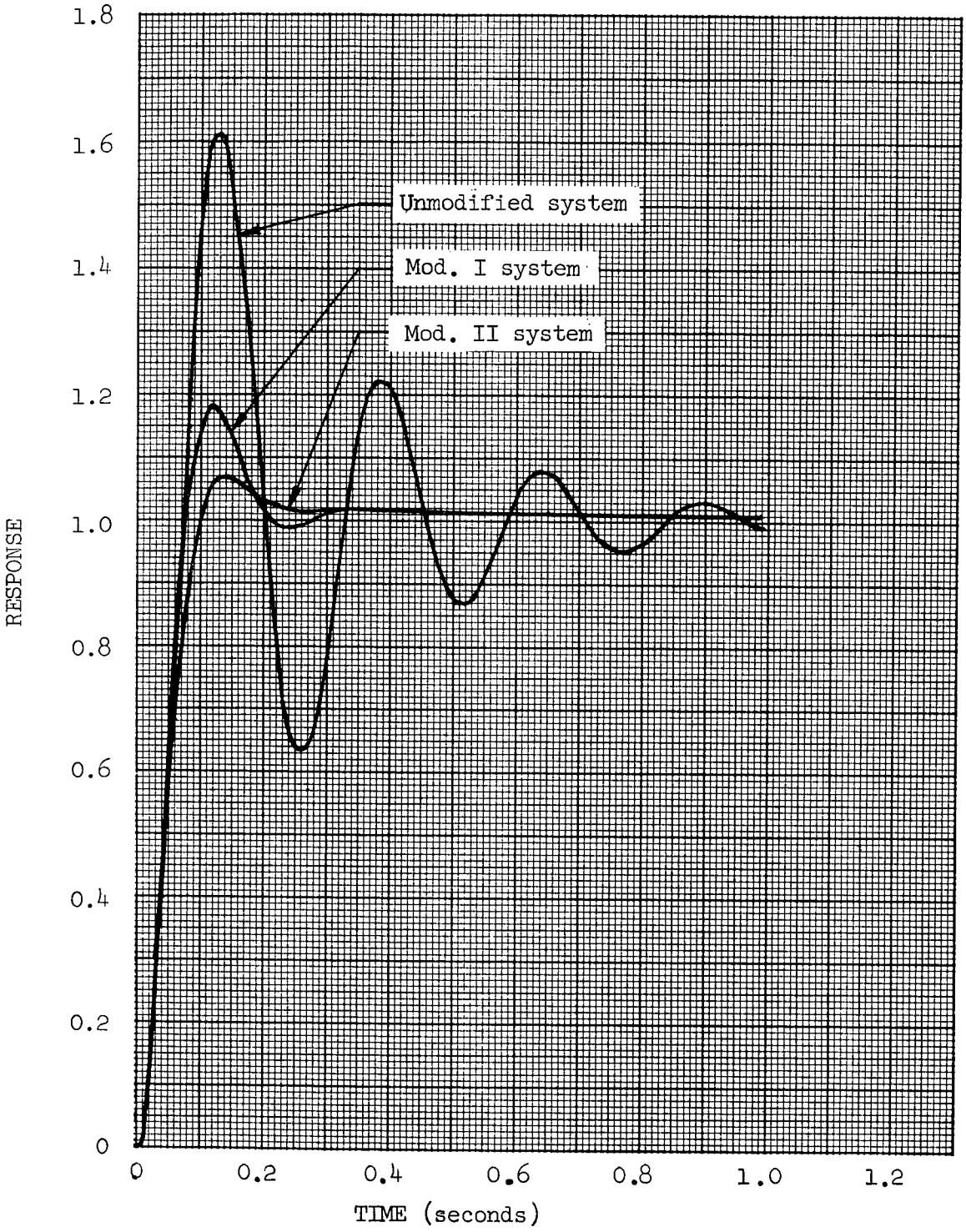

Figure 3. Comparison of Predicted Responses for Unmodified, Mod. I, and Mod. II Systems to a Step of Altitude.

Although these changes improved the damping, the overshoot was still larger than desired. Both components were then changed still further, and the step response for this modification (called Mod. II) was computed and the results are also shown in Figure 3. Since the computed step response for the Mod. II system appeared to be very nearly optimum, the altimeter components were changed to the Mod. II values. Actual response curves were then run on the system. The measured response values agreed quite well with the predicted values indicating that the system's response to a step input was greatly improved.

C. Investigation of Altimeter Video Pulse Signal-to-Noise Characteristics

When a simulated echo was injected into the altimeter at a level well above the receiver sensitivity, observations of the pulse at video showed the presence of a considerable amount of amplitude jitter. The appearance of this jitter remained essentially the same as the input signal level was varied over wide limits (from about 20 dB above the noise level of the receiver front end up to the maximum level at which the AGC system could control the video signal amplitude).

Experiments with the equipment indicated that although the AGC attenuator may add some noise to the video pulse, the major portion of the observed amplitude jitter was due to other causes. Among these other causes were: (1) frequencies generated in the timer clock-divider chain were leaking into the IF amplifier and beating with the received signal, (2) the receiver local oscillator was producing undesirable sidebands which produced a beat with the received signal, and (3) the distribution of IF and video gain was such that the received signal amplitude was reduced to a small fraction of the saturation level of the IF amplifier and thus accentuated the IF amplifier noise present in the output signal.

D. Conclusions

A theoretical analysis of the range tracking servo system in the track mode of operation has been performed, and a mathematical model of the servo system constructed. The model predicts the system's response to a step input of altitude with sufficient accuracy to make it a valuable analytical tool.

The original (unmodified) range tracking servo system was found by both analysis and experiment to be underdamped. The model was used to investigate the effect of circuit changes which were theoretically expected to improve the damping. Circuit changes for which the model predicted very nearly optimum damping were found. After incorporating these changes in the altimeter, laboratory experiments on the system indicated that the system response to an input step function was indeed close to that predicted by the model. The increase in damping effected by these changes also reduced the jitter of the servo system while tracking at a fixed altitude by approximately 2:1.

Studies were made to determine why the video signal-to-noise ratio was low. Three different problem areas were discovered. It was found that frequencies generated in the timer unit were being coupled into the IF amplifier and creating interference, that the local oscillator was producing strong spurious sidebands, and that the video signal-to-noise ratio was degraded by the existing distribution of gain between the IF and video amplifiers. Elimination of these problems improved the characteristics of the video pulse considerably.

For a complete detailed discussion of the investigation and results, see Technical Report No. 1.[2]

III. PERFORMANCE OF THE PHASE LOCK LOOP OF THE ODOP TRANSPONDER DURING SHORT TERM SIGNAL FADES

A. Introduction

Several problems associated with the ODOP (offset Doppler) transponder's phase tracking ability under varying conditions of signal fade or signal loss were studied. These problems were: (1) determination of the reacquisition time of the transponder phase lock loop after a received signal drop out, (2) determination of the received signal level at which the transponder phase lock loop will drop out of lock, (3) determination of the effect of a step of phase in the received signal on the phase lock loop.

Received signal variations which were considered included both instantaneous loss of the received signal and instantaneous fade from a strong signal to a weak signal. Results of these analyses are discussed in the following sections.

B. Loop Characteristics

A block diagram of the phase lock loop used in the ODOP transponder is shown in Figure 4.

Three quantities, which can be used to describe the loop are the lock frequency, the pull-in frequency, and the pull-in time. The lock frequency, $\Delta\omega_L$, is the maximum value of $\Delta\omega$ for which lock will occur without slipping a cycle. The pull-in frequency, $\Delta\omega_p$, is the maximum value of $\Delta\omega$ for which lock will eventually occur if the system is left undisturbed. The pull-in time, T_p, is the time in seconds for the system to achieve lock. These three quantities were used to analyze the behavior of the ODOP transponder phase lock loop.

The time constants and gain factors for the ODOP system were taken from the manufacturers data.[3,4] Two sets of characteristics of the ODOP transponder were obtained. One set was for strong signal conditions; the other set was for threshold conditions. For both

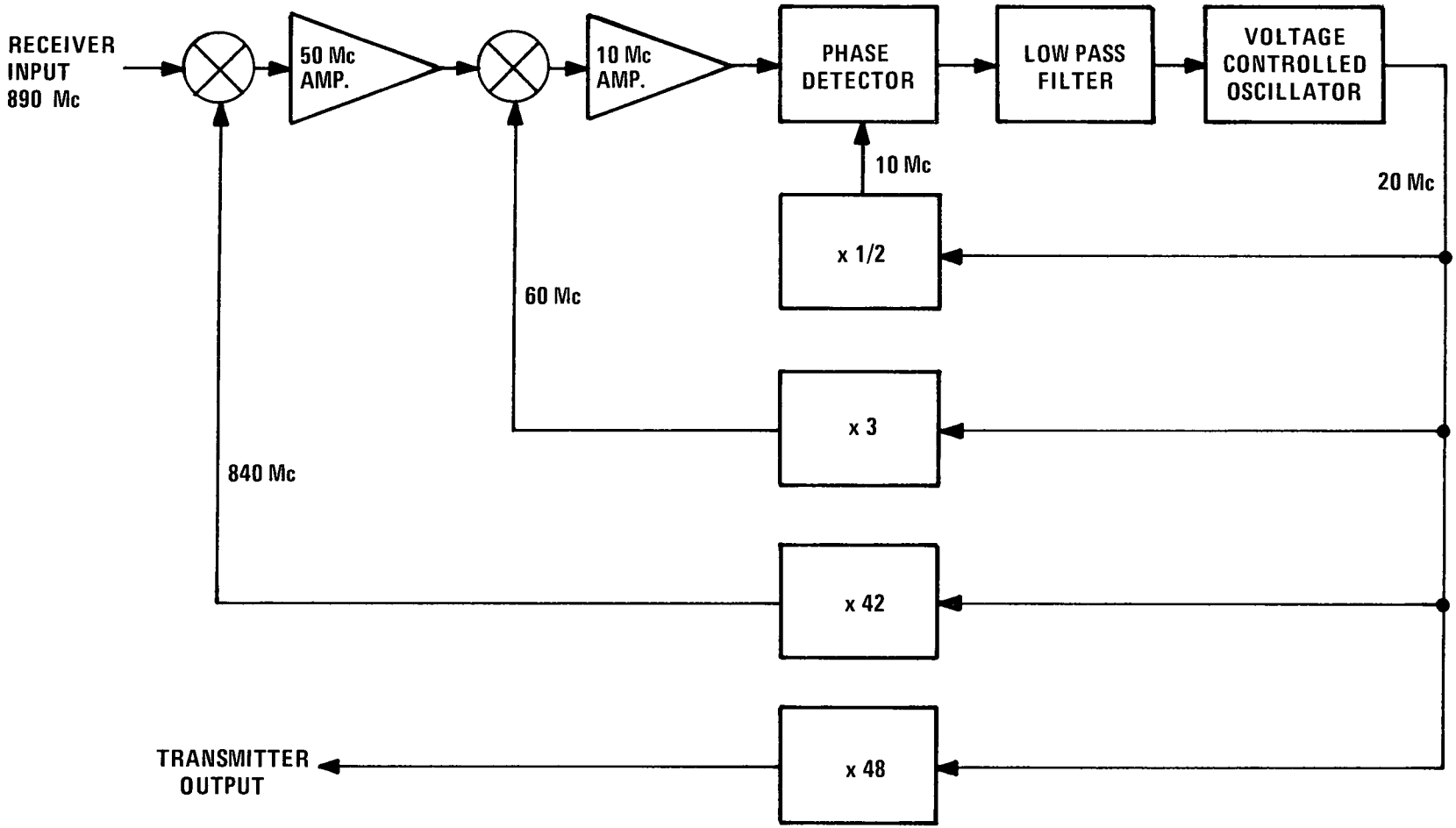

Figure 4. ODOP Transponder Phase-Lock Loop.

sets of characteristics the times required for the system to pull into lock were computed for various frequency differences. The results are shown graphically in Figure 5.

C. Phase-Lock Loop Voltage Decay Characteristics

The rate at which the frequency of the VCO returns to its natural frequency of oscillation following a signal drop-out depends upon the rate of decay of the voltage stored on the filter capacitors in the low-pass loop filter. Knowing the voltage-time relationship of the control voltage into the VCO would therefore allow calculation of the amount of VCO drift for a given drop-out period. An equation expressing VCO control voltage as a function of time after signal drop-out was developed and verified with laboratory measurements.

D. Signal Reacquisition Time

By combining the effects of oscillator drift during signal loss and the pull-in time for a known frequency difference, it is possible to estimate the time necessary to reacquire phase lock after a signal outage of known duration. It is assumed that the signal loss is complete and the voltage impressed on the VCO during the outage decays toward zero. As the voltage decays the oscillator will drift back towards its natural frequency, ω_o. The pull-in times required to re-lock after signal loss of various time durations were computed for a system with both strong signal characteristics and threshold signal characteristics. The results are shown graphically in Figures 6 and 7 for several values of Δf, where Δf is the difference between the signal frequency and the natural oscillator frequency.

E. Conclusions

A theoretical study of the characteristics of the phase-lock loop and associated circuits in the ODOP transponder has been made to determine if problems exist with respect to the transponder's

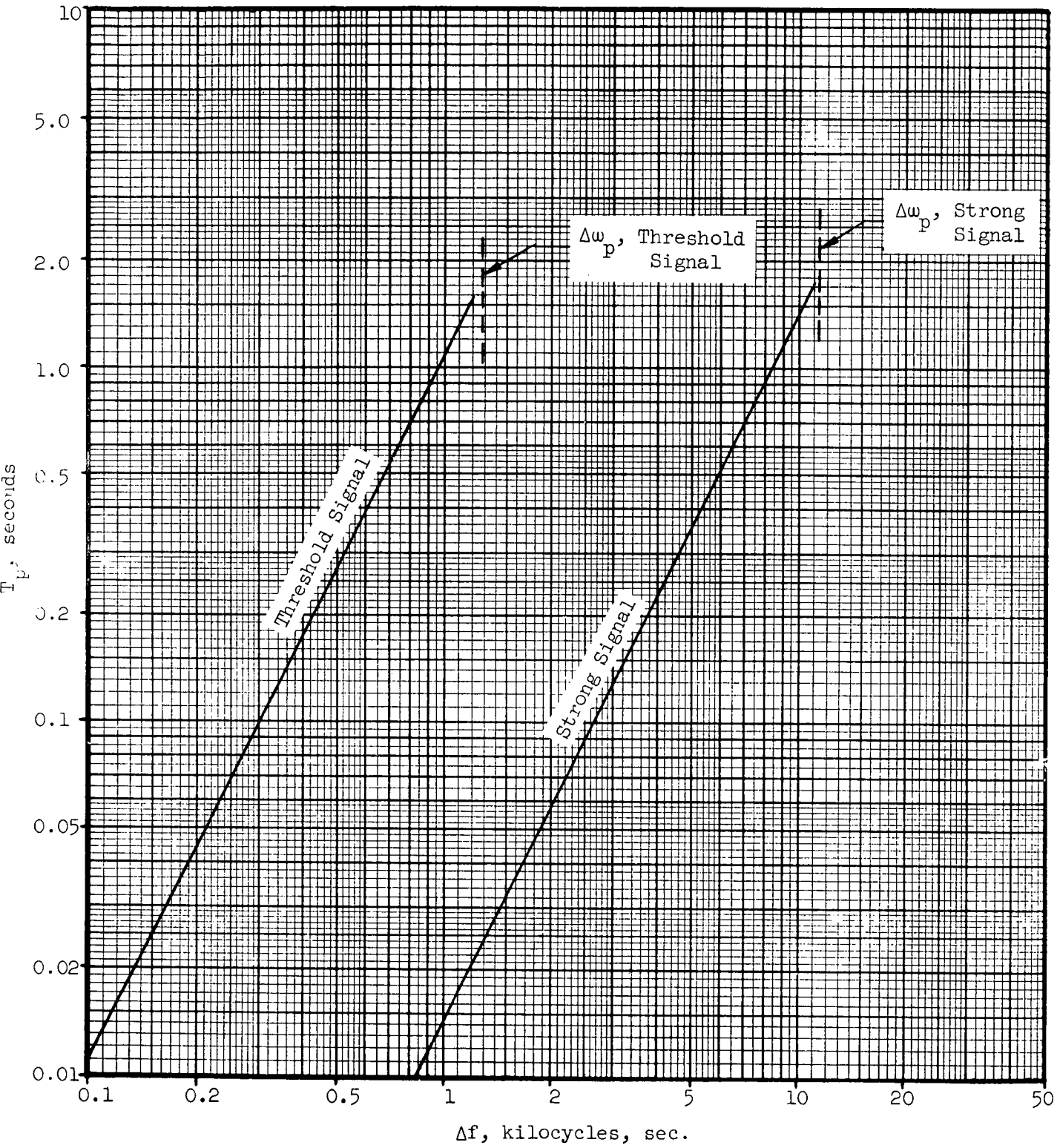

Figure 5. Pull-in Time for the Phase-Lock Loop of the ODOP Transponder.

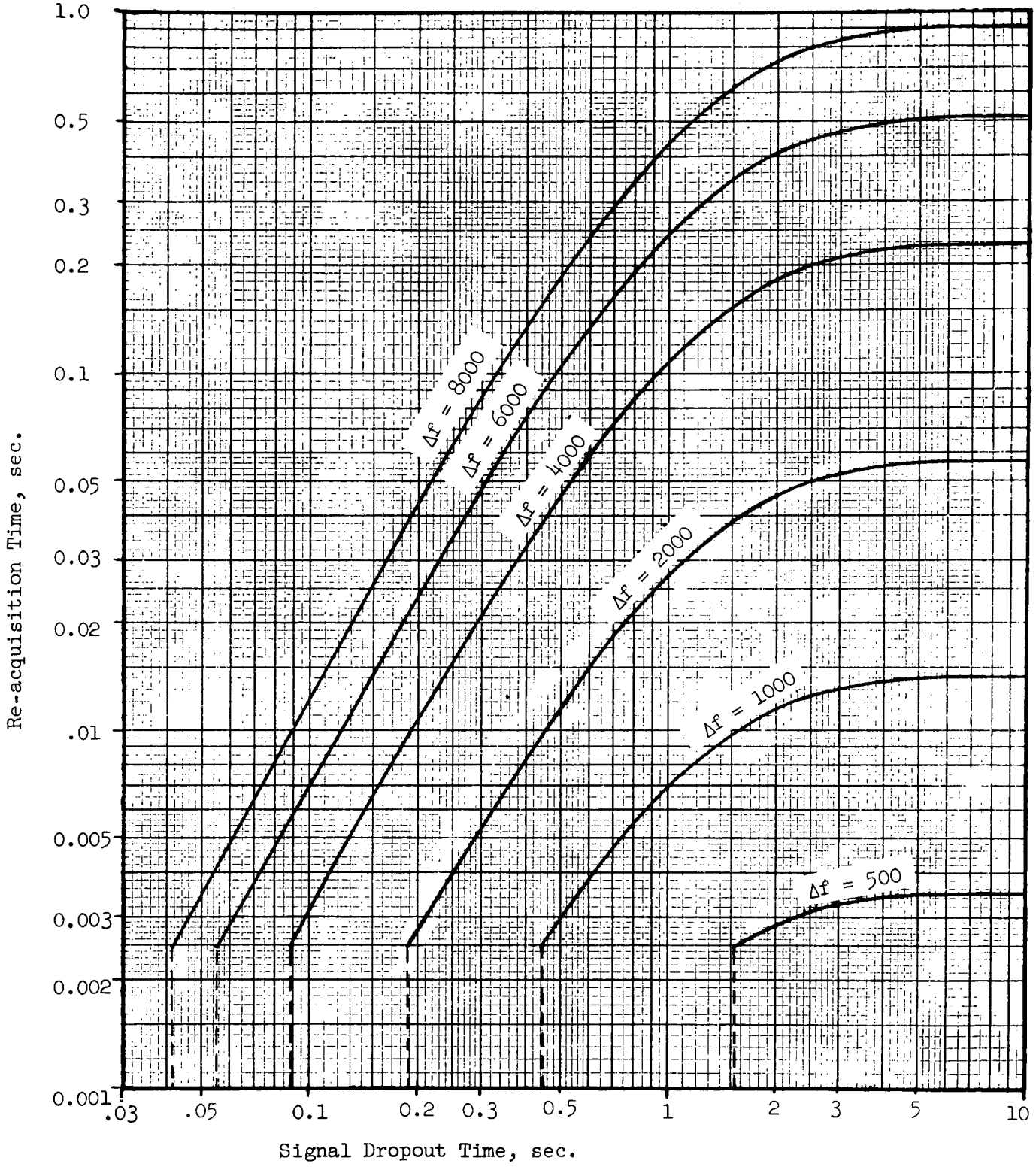

Figure 6. Time to Re-acquire Lock After Dropout of a Strong Signal.

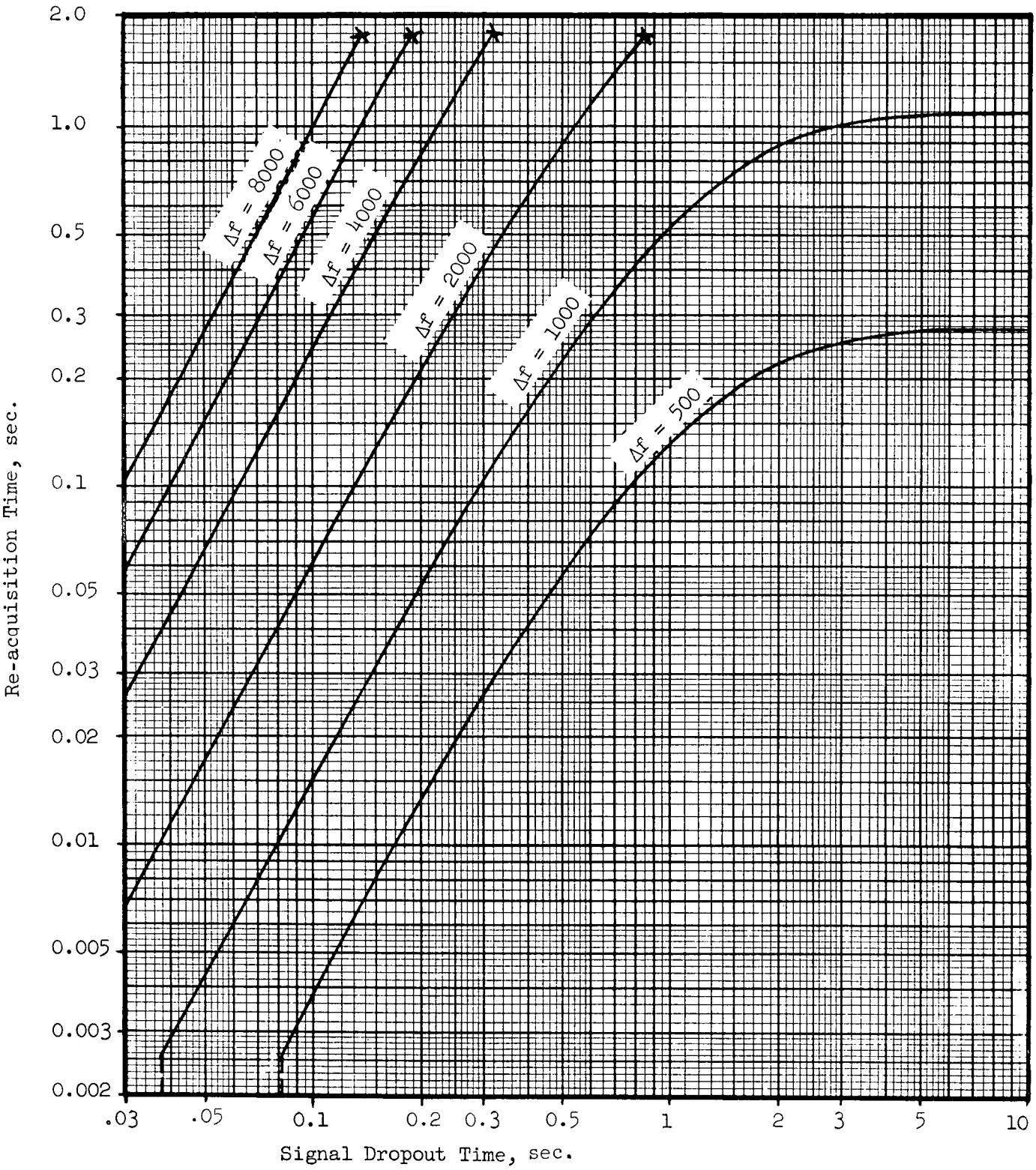

Figure 7. Time to Re-acquire Lock After Dropout of a Threshold Level Signal.

ability to maintain phase lock or reacquire lock in the presence of short term signal fades or signal drop-outs.

The results of these studies indicate that for the expected conditions of operation no difficulties will be experienced provided the frequency of the transponder oscillator is maintained very close to that of the transmitter oscillator.

Analysis showed that no difficulty in reacquiring phase-lock would be encountered from signal losses of 3 seconds or less duration provided the natural frequency of the transponder oscillator (after multiplication) is maintained with 1 or 2 kHz of the transmitter frequency.

For additional detail on the investigation and the results, see Technical Note No. 1.[5]

PRECEDING PAGE BLANK NOT FILMED

IV. RADAR RETURN EXPERIMENT SIGNAL PROCESSING EQUIPMENT

A. Introduction

The particular task covered by this section was that of designing and bread-boarding a signal processing system to be used in conjunction with a radar altimeter to obtain radar return signal data from orbital altitudes.

Radar altimeters are essentially range tracking radars whose input signals are derived from radar pulses reflected from the surface of the earth. In order to design range trackers so as to make optimum use of the information contained in the return signal, many of the echo characteristics must be determined. Very little factual data characterizing orbital echo signals have been obtained to date. To overcome this data gap, an experiment was planned in which a radar altimeter would be placed in an orbital vehicle, and the video pulse data telemetered to ground receiving stations. In addition to providing needed information for range tracker design, these data would be useful for other purposes. They would permit investigation of radar cross section versus angle of incidence, pulse stretching, and other echo characteristics.

The signal processing system described herein accepts signals from a radar altimeter and converts them to a form suitable for modulating a data link transmitter for transmission to ground stations. The signal processing equipment also provides amplitude and time calibration signals.

The approach to this phase of the program consisted of an initial overall review of the proposed return experiment from which information leading to a system block diagram of the signal processing equipment was derived. Following this, subsystem block diagrams were developed which provided the basis for the detailed circuit design.

For details of the experiment analysis and of the individual circuits shown in the system block diagram reference should be made to Technical Report No. 2.[6]

A breadboard of the complete signal processing system was constructed and was delivered to Marshall Space Flight Center.

B. System Parameters

The basic purpose of the signal processing equipment was to condition signals derived from the radar altimeter so that these signals were in form suitable for modulation of the data link transmitter. In addition, the signal processing equipment was to provide time and amplitude calibration of the radar return signal, and a system synchronizing pulse.

Signals obtained from the radar altimeter are:

1. a wide band video signal from an IF system with 7.5 MHz bandwidth,
2. a narrow band video signal from an IF system with a 1.5 MHz bandwidth,
3. a detected sample of the altimeter transmitter pulse,
4. a 1.327 MHz clock signal derived from the altimeter clock divider system,
5. the system PRF pulse,
6. a signal representing the end of the counter gate,
7. a 18 bit altitude signal,
8. a 16 bit time signal,
9. the reliability signal,
10. an analog signal representing automatic gain control voltage, and
11. an analog signal representing automatic frequency control voltage.

Supplementing the above altimeter derived signals is a 30 MHz IF amplitude calibration signal generated by the signal processing equipment. This calibration signal is fed into the altimeter IF system so that accurate amplitude calibration of the return signal may be obtained. An additional input was provided in the signal processing equipment for an analog temperature signal.

The signal processing equipment also generates additional video signals with specific time relationships to those signals obtained from the altimeter. These signals are:

1. a system synchronizing pulse,
2. fine timing marks for time calibration of the return signal when the altimeter is tracking, and

3. coarse timing marks for time calibration of the return signal when the altimeter is in the search mode.

In addition, the signal processing equipment furnishes a wide-band/narrow-band identification bit. This bit indicates which IF system is used to obtain the radar return video data.

To drive the data link transmitter, the signal processing equipment furnishes a composite output signal which is of the proper voltage and at the appropriate impedance level to drive the data link transmitter.

The block diagram of the signal processing system, Figure 8, shows the major subsystems which make up the signal processing equipment. All the signals shown in the left of the diagram, with the exception of the temperature signal, are obtained from the radar altimeter. Since many of the altimeter signals to be transmitted to the ground via the data link transmitter occur in time sequence, they are already in a form suitable for time-division multiplexing. The commutating system, a major portion of the signal processing equipment, is a two level commutating system. The video commutator shown in the system block diagram is used to switch between analog video data and digital data. The analog video data includes a sample of the transmitted pulse, the radar return pulse, and the amplitude calibration signal. Also transmitted along with this analog video data are a system synchronizing pulse and timing mark pulses. Video data are transmitted during the interval from approximately 12 microseconds ahead of the radar transmitter pulse to 3460 microseconds (mid-period position) following the transmitter pulse. The remainder of the PRF period is available for transmission of digital data since all radar return pulses for the altitudes of interest will be completely by mid-period. The video commutator is switched to its digital position at the mid-period time by switching pulses obtained from the signal processor clock divider system. Starting one-half period (of the 41.47 kHz clock) after the video commutator switches to the digital data position, the digital commutator sequentially samples 64 lines of parallel binary data. The half

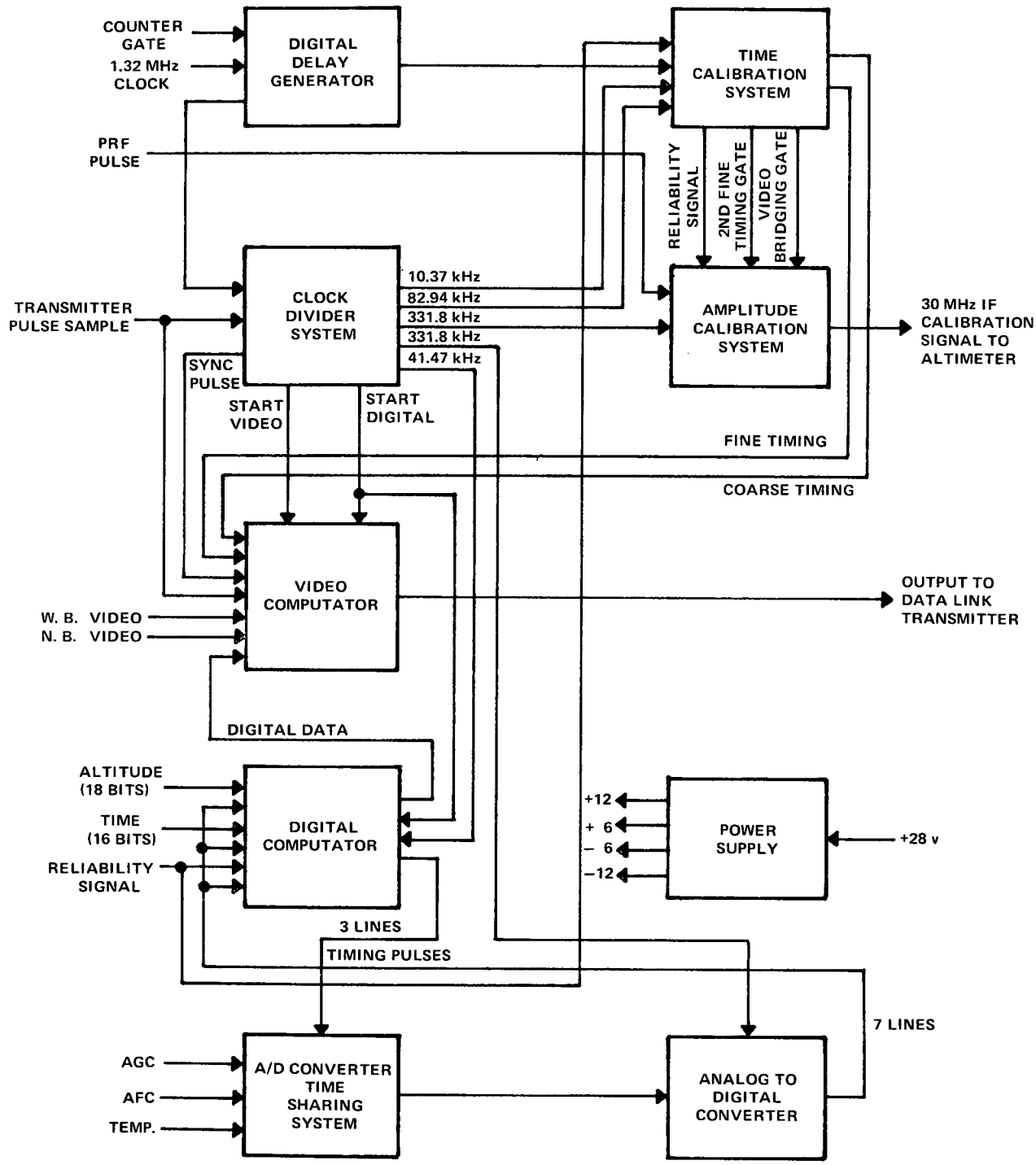

Figure 8. Signal Processing Equipment Block Diagram.

period delay prevents a "race" situation between the mid-period commutator start pulse and the first clock pulse which advances the digital commutator. This in turn prevents a possible ambiguity (equal to one clock period) in the position of the digital data transmission.

The binary inputs to the digital commutator, representing the AGC, AFC, and system temperature signals, are obtained from the analog to digital converter in the signal processing equipment. This is a seven bit converter which allows quantization of the input signals into 128 levels. The analog to digital converter, operating at a clock rate of 331.8 kHz can convert an analog signal of maximum value to its binary equivalent in 386 microseconds. The reset time of the converter is approximately 30 microseconds, hence the total time for the converter to reset and sample will not exceed 416 microseconds.

In order to make the system efficient time-wise, the digital data format is arranged so that transmission of converted analog data alternates with transmission of digital signals coming from the altimeter. This format allows the analog to digital converter to make the necessary conversion of an analog signal while digital data from the altimeter is being transmitted.

The clock divider system in the signal processing equipment utilizes the 1.327104 MHz clock derived from the radar altimeter clock divider chain; it provides the required clock frequencies to operate portions of the signal processing equipment. Clock frequencies provided by the system are: (1) 331.776 kHz for the analog to digital converter and the amplitude calibration system, (2) 82.944 kHz for fine timing marks, (3) 41.472 kHz for the digital commutator, and (4) 10.368 kHz for coarse timing marks. The clock divider system also supplies a pair of one microsecond system synchronizing pulses spaced 3.014 microseconds apart and placed approximately 12 microseconds ahead of the transmitter pulse. In addition, the switching pulses for the video commutator are generated by the clock divider system.

Two modes of operation for the time and amplitude calibration system are used in the signal processing equipment. One mode is used when the altimeter is searching for a radar return signal to track and the other is used when the altimeter has acquired a return signal and is tracking this signal. The altimeter reliability signal indicates which mode of operation the altimeter is in and switches the signal processor time and amplitude calibration systems accordingly.

During search operation of the altimeter the time calibration system in the signal processor provides a chain of coarse timing marks that appear in the output signal during the time that the video commutator is switched to its video position. These timing marks are one microsecond pulses derived from the 10.368 kHz output of the signal processor clock divider system. This provides a chain of timing marks spaced every 96.45 microseconds during the active radar time of the system. The first timing mark in the coarse timing mark chain occurs 60.28 microseconds after the video commutator switches from its digital to its video position. These coarse timing marks provide a time calibration for the return video signal when the altimeter is not in the track mode.

The amplitude calibration signal is injected into the altimeter during the 100 microsecond period immediately following the transmitter pulse in order to avoid possible capture of the tracking gate during the search mode. In this mode, the range tracker is active over the entire sweep range except for the 100 microsecond period which is blanked out. If a calibration signal were injected during any other time position, it would appear as a very attractive target and could capture the tracking gate.

The purpose of the 100 microsecond blanking period is to allow the transmit-receive (TR) devices in the altimeter to recover from overload effects caused by pulsing the transmitter. The 100 microsecond period is overly conservative; however, the actual recovery time of the TR devices is stated to be less than 20 microseconds. Thus the calibration signal can be injected during the period between 20 and 100 microseconds following the transmitted pulse. The amplitude

calibration system which must be operative during search mode is designed to do this.

The amplitude calibration signal was adjusted to start at -102 dBm and step up in 6 dB steps to -60 dBm -- a range of 42 dB -- which will provide adequate calibration levels for the radar return signals expected. Each step in the amplitude calibration signal is 6.03 microseconds in length, with the exception of the -90 dBm step, which is double length, and the -72 dBm step, which is triple length. These double and triple length steps allow the exact levels of the amplitude calibration signal which appears in the composite video signal to be identified readily. The total time required for the amplitude calibration system to completely step through all calibration levels is 66.3 microseconds. Thus the amplitude calibration signal can be placed in the 20 to 100 microsecond period following the transmitter pulse, with some time to spare.

When the radar altimeter goes into the track mode of operation, the reliability signal from the altimeter activates switching circuits to change the time and ampliude calibration systems to their track mode of operation. When operating in this mode, both the timing marks and the amplitude calibration are placed in close time proximity to the radar return pulse. This arrangement permits an expanded sweep oscilloscope display of the timing marks, video pulse, and calibration signal. Such a display would show, in sequence, the first timing mark, the video pulse, the second timing mark, and the amplitude calibration signal. This entire display is confined to a time interval of less than 400 microseconds.

Accurate positioning of the time and calibration signals is accomplished by generating a delay of precisely 6896 microseconds from the end of the previous counter-gate. Since the counter gate ends at the leading edge of the radar echo pulse and the pulse repetition period is 6944 microseconds, the delay of 6896 microseconds terminates 48 microseconds before the next echo pulse arrives. The delay itself is produced by the digital delay generator shown in Figure 8.

The output of the digital delay generator is used to open a gate of such length that at least one of a chain of one-microsecond timing marks (spaced 12.06 microseconds apart) will be gated into the video system of the signal processor. At the end of the first timing mark gate a delay of 250 microseconds is generated which provides time for the occurrence of the stretched video return pulse. At the end of the 250 microsecond delay a second timing mark gate is opened to again pass at least one of the chain of timing marks.

At the end of the second timing mark gate the amplitude calibration system is placed in operation. This system produces the same form of calibration signal as that used in the search mode of operation, namely an eight level signal that steps from -102 dBm to -60 dBm in steps of 6 dB.

Since the amplitude calibration signal always occurs a fixed time away from the end of the counter gate the amplitude calibration signal cannot be locked onto by the altimeter. Thus in the track mode of operation of the altimeter a timing mark is placed ahead of and behind the video signal and the second timing mark is followed by the amplitude calibration signal. The time relationship between system signals when operating in the track mode is shown in Figure 9.

The signal processor contains its own power supply which operates from the 28 volt vehicle supply. This supply furnishes +12, +6, -6 and -12 volts from a dc to dc converter and regulated power supplies.

C. Conclusions

A breadboard version of the signal processing equipment for use in a contemplated radar return experiment has been constructed. The equipment was designed to time-division multiplex signals obtained from a radar altimeter and to deliver these signals in the proper form to modulate a data link transmitter. The signal processing equipment met these requirements satisfactorily and demonstrated the feasibility of the approach used.

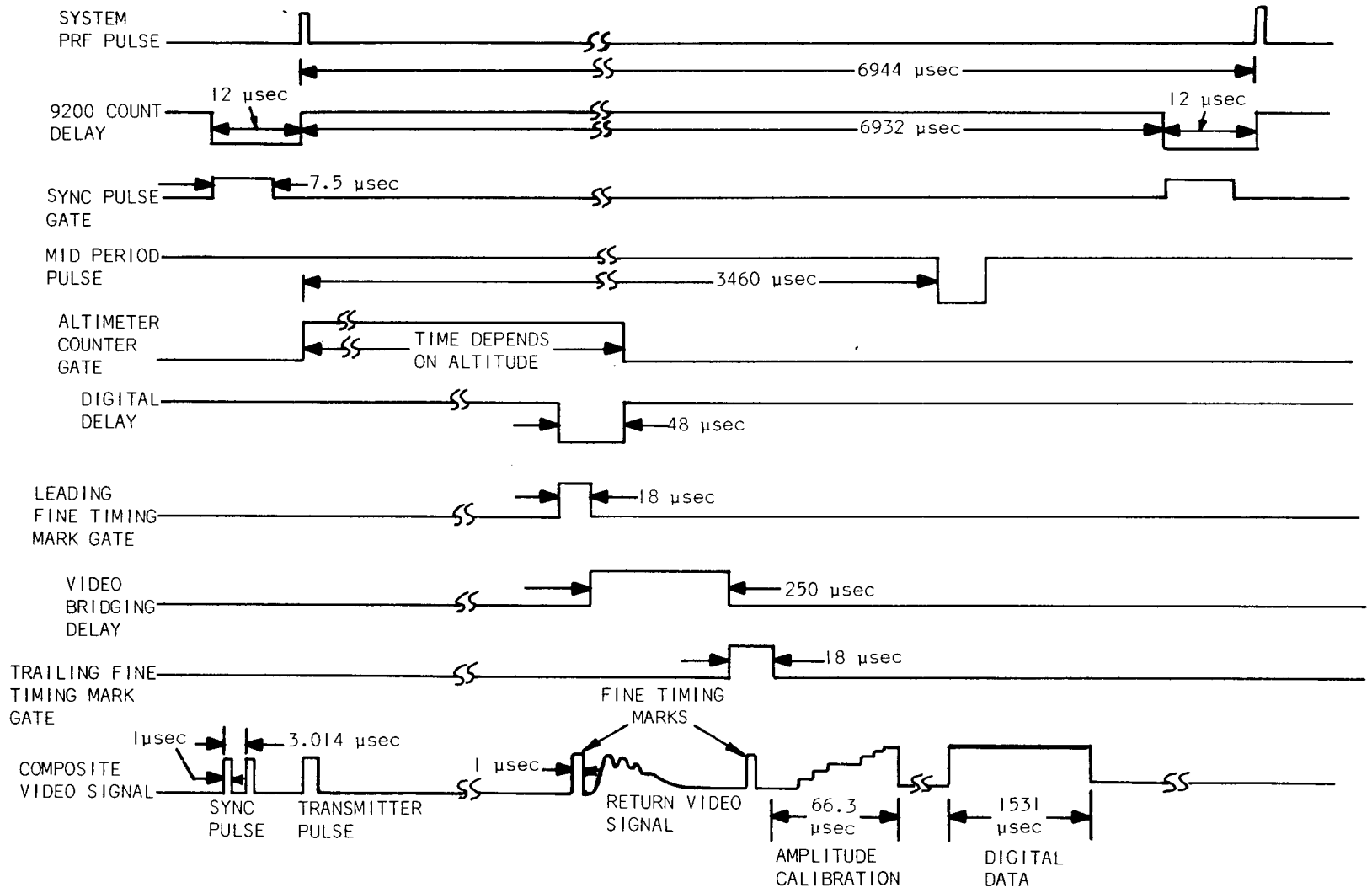

Figure 9. Timing Diagram for Signal Processor Operating in the Track Mode.

From experience with the breadboard system no difficulty is foreseen in packaging the equipment for use in a vehicle environment.

V. COMMAND AND COMMUNICATIONS SYSTEM SPECTRAL STUDIES

A. Introduction

The particular task covered by this section was that of calculating the frequency spectra for various portions of the Command and Communications System (CCS). The section presents some results of the calculations, and compares calculated values with measurements actually made on the system in the laboratory.

Methods were derived for calculation of the frequency spectra of (1) the baseband signal at the output of the command modulator for an alternating bit pattern and an arbitrary sub-bit pattern, (2) the baseband spectra of the range code, (3) the output of the frequency modulated command subcarrier generator, and (4) the output of the up-link signal generator at S-band.

The S-band spectra were obtained for modulating signals into the phase modulator consisting of (1) the command data subcarrier with the baseband modulation applied (2) the range code, and (3) the range code and the unmodulated command data subcarrier.

The methods derived mathematically for the calculation of the various spectra were programmed on a Burroughs B-5500 computer. The computational results provide the details of the spectra at the outputs of the various systems in the Command and Communications System. These results can be used to determine the spectrum occupancy of the various signals.

For a detailed discussion of the mathematical analysis, computer programs, and examples of computer printout reference should be made to Technical Report No. 3.[7]

B. System Description

The generation of the output signal of the CCS up-link transmitter is rather complex and involves a number of steps. The essential elements of the signal generating equipment are shown in the block diagram of Figure 10. The output of a 1 kHz oscillator is passed through a frequency doubler to obtain a 2 kHz sine wave.

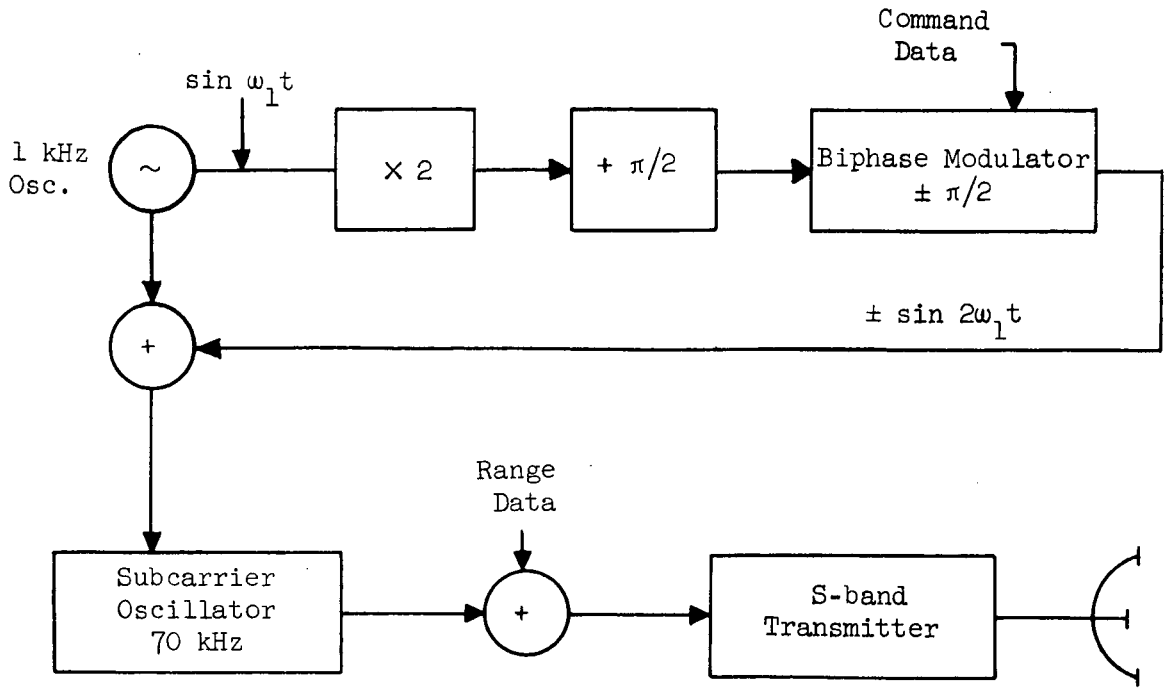

Figure 10. CCS Up-Link Transmitter.

This 2 kHz wave is then shifted $\frac{\pi}{2}$ radians in phase and passes through a biphase modulator which shifts the phase either $+\frac{\pi}{2}$ or $-\frac{\pi}{2}$ radians depending on a digital data stream arriving at 1000 bits per second. The output of the biphase modulator is then summed with the original 1 kHz wave of equal amplitude, the phases of the two waves being such that they pass through zero crossings at the same time. The output of the summing network is frequency modulated onto a 70 kHz subcarrier with the modulation level adjusted to give 5 kHz peak frequency deviation. The output of the FM subcarrier generator is phase modulated onto the S-band carrier. The modulation level is adjusted to give a maximum phase deviation of ± 1.22 radians.

The digital data stream which determines the phase shift introduced in the biphase modulator is actually composed of two parts. Command data is fed to the system at the rate of 200 bits per second, but each "bit" of data is injected into the biphase modulator as 5 "sub-bits". The particular 5 sub-bits chosen to represent a "one" data bit constitutes a code which is chosen prior to launch

and is fixed for the flight. Once the sub-bit configuration is chosen to represent the "one" data bit, the complement of that set is the sub-bit code for the zero data bit. The sub-bit codes can be varied from one flight to the next. Thus the maximum "bit rate" at which command data is transmitted is 200 bits/sec, and the maximum sub-bit rate at which the biphase modulator switches is 1000 bits/sec.[8]

In addition to the command data entering the S-band phase modulator, there is present at times (but not always) a pseudo noise stream of rectangular pulses. These pulses, the range data code, are generated from a basic frequency of 498 kHz, so that the basic pulse interval is approximately 1 microsecond. The modulation level for this pulse stream is adjusted to give a maximum phase deviation of the S-band carrier of ± 0.6 radians.

C. Baseband Spectrum

The baseband spectrum is composed of two parts. One of these is the reference 1 kHz signal which is summed with equal amplitude to the output signal of the biphase modulator. The 1 kHz reference signal simply places a component in the baseband spectrum with an amplitude of E_o.

A graph of the amplitude spectrum corresponding to the biphase portion of the signal is shown as the solid lines in Figure 11.

To obtain the complete baseband spectrum the 1 kHz reference signal component must be added to the output spectrum of the biphase modulator. This component is shown in Figure 11 as the broken line.

As a check on the calculated values, a laboratory version of the biphase modulator was constructed and the components of the output spectrum corresponding to the calculated components were measured. The measured values are indicated in Figure 11 by the dots. The small differences could easily be due to distortion in the laboratory model of the modulator.

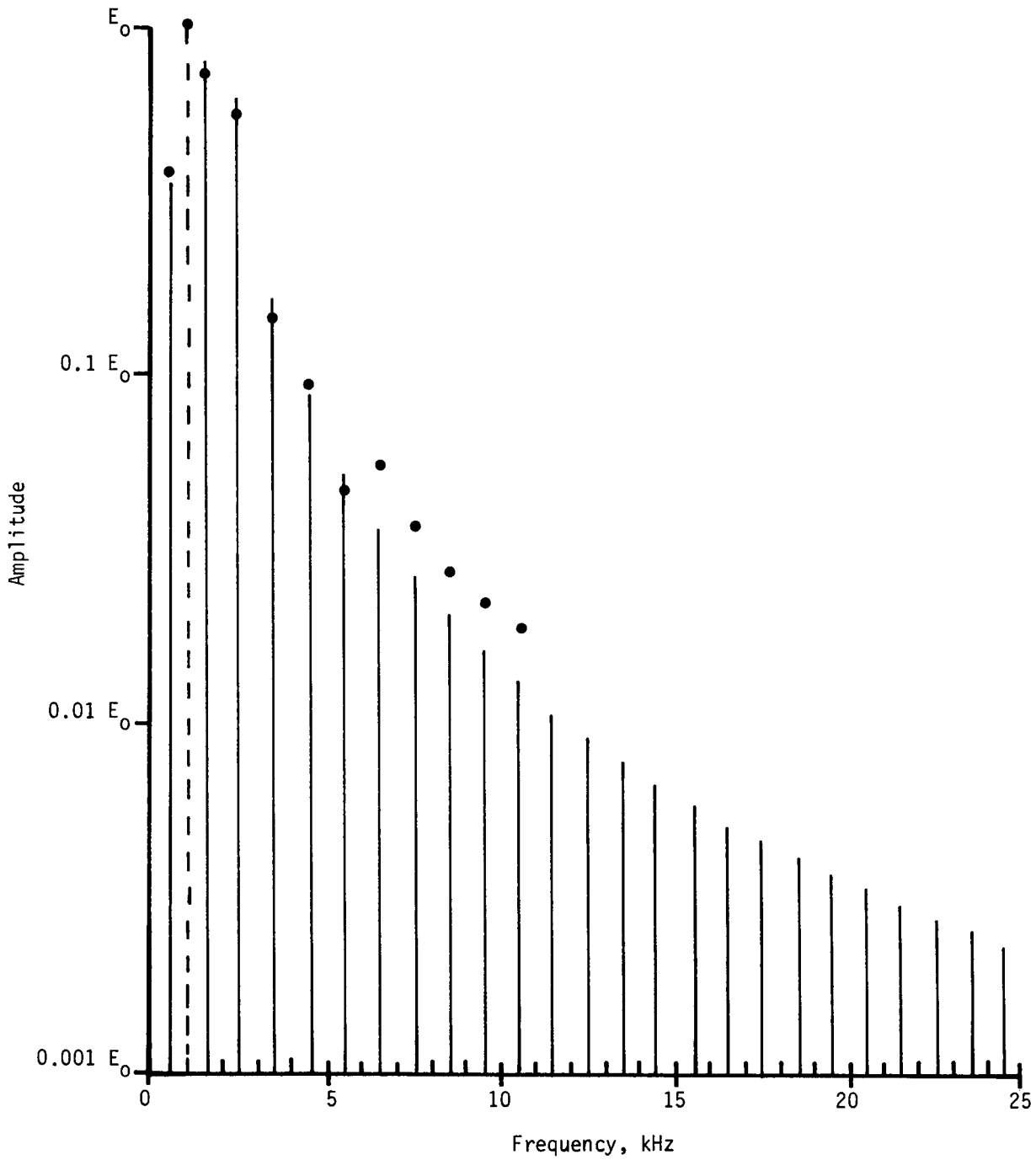

Figure 11. Computed Baseband Spectra of the Command Modulator. Comparative Measured Values are Indicated by Dots.

D. FM Spectrum

A computer program, written in ALGOL compiler language for the Burroughs B-5500 computer, was constructed to evaluate the FM spectrum. Using the computer program, the output spectrum of the FM subcarrier generator was computed for $\lambda = 2.84$ and a sub-bit pattern of 1, -1, 1, -1, 1. The value of λ is that which corresponds to a 5 kHz peak deviation of the FM carrier when modulated by the baseband command data signal.

As a check on the accuracy of the prediction technique, the predicted values were compared with measured values obtained from a laboratory version of the circuit. To effect the laboratory setup, a breadboard model of the biphase modulator was constructed. This model was then used to frequency modulate a carrier and the output spectrum was displayed on a spectrum analyzer and photographed. Measurements taken from the photograph were then compared with the predicted values. The measured values were normalized to the computed values by adjusting the measured carrier until it equaled the predicted values. All other measured values were scaled proportionately. These measured values along with the predicted values are shown in Figure 12.

E. S-Band Spectrum

1. General Approach

The output of the FM modulated subcarrier oscillator is phase modulated onto the S-band carrier. Before being applied to the S-band transmitter, however, it is summed with the range data code (a stream of digital data) when this code is present. Consequently the output S-band signal is the result of these two modulating signals. The range data code will probably be generated only part of the time, hence the modulating signal applied to the S-band transmitter is at times only the output of the FM subcarrier oscillator, while at other times the modulating signal is the oscillator output plus a stream of digital data made up of pseudo noise sequences.

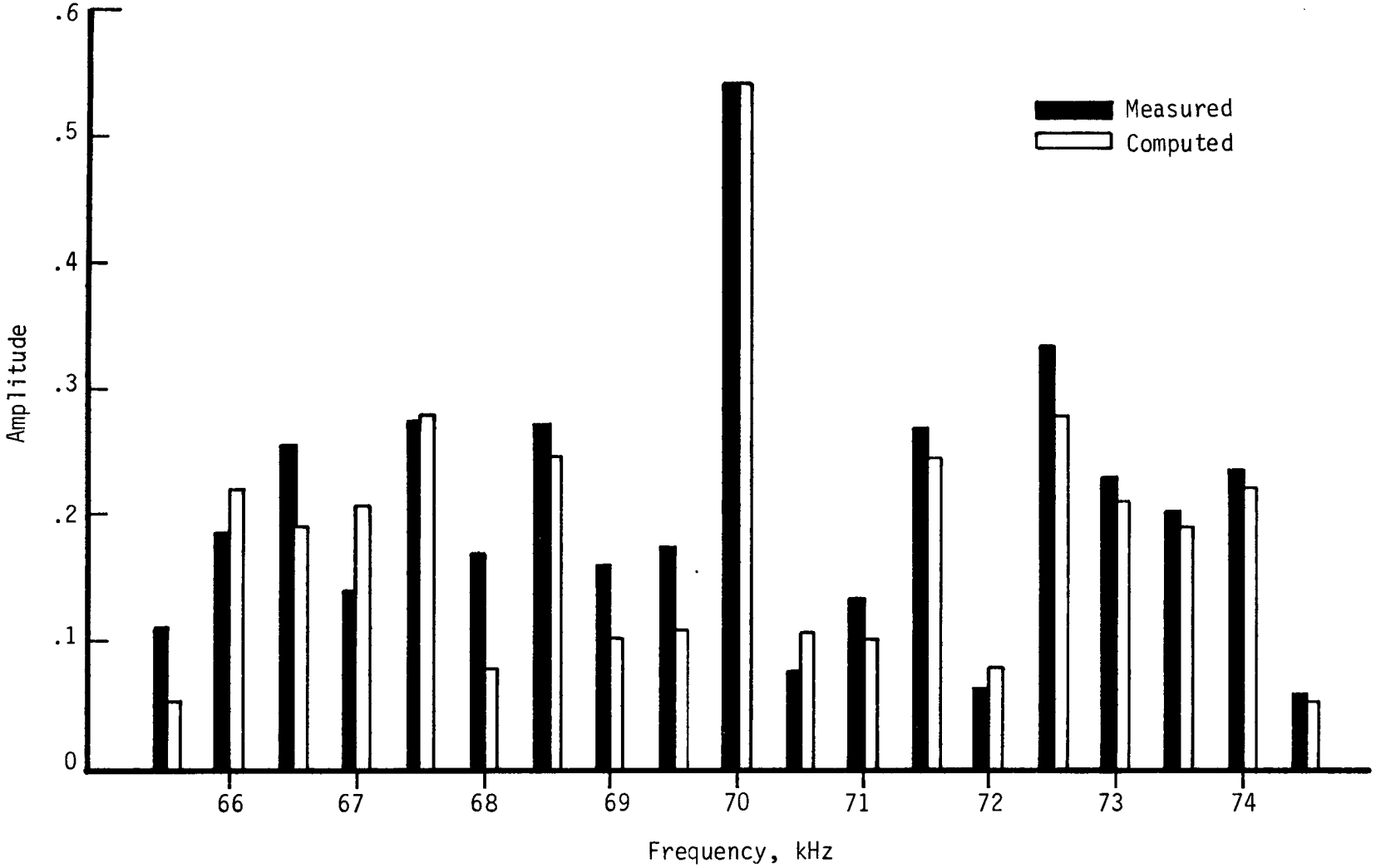

Figure 12. Comparison of Measured vs Computed FM Spectra $\lambda = 2.84$ (5 kHz peak deviation), Sub-Bit Pattern 1, -1, 1, -1, 1.

Although it is possible to derive mathematical expressions for the spectrum at the S-band output, there are practical problems involved in calculating the spectrum due to the large number of lines involved. General consideration of the two signals modulating the S-band transmitter indicate that the command data alone will produce a spectrum with line spacings as small as 100 Hz, while the range data alone will produce lines at wider spacings which spread over several Megahertz. The interaction of these two will produce a spectrum several Megahertz wide with lines at 100 Hz spacing. Calculating the tens of thousands of lines in a sample spectrum (for fixed command data code and fixed range data code) would tax the capabilities of the largest computers. Also it is somewhat doubtful if the fine detail in the entire spectrum would really provide any useful information.

As a method of approach in analyzing the S-band spectrum, the problem was divided into three sub-problems. First, the S-band spectrum for the command data alone was calculated. Second, the S-band spectrum due to the range data alone was computed. Finally, the spectrum produced when both signals modulated the S-band transmitter was computed, but with the input from the command data channel being limited to the unmodulated subcarrier. By considering the subcarrier without modulation, the close spacing of spectral lines that was caused by the command data modulation was eliminated. Although neither of the three types of calculations that were made produced the output spectrum in its entirety, the results of the calculations do permit determination of the nature of the S-band spectrum.

2. S-Band Spectrum of the Command Data

A computer program was constructed for computing the S-band spectrum with only the sub-carrier oscillator output, $e_{FM}(t)$, as input to the phase modulator; the range data code was not included. The computer program was run to obtain this S-band spectrum for

alternating sub-bits. The resulting spectrum contains so many components at 500 Hz spacing and is spread over such a wide range that it was not feasible to present the entire spectrum in a single graph. However, Figure 13 shows a curve which passes through the highest line in each subgroup. Thus this curve is an envelope of the entire spectrum. For additional information on the spectrum, including detailed graphs of the first five sideband groups, see Technical Report No. 3.[7]

3. S-Band Spectrum of the Range Data

A computer program was constructed for calculating the output spectrum when only the range data signal was modulating the S-band transmitter. Using this program, the output spectra were computed for various range data codes. For the first of these calculations, an alternating bit pattern was used for the range code rather than a pseudo-noise sequence. The number of bits in the alternating sequence was odd so that the modulating wave form was not strictly a square wave. An example of the computed and measured spectrum for a code consisting of 29 alternating bits is shown in Figure 14. Spectra were also computed for a number of pseudo noise sequences of range data bits. As examples of the results, the computed output spectra for a sequence of length 15 bits is shown in Figure 15.

4. Total S-Band Spectrum

A computer program for this calculation was constructed and the output spectrum of the S-band transmitter when modulated with both the sub-carrier and the range data was computed for several different pseudo-noise codes. For verification of the calculations, measured spectra were obtained in the laboratory from the S-band transmitter when similar modulations were applied. Even with the modulation removed from the subcarrier, the output spectrum contained so many lines that detailed comparison of measured and

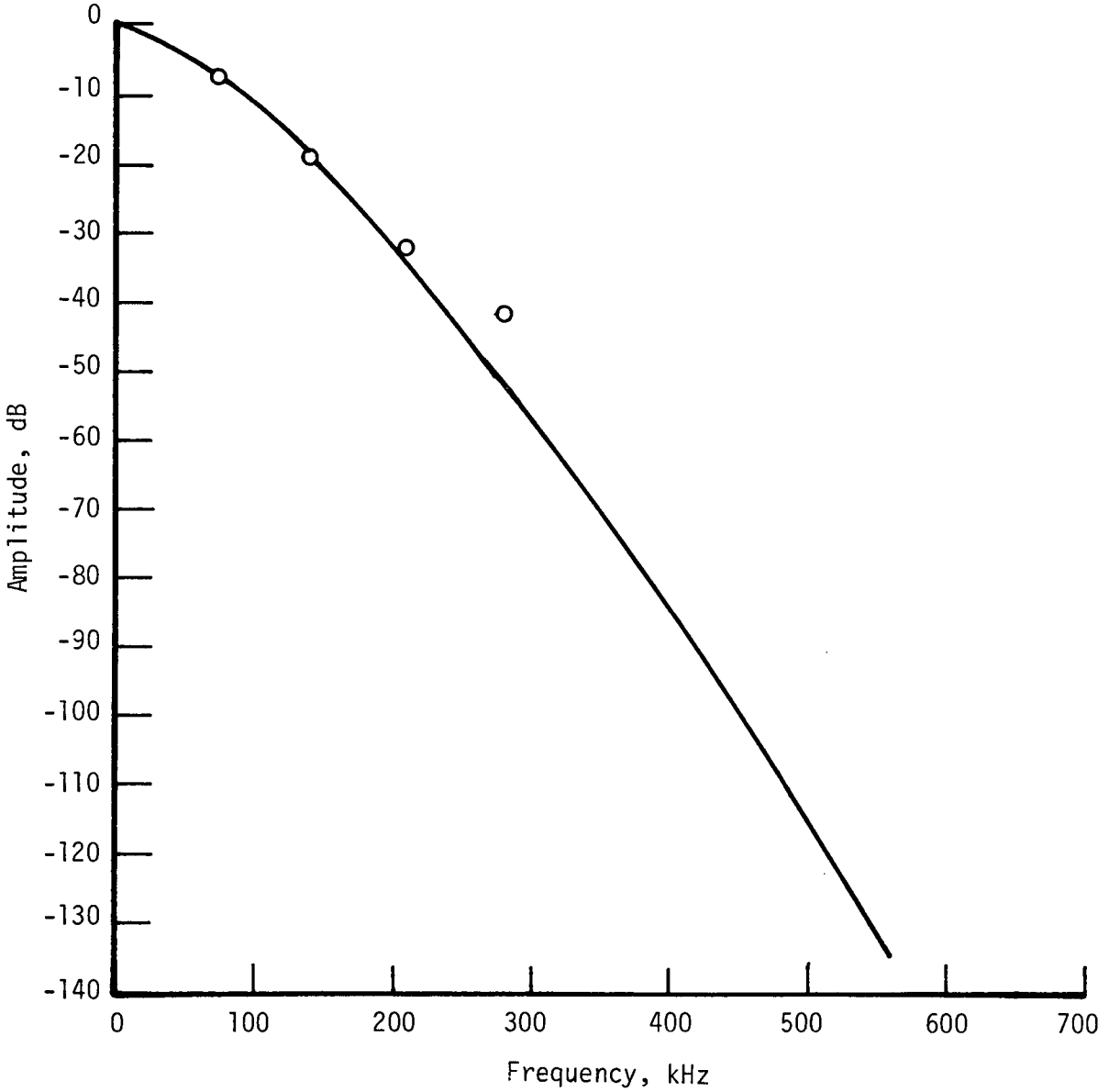

Figure 13. Envelope of Sidebands of S-Band Spectrum for Command Data Modulation.

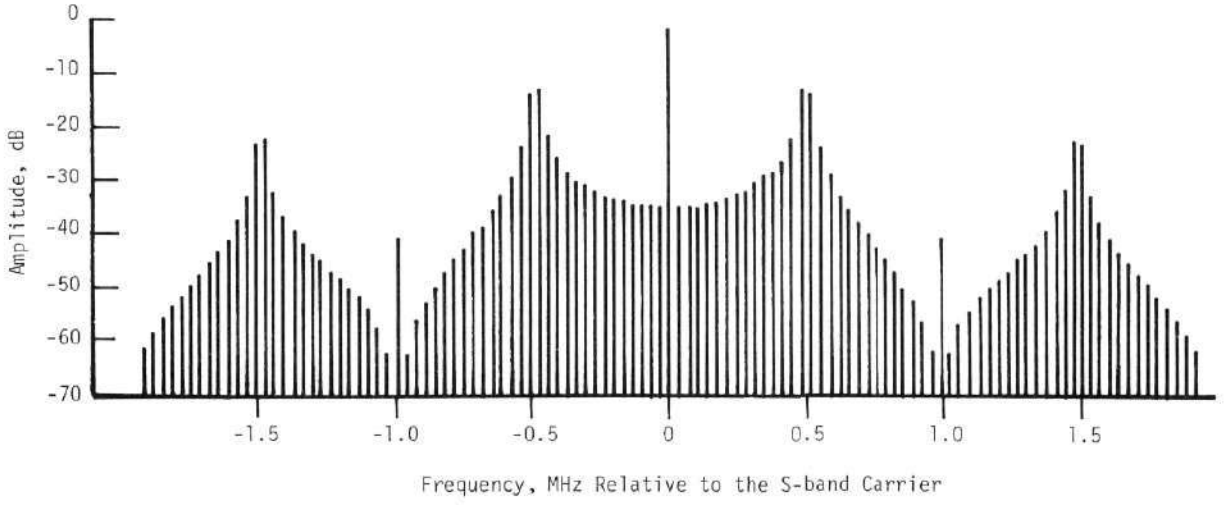

(a) Computed

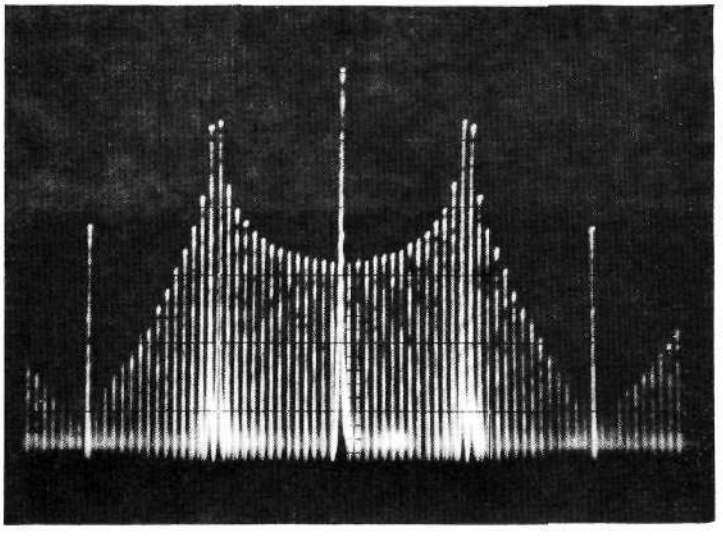

(b) Measured:
Horizontal: 300 kHz/cm
Vertical: 10 dB/cm

Figure 14. Computed and Measured S-Band Spectra for a Modulating Signal Consisting of 29 Alternating Bits Applied to the Range Code Input of the Phase Modulator, $\beta_2 = 0.6$.

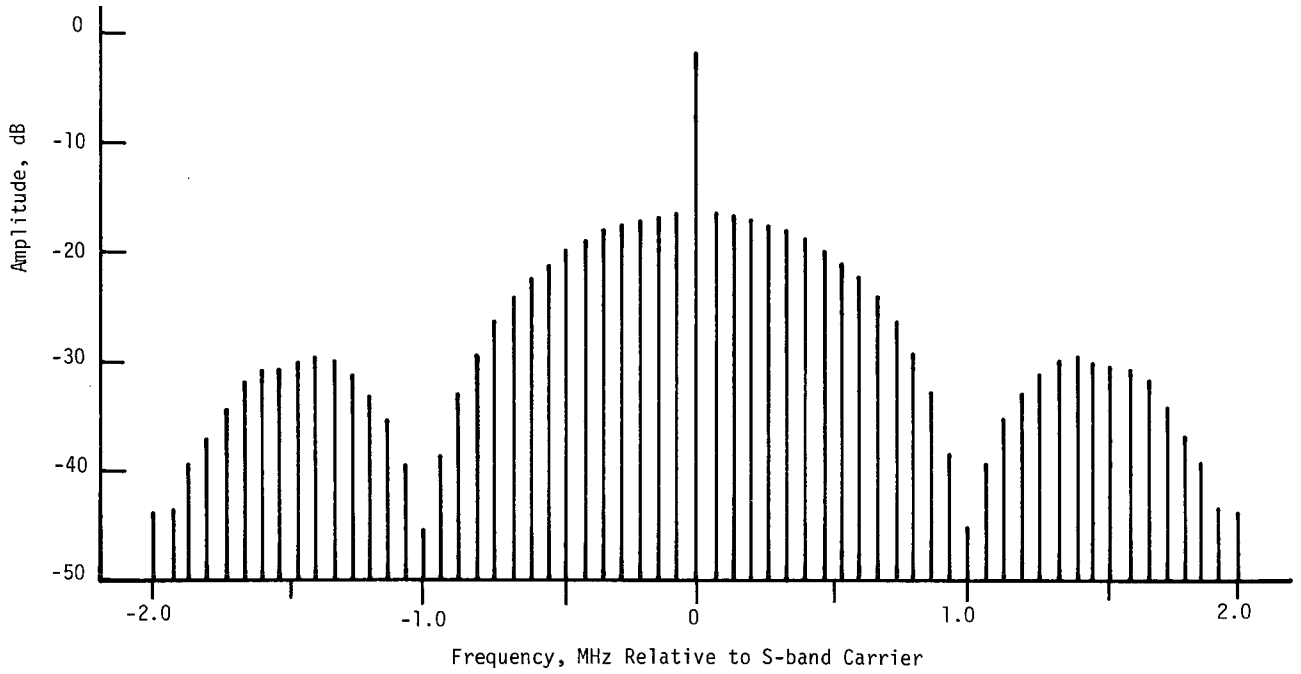

Figure 15. Computed S-Band Spectrum for a Modulating Signal Consisting of a 15 Bit Pseudo Noise Code Applied to the Range Code Input of the Phase Modulator, $\beta_2 = 0.6$.

computed values could easily be made only for very short range data codes. For the three bit code 1, -1, 1, a comparison of the measured and computed values for a number of lines in the center of the spectrum is shown in Figure 16. The measured values were read from a photograph of the spectrum obtained in the laboratory and were normalized by making the carrier levels equal.

F. Conclusions

Methods have been developed for the calculation of the frequency spectra of (1) the baseband command data signal, (2) the baseband range code signal, (3) the frequency modulated output of the command subcarrier generator, and (4) the output of the S-band up link signal generator. The S-band spectrum was obtained for modulating signals

applied to the S-band phase modulator which consisted of (1) the modulated command data subcarrier, (2) the range code signal, and (3) both the range code and the unmodulated command data subcarrier. Good agreement has been obtained between the calculated and measured values. The computer programs developed to implement the calculation from the mathematical derivations can be used to study the effect of variation in system parameters, such as modulation indices, on the spectra obtained for the various systems.

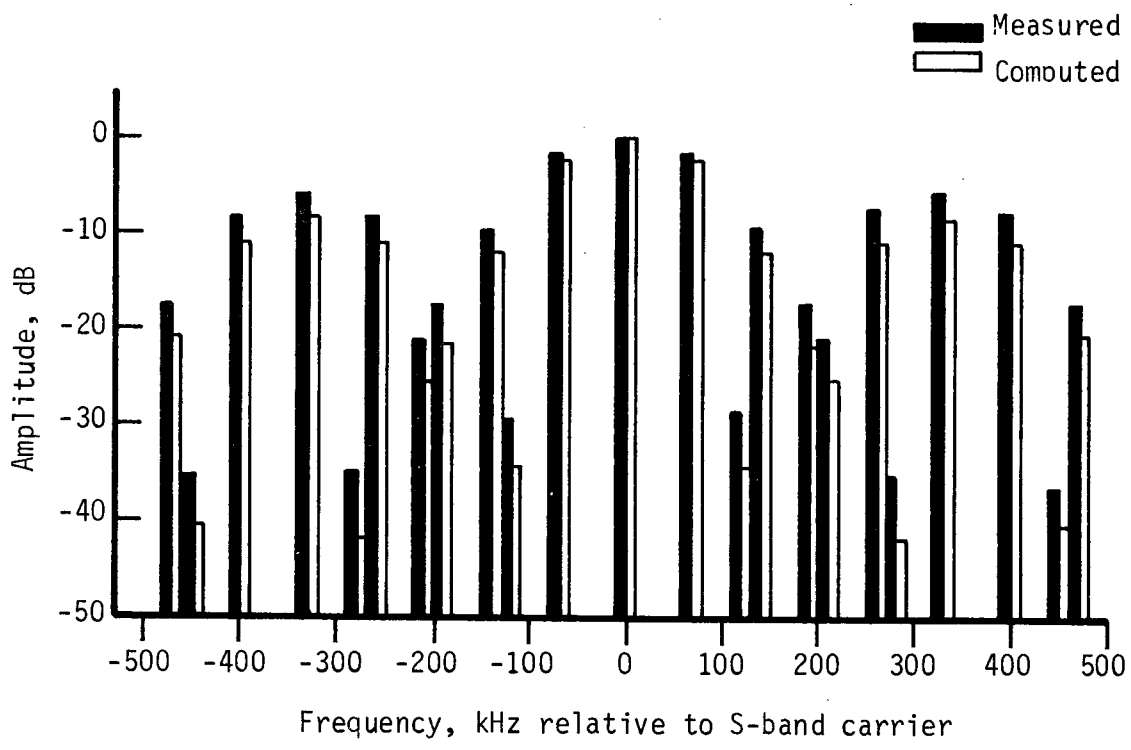

Figure 16. Comparison of the Computed and Measured Spectral Components of the S-Band Spectrum for a Modulating Signal Consisting of a 3 Bit Pseudo Noise Code and the Unmodulated 70 kHz Command Data Subcarrier Applied to the Input of the Phase Modulator, $\beta_1 = 1.22$, $\beta_2 = 0.6$.

VI. SOME INTERMODULATION CONSIDERATIONS IN THE CCS DOWN-LINK DATA DEMODULATORS

A. Introduction

Initial data received over the CCS down-link telemetry channel on Saturn-Apollo flight AS-501 exhibited error rates that were thought to be excessive. This experience prompted an investigation into possible causes of excessive error rates in the CCS telemetry channel. Reduction of the data at a later date showed that the error rates experienced were consistant with predictable rates and that system performance was essentially in conformance with theoretical expectations. The investigation of excessive error rates did reveal the possiblity of system degradation in the Unified S-band System (USB) due to intermodulation products created by the data demodulator in the ground receiver.

The ground receiver used in the investigation is the prototype model of the Generalized Concept Receiver (GCR).[9] This receiver is a triple conversion phase lock receiver utilizing sinusoidal phase detectors. Other than the triple conversion feature, it is similar to the double conversion phase lock receivers used in the Manned Space Flight Network. The objective of the investigation was to determine how intermodulation distortion could be produced in the demodulators.

The investigations that were made and a summary of the results are described briefly in the following sections. For a more detailed discussion of the investigation and the results, see Technical Note No. 2.[10]

B. Loop Characteristics

The USB system was designed to provide command, communication, telemetry, and accurate range and range rate information for all ranges up to and greater than lunar distance. The system has a single radio frequency channel and utilizes subcarriers for the

command, communication, and the telemetry functions; a pseudo noise (PN) code is used for range information. In the CCS the range code clock frequency is approximately 498 kHz, the up-link command data subcarrier is 70 kHz, and the down-link telemetry subcarrier frequency is 1024 kHz. The command data baseband signal is frequency modulated on to the 70 kHz command subcarrier with a peak deviation of 5 kHz; the range information is obtained by the use of PN sequences clocked at the range code clock rate; and the down-link telemetry data is biphase modulated onto the 1024 kHz telemetry subcarrier.

Because several signals are present simultaneously, intermodulation products can be generated in the non-linear data demodulators; the resulting distortion can cause system degradation. The degradation of the telemetry channel by intermodulation products involving the turned-around command data subcarrier received particular emphasis in this investigation.

The vehicle transponder receiver and the ground receivers are both phase lock receivers. The carrier tracking section of the receivers can be analyzed as a second order automatic control system in which (during the time the loop is locked) the variable to be controlled is the phase of the reference voltage-controlled oscillator (VCO). The phase of this oscillator is forced by the phase lock loop to be approximately in quadrature with the phase of the received signal at the phase detector. The receiver demodulates the various data signals from the modulated carrier by using a reference signal derived from the coherent VCO. A simplified block diagram of the phase lock receiver is shown in Figure 17. The S-band signal is heterodyned down to an intermediate frequency with a local oscillator frequency obtained by multiplication of the VCO frequency. This IF signal is applied to one input of the loop phase detector, a reference signal derived from a crystal oscillator and a 1 MHz frequency standard is applied to the other input. The phase detector output is an error voltage

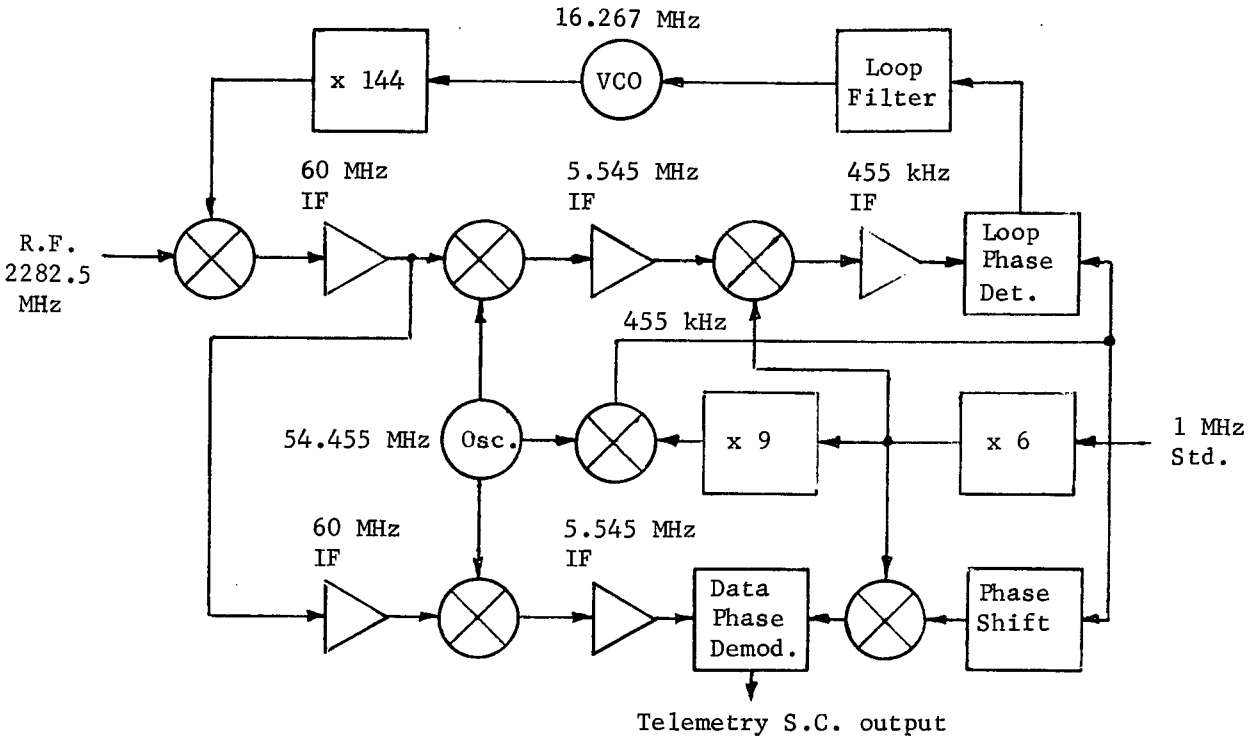

Figure 17. Simplified Block Diagram of a Phase Lock Receiver.

proportional to the sine of the phase between the IF signal and the reference signal. This error voltage is passed through a lag network and used to control the frequency of the VCO. The closed loop system controls the frequency of the VCO to maintain a quadrature phase relationship between the two phase detector inputs. With high gain loops the quadrature phase relationship will be closely approximated, but static and dynamic tracking errors can occur.

C. Intermodulation and Subcarrier Suppression Considerations

Demodulation of the input signal is accomplished by applying the signal to be demodulated to one input of a phase detector and applying a reference signal to the second input. The phase demodulator operates much like a perfect multiplier. If the phase

relationship between the input signal and the reference signal is correct, then after low pass filtering of the detector output, the sine of the modulating signal will be recovered. For small deviations in the phase relationship of the two signals, the recovery of the modulation is essentially linear.

Since the phase demodulator has a sinusoidal transfer characteristic, intermodulation distortion can occur if there is an appreciable phasing error at the demodulator inputs. The distortion appears as AM sidebands around a subcarrier frequency. The frequencies of these sidebands can be shown to correspond to the sum and difference frequencies of the two subcarriers.

A phasing error at the demodulator will also cause a reduction in the detected subcarrier amplitude.

Thus two problems are introduced if a phasing error exists in a phase lock receiver; intermodulation distortion, and reduced signal power from the detector. The magnitude of these problems is dependent on the amount of phase error and the modulation indices chosen for the subcarriers. The calculated subcarrier suppression and the amplitude of the AM sidebands produced by various phase errors at the data demodulator are shown in Table I.

TABLE I

INTERMODULATION AND SUPPRESSION EFFECTS ON TELEMETRY SUBCARRIERS

Phase Error (degrees)	Suppression Relative to no Phase Error (dB)	Amplitude of 70 kHz AM (percent)
15	0.3	22.1
30	1.2	47.6
45	3.0	82.8

Verification of the theoretical results discussed above was obtained in the laboratory using the Interstate GCR and a CCS transponder. The tests were made only with static phase errors simulating the phasing errors which might be encountered in the use of the USB system. Typical modulation indices and actual subcarrier frequencies were used in the tests. The command subcarrier frequency used was 70 kHz with a modulation index of 0.75 radian, and the telemetry subcarrier frequency used was 1024 kHz with a modulation index of 1.22 radians. The measured amplitude of the AM for various phase errors differed from the predicted values at phase errors of 15, 30, and 45 degrees by 0.5, 0.9, and 1.3 percent respectively.

The effects of the intermodulation distortion on the detected signal were also observed in the laboratory. For these tests the telemetry subcarrier was modulated with a 36 kHz square wave (simulating a data stream at the normal bit rate of the channel), and the waveform of the bandpass filtered signal into the telemetry demodulator as well as that of the demodulator output was observed and photographed. The results are displayed in Figure 18.

D. Conclusions

The results obtained theoretically and verified experimentally in the laboratory show that a phase error in the tracking loop of a phase lock receiver can introduce distortion of the signals in a multiple subcarrier system. The distortion was shown to be in the form of amplitude modulation of one subcarrier by the other. The amount of modulation was shown to be a function of the modulation indices used and of the amount of phase error present. It was also shown that the phase error produces suppression of the subcarrier.

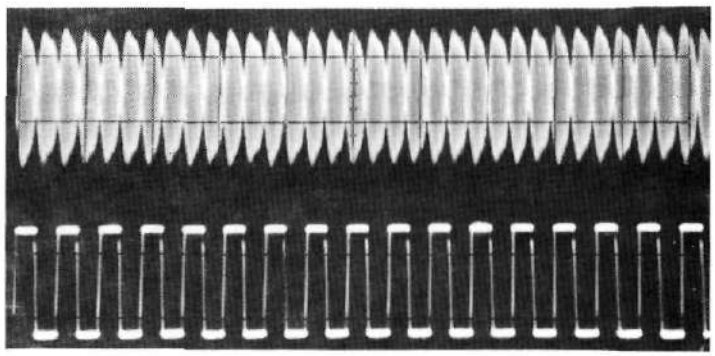

Detected Signal with a 0° Reference Phase Error.

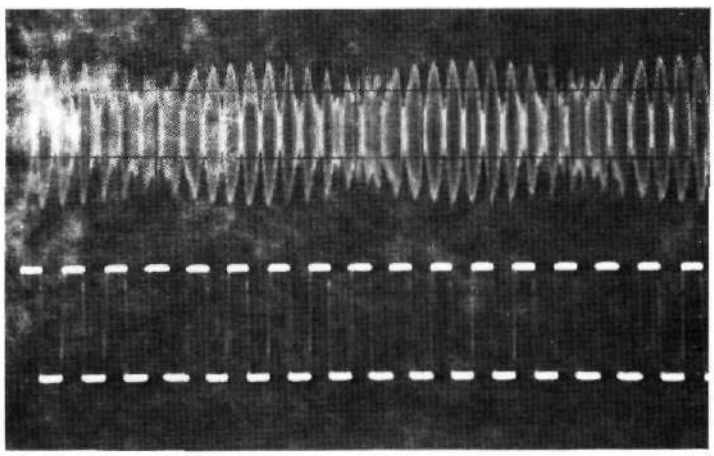

Detected Signal with a 20° Reference Phase Error.

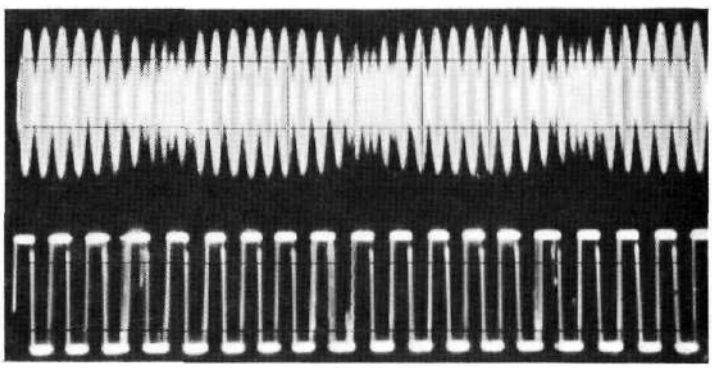

Detected Signal with a 40° Reference Phase Error.

Figure 18. Effect of Intermodulation on the Detected Square Wave Telemetry or the Indicated Reference Phase Errors.

VII. AN INVESTIGATION OF THE ERROR-RATE PERFORMANCE OF THE CCS COMMAND DATA DEMODULATOR

A. Introduction

This section summarizes an investigation which was concerned with the error-rate performance of the command demodulator (module A-10) of the Command and Communication System (CCS) transponder. Of particular interest was the performance of the command demodulator when operating in the region just below threshold (i.e., below approximately 12 dB input signal-to-noise ratio). Experimental observation showed that the error-rate performance obtained for the signal from the demodulator was worse than that obtained for a simulated signal having the same signal-to-noise ratio and bandwidth. The simulated signal was the command data baseband signal which consisted of the biphase modulated 2 kHz waveform summed with the 1 kHz reference signal with added white noise. Detailed discussions of the investigation are contained in Technical Report No. 5.[11]

B. System Analysis

An investigation was made of the manner in which various sections of the command demodulator influenced the characteristics of the demodulated output signal. The goals of the investigation were: (1) to determine if the command demodulator was operating as theory predicted, and (2) to determine the reason for the observed error-rate behavior.

As a preliminary to the investigation, a review was made of the theoretical behavior of FM demodulators, with noisy input signals. Papers by Frutiger,[12] Rice,[13] and Malone[14] provided a basis for the analysis of FM detector characteristics for two regions of interest, i.e., for high signal-to-noise ratios and for signals just below threshold.

Experimental measurements at high signal-to-noise ratios agreed with the signal-to-noise performance predicted from the theoretical

considerations. Measurements were also made which agreed with Rice's results for the region just below threshold. The predicted and measured signal-to-noise performance is shown in Figure 19. Because of the close agreement, it was concluded that on a signal-to-noise basis the command demodulator was operating properly and that the degradation of error-rate performance in the region below threshold could not be attributed to the signal-to-noise performance of the command demodulator alone.

Analysis of the character of the noise present at the output of the demodulator, when operating below threshold, resulted in a refined simulation signal for the output of the demodulator. This new signal consisted of the baseband signal, plus noise with an amplitude spectrum proportional to frequency, and impulses, with the same amplitude and at the same rate as those produced by the command demodulator. As shown in Figure 20, when this test signal was used as the input to the decoder, the error rates produced were very close to those obtained when the output of the command demodulator was used for the drive signal into the decoder. Figure 20 also shows the error-rate performance for decoder inputs consisting of (1) baseband signal plus white noise, and (2) baseband signal plus noise with an amplitude spectrum proportional to frequency. In each case, all signals have the same low-pass bandwidth as the demodulator output.

During the course of the investigation, it was noted that the amplitude limiters in module A-10 changed characteristics with changes in input signal amplitude. Comparisons of the A-10 limiters with the theoretical performance expected and with symmetric limiters which were constructed in the laboratory indicated that improvement in the A-10 limiters could be attained. The imperfect limiting did not, however, appreciably affect error-rate at the decoder output.

C. Conclusions

The overall conclusion of these studies is that the command demodulator was operating properly and that the error-rate performance obtained was as expected.

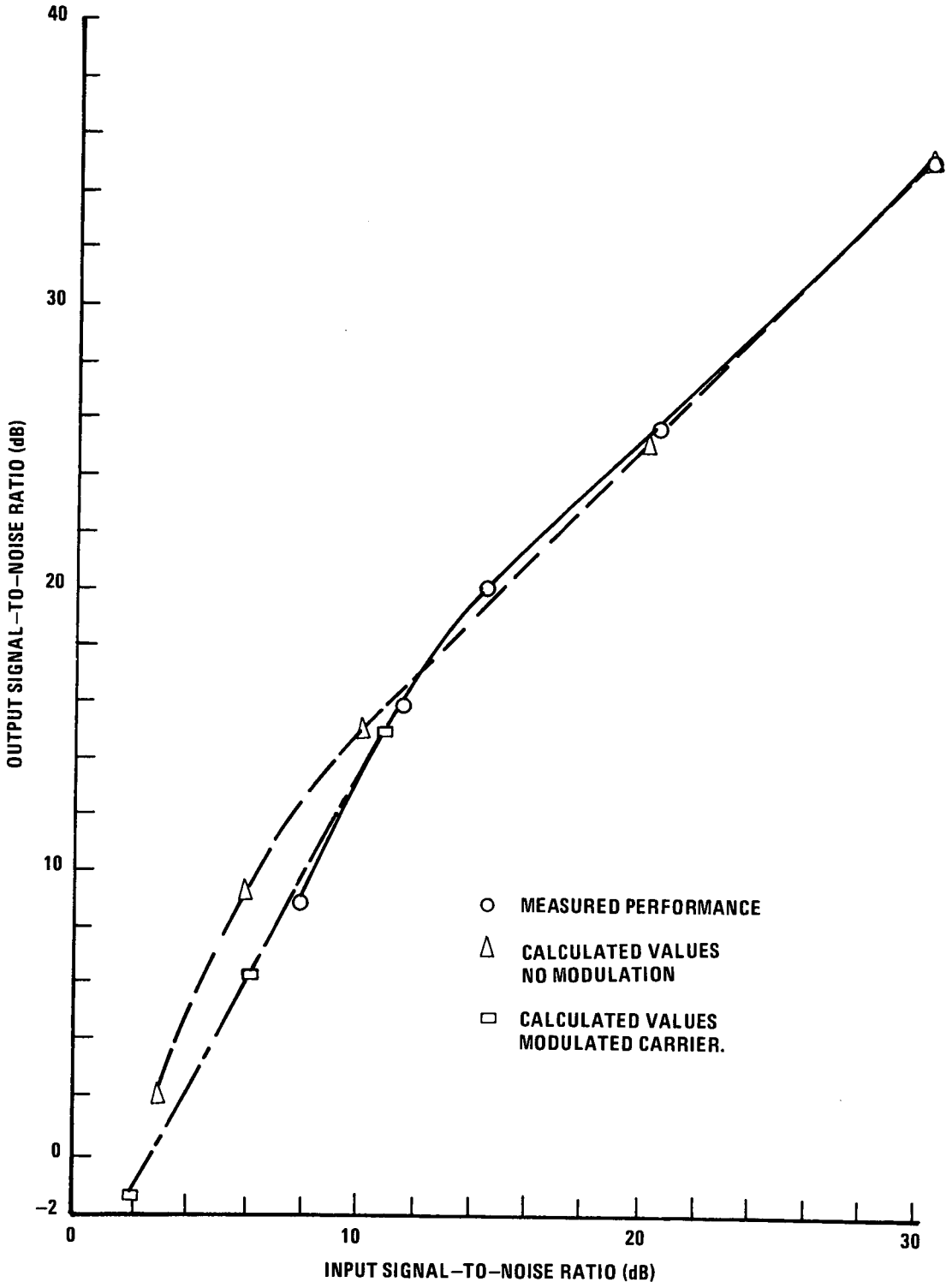

Figure 19. Predicted and Measured Signal-to-Noise Performance of the CCS Command Demodulator.

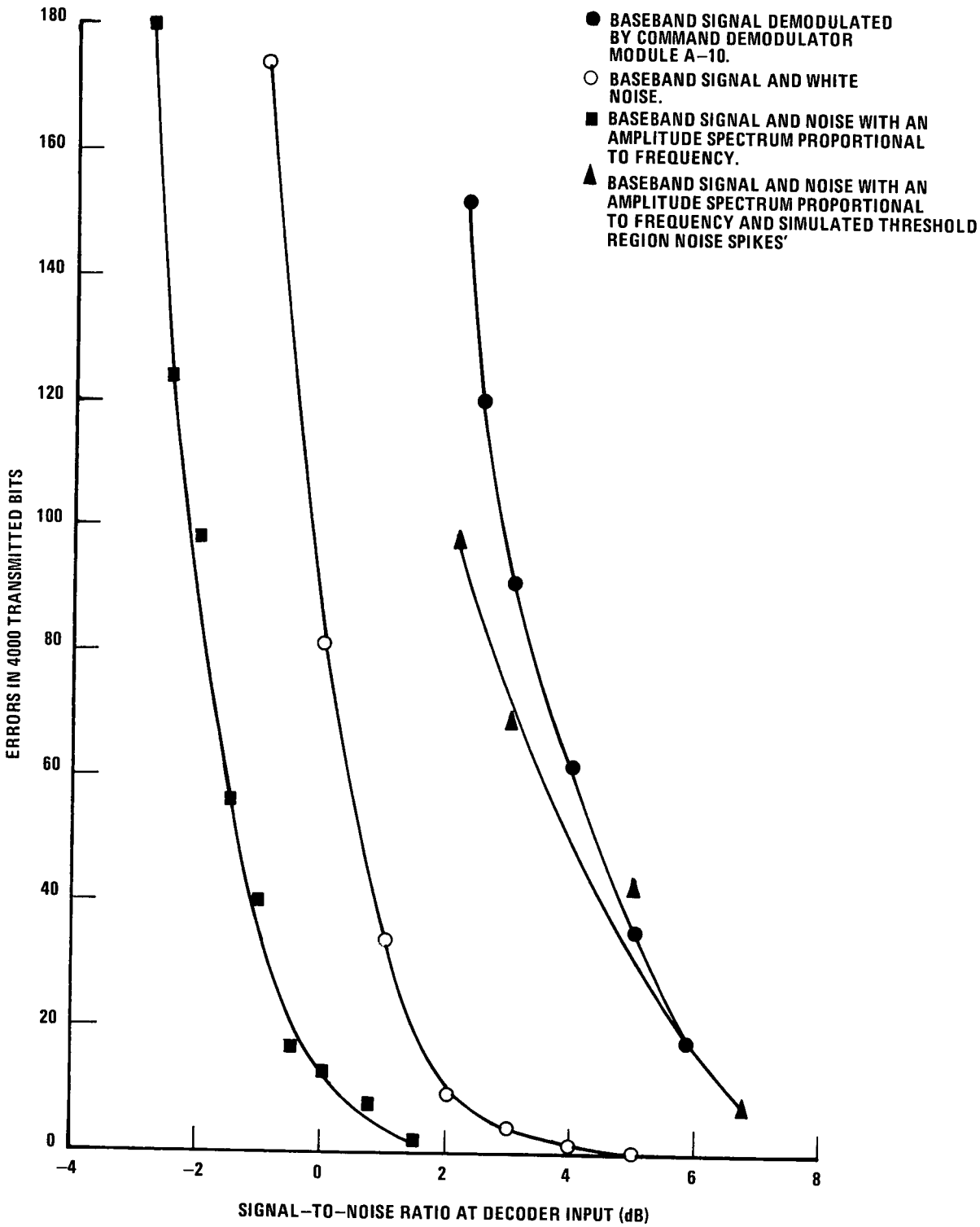

Figure 20. Error-Rate Performance for the Indicated Signals at the Input to a Command Decoder.

VIII. A STUDY OF FLAME ATTENUATION OF TELEMETRY TRANSMISSIONS FROM SATURN VEHICLES

A. Introduction

Adverse RF propagation effects have long been associated with the powered phases of rocket flights while in the atmosphere. The more severe of these effects have been attributed to the presence of a turbulent plasma in the rocket exhaust trail, and have been characterized as "flame attenuation." Flame attenuation of RF signals has been reported, on certain flights, to be tens of decibels, with complete loss of signal lasting into the tens of seconds.[15] Flame attenuation could, therefore, produce signal degradation, or possibly total disruption of RF signal links which carry command, telemetry, and range-safety command destruct signals.

B. Analysis of Flame Attenuation Effects

In this investigation an attempt was made to form an empirical prediction model based on actual recordings of telemetry signal strength, obtained during the time of the attenuation effects for a Saturn 200 and a 500 series flight. A specific objective was to examine the dependence of RF signal attenuation on four parameters associated with rocket exhaust flame. The parameters considered were: (1) flame angle, (2) vehicle altitude, (3) angle of the transmission path into the exhaust plume, and (4) frequency.

Data analysis included the removal of the free space loss from the recordings of telemetry signal strength for receiving stations of the Central Instrumentation Facility and Cape Telemetry Station IV, the only stations for which data were available which experienced flame attenuation. An unsuccessful attempt was made to remove vehicle antenna effects from the data. A typical plot of relative signal strength as a function of range time after the removal of the space loss is shown in Figure 21. Were it not for the flame effects, the curves shown in Figure 21 would be straight horizontal lines.

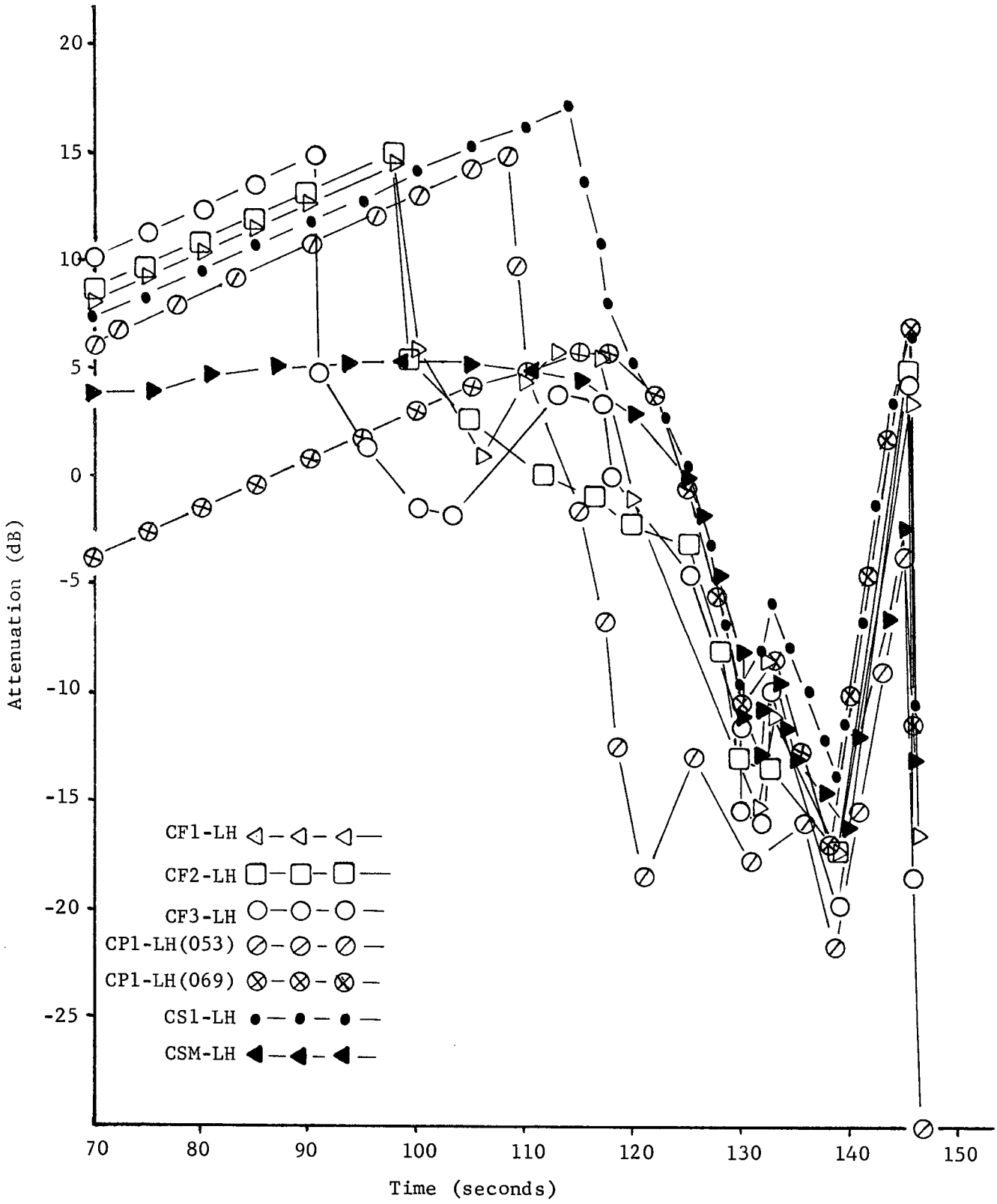

Figure 21. Attenuation Due to Flame Effects of the "A" Signals Received at CIF for Flight AS-502.

Based on these reduced data an empirical model for predicting flame attenuation effects for signals received at the Central Instrumentation Facility and at Cape Telemetry Station IV was constructed. This model has been implemented as a computer program and should be useful in predicting flame attenuation on future Saturn V flights.

The data upon which the model was based indicated that telemetry signals transmitted from Saturn-Apollo vehicles, during the time of first-stage boost, can be affected by passing near or through the engine exhaust plume. The effect appears to be multipathing caused by reflection and refraction at the plume boundary. The multipathing can produce signal enhancement in some cases, and signal reduction in others. The maximum flame attenuation that is likely to occur during first-stage boost is only approximately 20-25 dB, and since the range to the receiving stations located astern of the vehicle is relatively short, there is sufficient signal strength such that 25 dB of attenuation appears to pose no real threat of signal loss.

C. Conclusions

The attenuation is definitely dependent on the position of the transmission path relative to the exhaust plume. Since the look-angles, the plume width, and the vehicle altitude are all changing with time, the exact dependence on each of these factors cannot be easily determined. Also no dependence on frequency was found in the telemetry data examined. It should be pointed out, however, that almost all of the telemetry data examined were confined to a very narrow band of frequencies. Experiments specifically planned for studying the flame attenuation effect would be required to produce sufficient data to establish the functional dependence on each parameter. The expense of such experiments does not seem warranted.

Details of this investigation are discussed in Technical Report No. 4.[16]

20

PRECEDING PAGE BLANK NOT FILMED

IX. DESIGN OF A SLOW SCAN DIGITAL TELEVISION SYSTEM

A. Introduction

A digital television system was designed for transmitting picture information through a telemetry channel. The system consisted of an encoding and a decoding device. The encoding section was designed to take picture information from a standard American monochrome TV camera, encode it in digital form, and deliver it to the telemetry channel at a suitable data rate. It also generated all necessary synchronization signals. The decoding system was designed to convert the information received over the channel into a slow scan picture display.

Actually two systems were designed, one for transmission through a telemetry channel capable of operating at a rate of 144 kilobits per second, the other for a channel with a 72 kilobit per second capacity. The two systems have many simularities and are described in detail in Technical Report No. 8.[17]

B. System Design

The method of adapting the encoder to a standard TV camera was simple; the encoder merely sampled the video data at the horizontal scan rate (144 kilobit system) or at one-half the horizontal scan rate (72 kilobit system). Consecutive points thus sampled lay along a vertical line, and the decoding and display equipment re-constructed the picture with vertical scan lines. The 144 kilobit system required one frame time (1/30 second) to generate a complete vertical line, while the 72 kilobit system required 2 frame times. After a vertical line was completed, the sampling time was changed by an amount corresponding to one horizontal resolution element so that the next vertical line would be sampled. The system provided for more than one mode of operation with different horizontal resolutions, a nominal resolution of 300 horizontal elements will be referred to in the following.

Video intensity was converted to a six bit digital code which allowed sixty-four shades of grey to be transmitted. Three bits of fixed code were added to the video data so that the standard word being transmitted over the telemetry channel contained nine bits. The extra bits were utilized to prevent false synchronization.

The 144 kilobit system is the simpler of the two and will be described briefly. A block diagram of the encoding system is shown in Figure 22. The clock and divider system provides synchronization signals for both the camera and the encoder. The sampling time is determined by the sampling pulse generator which contains two counters. Each of these counts up to the number of horizontal resolution elements (300) and then resets. One counter runs at 4.725 MHz and runs through its entire count cycle during one horizontal line scan. The other counter runs at 30 Hz, advancing one count for every frame time, and coincidence of the two counts causes a sampling pulse to be generated. Essentially the fast counter produces a sampling rate such that one sample is taken at the same relative position on each horizontal line, while the slow counter advances the sampled position horizontally by one resolution element after each vertical line is completed.

When a sampling pulse occurs, a sample of the video is taken and converted to the six bit digital code in the analog-to-digital converter. The remainder of the encoder consists of buffers to store the digital code until it can be fed into the telemetry link, a sync data generator, a word counter, and a commutating system.

The use of a standard TV frame time (during which the system transmits a single vertical line) is shown in Figure 23(a), and the first sync interval is shown expanded in Figure 23(b). The first ten words are used to establish word sync, and words 12-14 provide frame sync. The all-zero contents of words 2-5 are the key sync detection point; no other all-zero words occur. The frame counter is transmitted next (three times to provide redundancy) and is used at the display to horizontally position the following

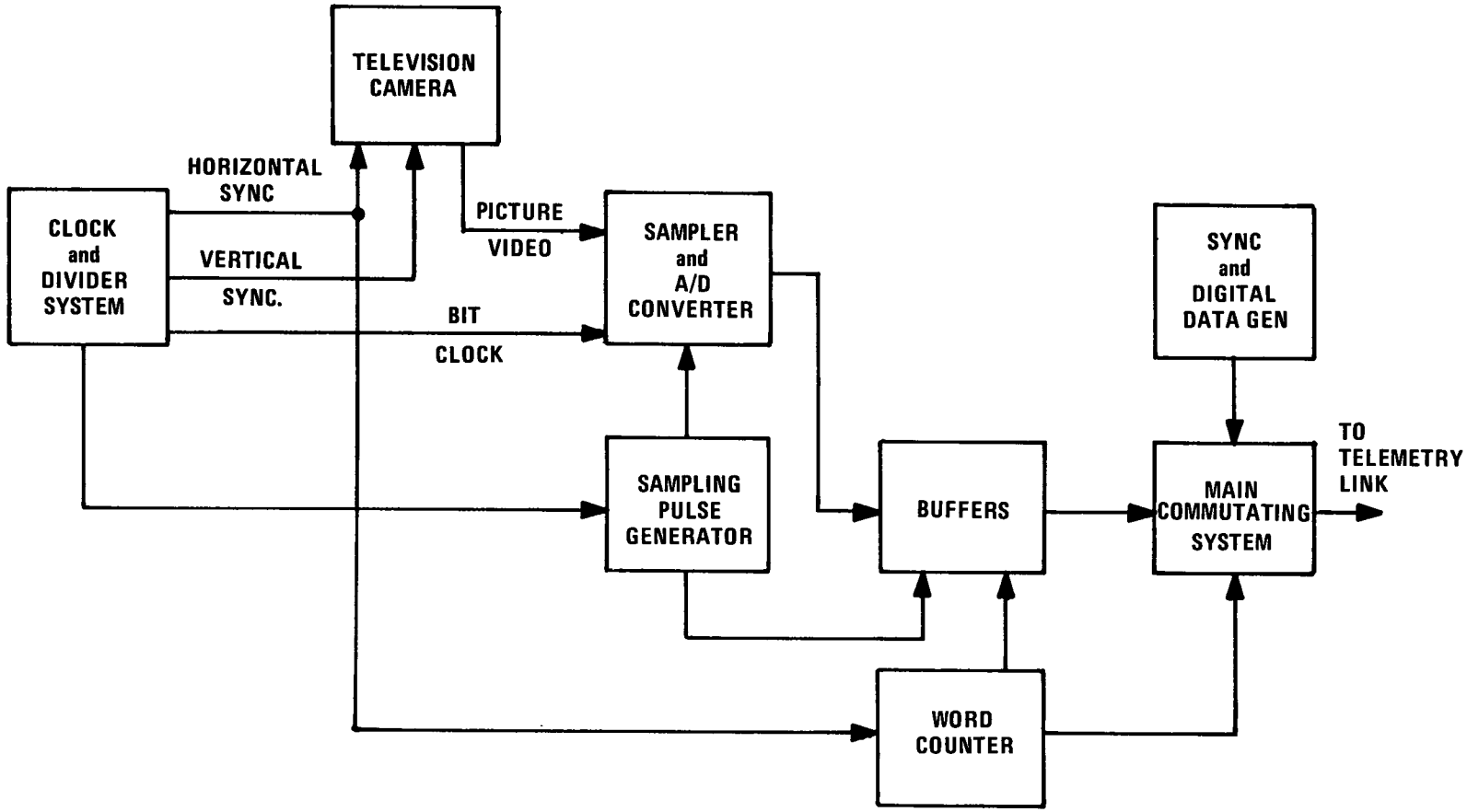

Figure 22. Simplified Block Diagram of Encoder.

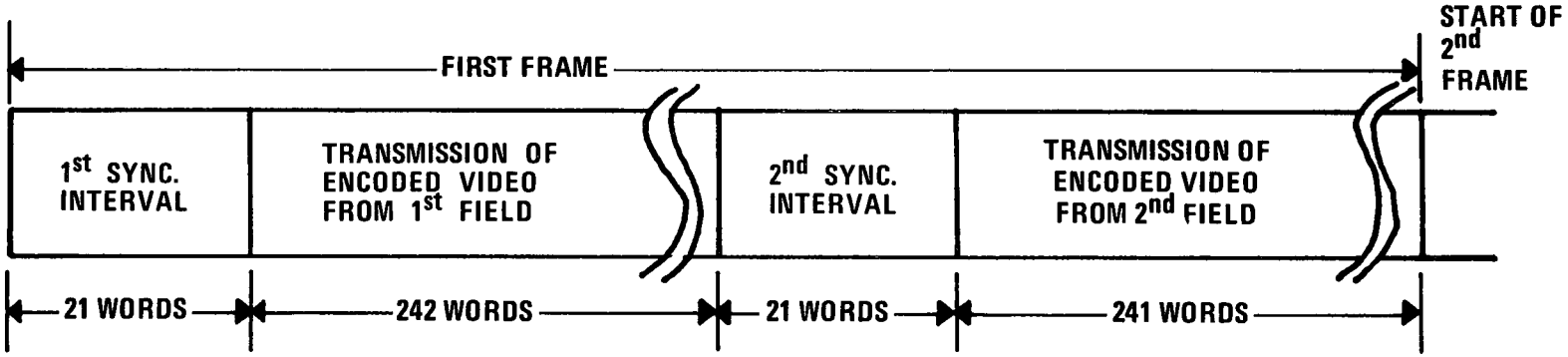

(a) GENERAL DATA FORMAT FOR ONE FRAME OF TELEVISION PICTURE

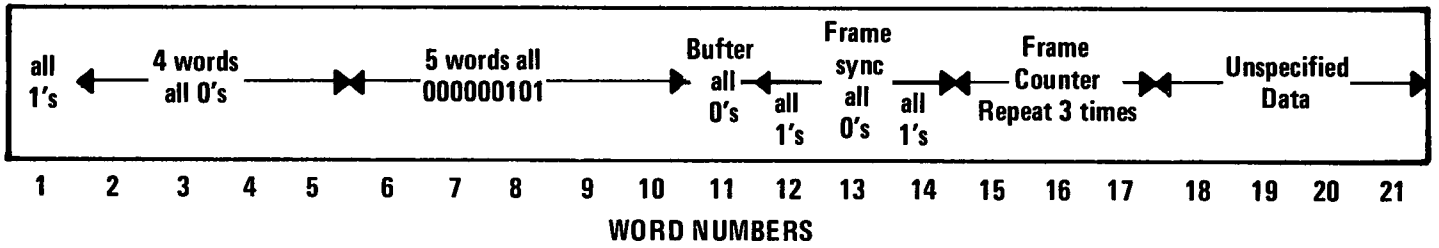

(b) FIRST SYNCHRONIZATION INTERVAL DATA FORMAT

Figure 23. Television Frame Interval and Telemetry Data Format.

video stream. The second sync interval is not used by the system; other data could be inserted into the second sync interval provided no all-zero words are used.

The decoder is shown in the block diagram of Figure 24. The telemetry data flows into a bit sync generator whose output is used to synchronize a local clock with the received bit times. When the string of zeros indicating a synchronization interval enters the sync recognition circuit, the word sync detector is armed, and syncs on words 6-10 [Figure 23(b)]. Picture sync is then obtained from words 12 through 14 [Figure 23(b)], which also resets the word counter in the decoder. This word counter is used in generating the vertical deflection of the display device; it also provides information for the blanking generator, gating information for the horizontal position digital-to-analog converter, and (together with the bit sync generator output) synchronizes the intensity digital-to-analog converter.

The telemetry word number in the word counter is fed to the vertical digital-to-analog converter to generate vertical positioning information. To determine the horizontal position of the line, the transmitted contents of the encoder frame counter is gated into the horizontal digital-to-analog converter at the decoder. Intensity information is decoded by the intensity digital-to-analog converter (Figure 24) after it is synchronized by the outputs of the bit sync generator and the word counter. This converter decoded the six bits of the telemetry words which contain video brightness information.

The system designed to operate with a 72 kilobit per second telemetry channel is somewhat more involved than the system described but uses essentially the same method of encoding and decoding as the picture.

C. Conclusions

A system has been designed which provides the capability of transmitting picture information produced in accordance with

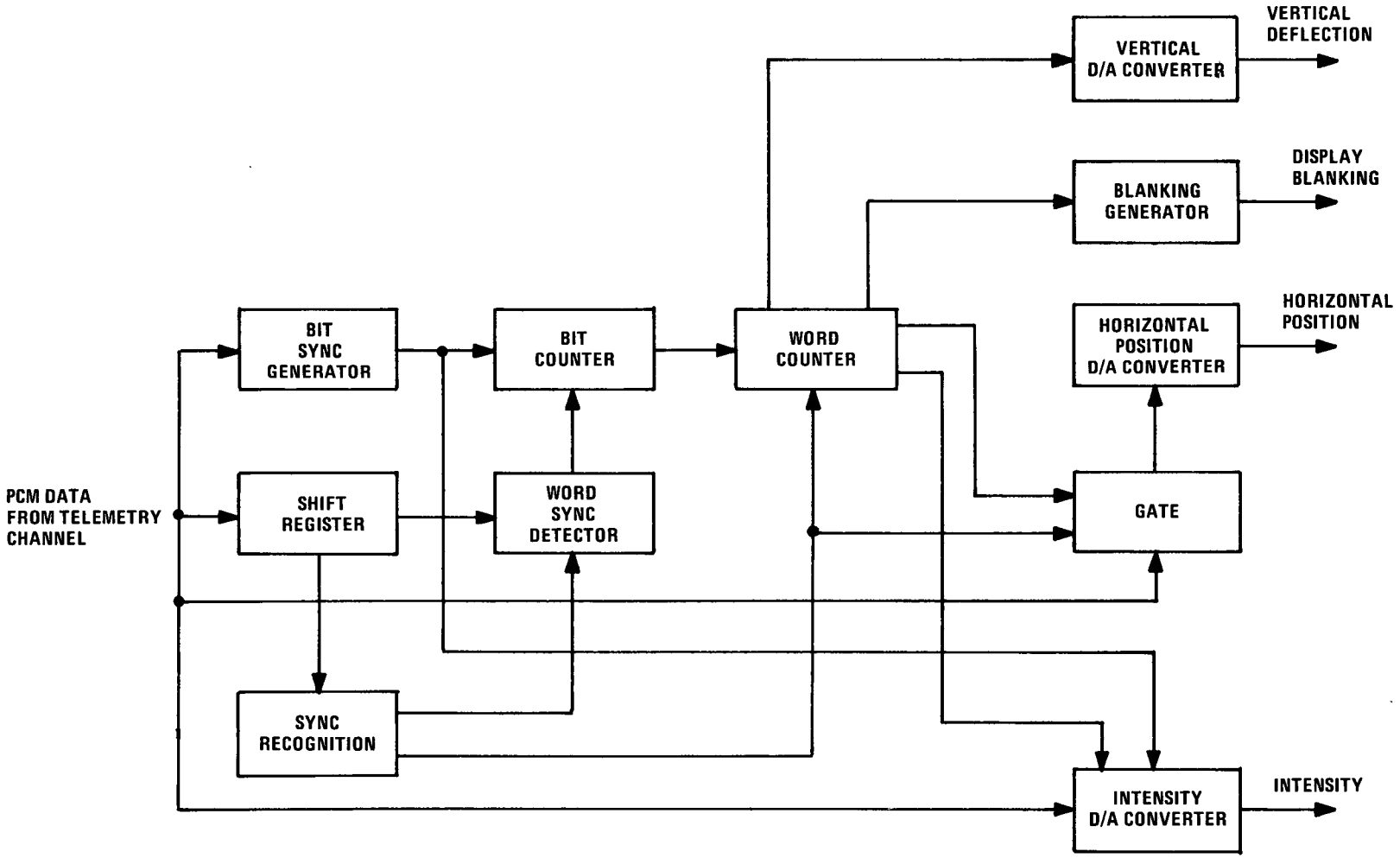

Figure 24. Simplified Block Diagram of Decoder.

American monochrome television standards over a digital transmission channel. Two system designs were actually completed; one transmits data at the rate of 72 kilobits per second over the telemetry channel, while the other transmits data at twice this bit rate. Methods of interfacing the television system with the telemetry channel were developed. The system was designed for the transmission of picture information whose content changes slowly with respect to the time required for the transmission of a picture. The system design provides redundancy in synchronization which should reduce the chance of losing appreciable parts of a picture due to telemetry channel errors. Errors in isolated picture elements were considered to be less important and their effect could be reduced by picture processing techniques after reception. The received picture is reproduced as a series of vertical slow scan lines which may be photographed or displayed on a storage tube for viewing. The capability of changing the horizontal extent of a picture or its horizontal resolution is included in the system design.

Picture transmission systems such as the one designed in this task would be particularly useful in spacecraft applications where transmitter power is limited and the advantages of digital transmission are attractive.

PRECEDING PAGE BLANK NOT FILMED

X. AN INVESTIGATION OF SOME PROBLEMS INVOLVED IN ADDING AN ADDITIONAL SUBCARRIER TO THE CCS DOWN-LINK

A. Introduction

This section describes the results of a study that was conducted to determine the capability for and the effect of adding another telemetry channel to the down-link portion of the Command and Communication System (CCS). A major limitation of the ability to add additional channels to multiple subcarrier, phase-modulated systems is the generation of intermodulation and cross modulation products within the nonlinear elements of the system. Consequently, emphasis was directed to the investigation of the nonlinear performance of the phase modulator and phase demodulator which are the principle elements of the down-link portion of the CCS considered in this investigation. The demodulator is a diode phase detector which can be generally characterized by a sinusoidal input-phase versus output-voltage relationship. The modulator is a varactor phase modulator which is normally characterized by a linear input voltage versus output phase relationship. The investigation included theoretical analyses of the modulator and demodulator, experimental tests on the CCS down-link with several subcarriers present, and computer simulations of the modulator and demodulator.

B. Approaches to Adding An Additional Telemetry Subcarrier

Two approaches to adding another telemetry channel to the CCS down-link were considered. The first was to add a distinct subcarrier whose frequency is chosen such that it would have a minimum effect on other telemetry channels. The second method was to insert a "quadrature" subcarrier which is identical in frequency to the existing telemetry subcarrier (i.e., either plus or minus 90° relative to the present subcarrier). The new subcarrier and the original subcarrier are modulated by independent data streams.

The method of modulation in either case is restricted to biphase modulation of the subcarriers. Both methods of obtaining an additional telemetry link were investigated.

A nonlinear, sinusoidal, phase demodulator was studied to determine what intermodulation components were generated when its input signal consisted of a carrier phase modulated by one, three, and four subcarriers. The demodulator performance was simulated with a digital computer program. The nonlinearity was modeled as a sinusoid and the output spectra for several input signals were computed using a computer program adapted from the spectral calculations to these computations. Experiments were conducted to verify theoretical results. Measured data showed that components other than those predicted were present. Further investigation showed that these components were due to the nonlinear phase modulator. The measured phase versus modulating voltage characteristic of the transponder phase modulator is shown in Figure 25. This nonlinearity was modeled and its effect included in the computer simulation. Data from subsequent simulations showed good correlation with experimental results.

C. Conclusions

Analysis showed that no new intermodulation components are generated by a nonlinear detector if a subcarrier is added in phase quadrature with the present telemetry subcarrier. Although no new components are generated by a detector operating on quadrature subcarriers it was found that the nonlinearity caused a reduction in output signal power.

Details of this investigation and a listing of the computer program used are contained in Technical Report No. 6.[18]

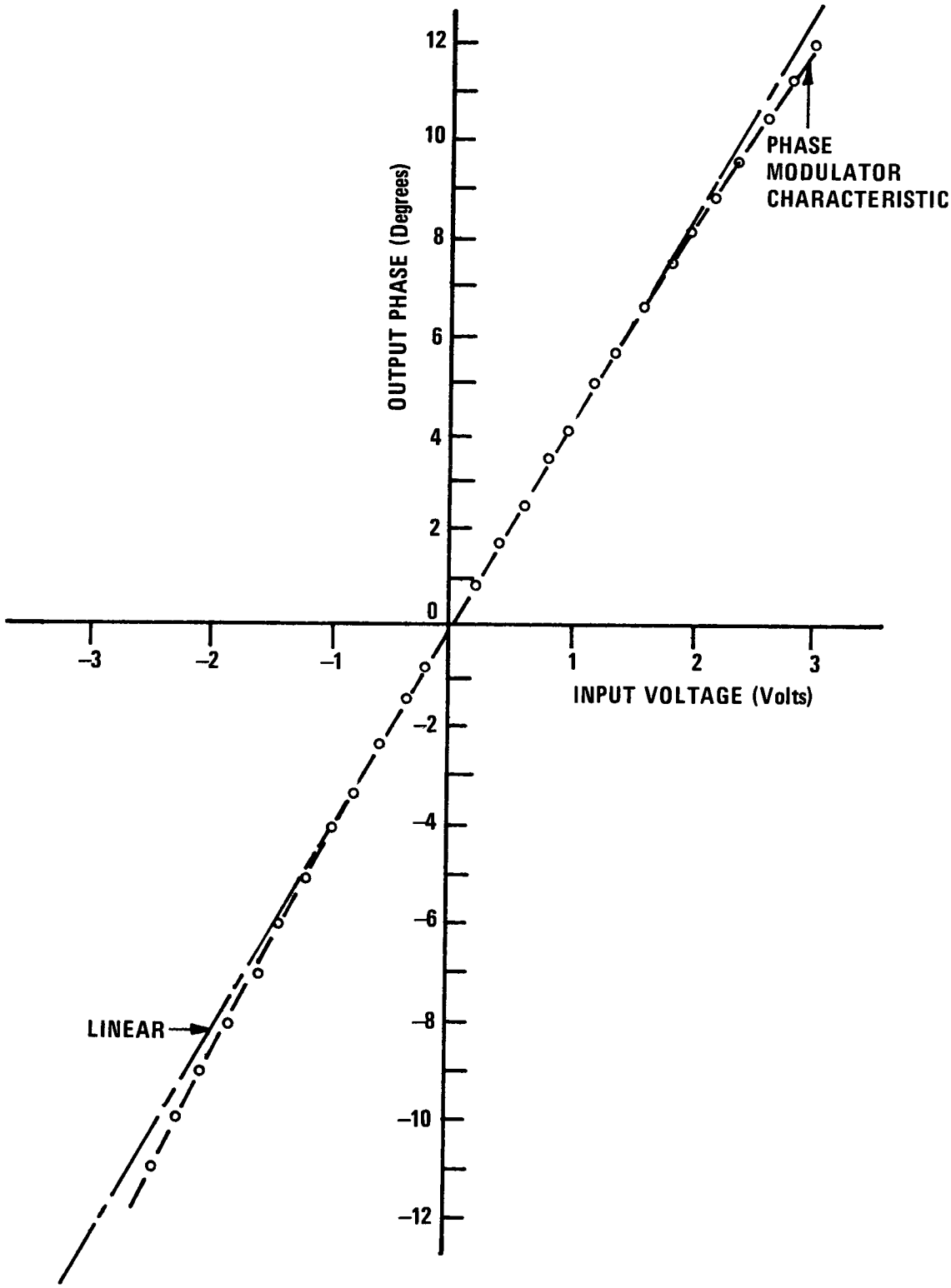

Figure 25. CCS Down-Link Phase Modulator Characteristics.

PRECEDING PAGE BLANK NOT FILMED

XI. DOWN-LINK SPECTRA

A. Introduction

During preflight testing of the Command and Communication System (CCS) it was observed that unwanted sidebands of significant amplitude were generated when the telemetry subcarrier was modulated. These sidebands lay close to the S-band carrier frequency and posed the threat that the ground receivers might phase lock on the sidebands when control was transferred from one station to another. An investigation into the origin and nature of these sidebands has been carried out in which a square-wave modulating signal was applied to the telemetry subcarrier to simulate PCM data.

The investigation was both theoretical and experimental. Equations for the S-band spectrum were derived and computer programs were used to compute the S-band spectrum for various modulating signals. While the computed spectra were regarded as the major output of the study, these results were confirmed by measurements made in the laboratory. Good agreement was found between computed and measured values in each case.

B. System Description

The CCS is a unified carrier system which combines the functions of command, communications, and ranging on a single radio frequency carrier. In a prior study the spectrum of the up-link portion of the system was investigated. The mathematical derivation of the spectrum is detailed in the report on that study.[7]

Since the up-link and down-link systems have many simularities, many of the techniques used for the up-link calculations could be applied to calculating the down-link spectrum. For both links the data begins as a PCM digital stream which is biphase modulated onto a sine wave subcarrier. The two differ in that the data rate and sine wave frequency are different; also the biphase modulation is synchronous in the up-link portion and non-synchronous in the down-link portion.

C. Computer Analysis of Spectra

The original computer program developed for the up-link calculations utilized convolutions to generate the spectra. The program, originally written in ALGOL for a Burroughs B-5500 computer, was rewritten in FORTRAN for a UNIVAC-1108 computer along with modifications to handle the down-link calculations. The conversion made available the larger core memory and higher speed of the 1108.

This program was used for many of the calculations, but its inherent limitations restricted the width of the baseband signal that could be processed. The trouble lay primarily in the necessity of having three large arrays in core storage simultaneously in order to efficiently compute a convolution. A study was then made of the fast Fourier transform (FFT) and a routine was developed for rapidly calculating both the transform and its inverse as an "in-place" operation. This program provided faster computation of the spectra and also allowed wider bandwidth signals to be processed.

The convolution program was tested by several runs using idealized baseband spectra for which the spectrum was theoretically known. The two cases consisted of applying to the phase modulator input (1) two-tone phase modulation, and (2) the telemetry subcarrier which had been modulated with a wideband (ideally unlimited) square-wave. These runs showed that the program performed satisfactorily for modulation indices encountered in the CCS. (1.22 for the telemetry subcarrier.) The S-band spectrum for the wideband modulated subcarrier is shown in Figure 26. This spectrum was calculated with the widest baseband spectrum that the convolution program could handle, ± 11 MHz. The spectrum agrees with the theoretical spectrum for an unlimited baseband signal except for the frequency components at a level of approximately -67 dB. It was suspected that these components were produced by the truncation, and this suspicion was confirmed after the FFT program was developed. Figure 27 shows the same spectrum computed (with the FFT program)

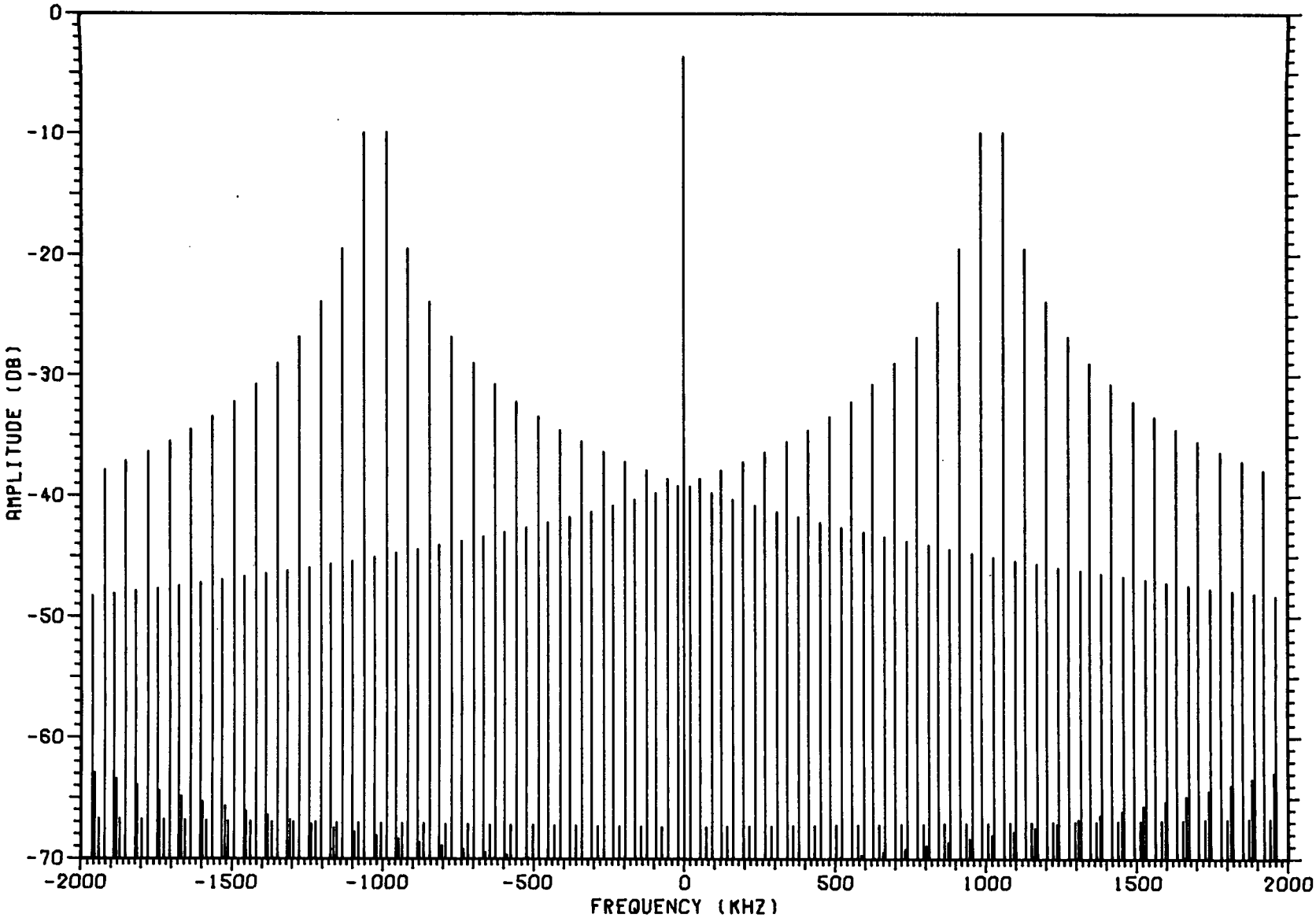

Figure 26. Computed S-Band Spectrum Produced by a Baseband Signal Truncated at ± 11 MHz.

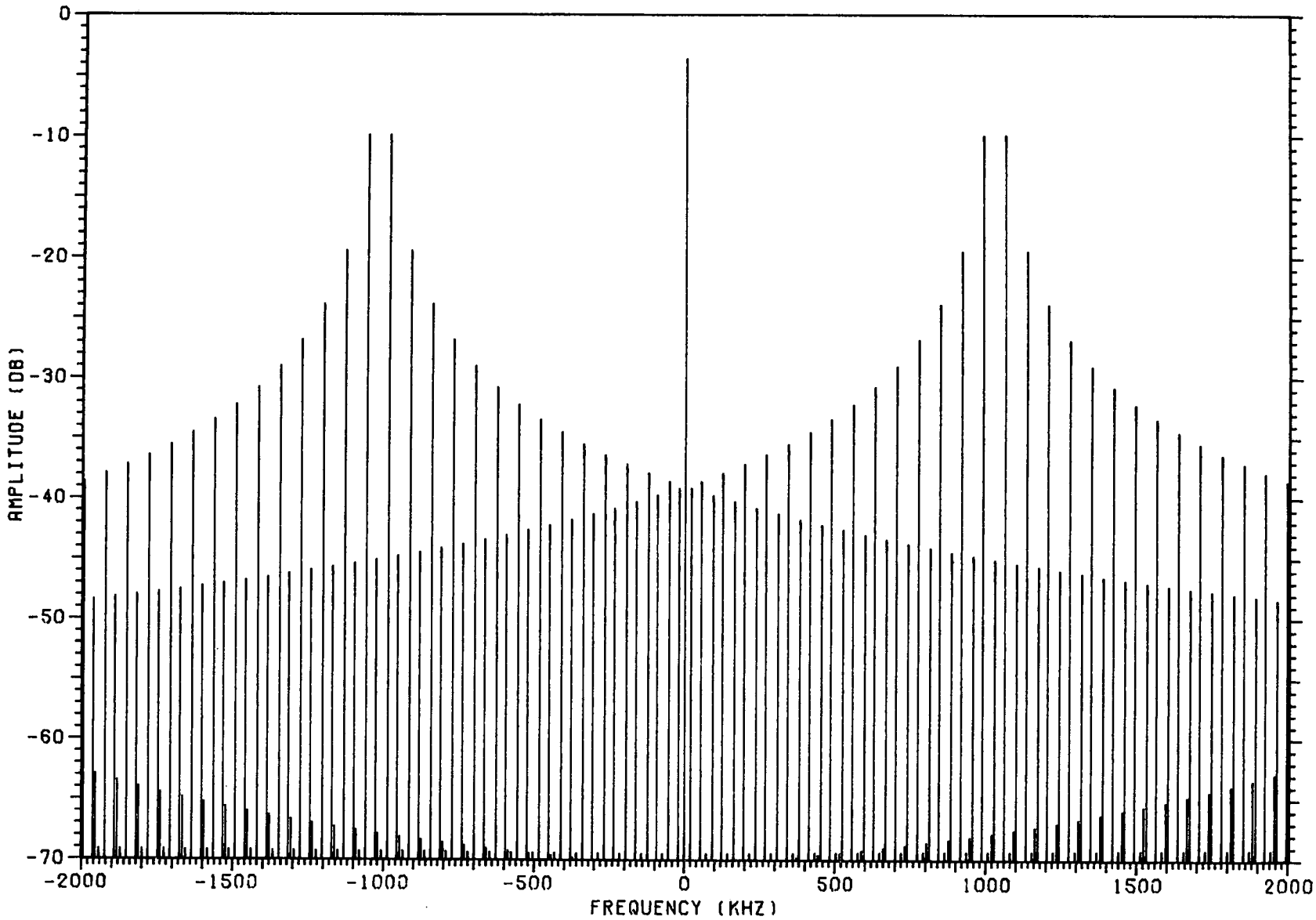

Figure 27. Computed S-Band Spectrum Produced by a Baseband Signal Truncated at ± 16 MHz.

for a baseband width of ± 16 MHz. Note that the spurious components were reduced approximately 3 dB by using the wider bandwidth.

These computer programs were used to study the effects on the S-band spectrum of various filter functions applied to the telemetry subcarrier baseband signal. Any realizable system will have some finite bandwidth which will limit the spectrum that can be passed. To investigate this area, computer simulations of filter functions were developed for RC low-pass and high-pass filters, the CCS transponder bandpass filter, and a rejection filter for the third harmonic of the telemetry subcarrier frequency. These routines were developed for use with the convolution program and each could be called any number of times and in any desired sequence. Thus it was possible to simulate multi-stage filter effects.

An example of the calculations is the spectrum obtained for a filter function applied to the baseband signal that approximated the frequency response of the down-link S-band modulator. The actual response of the modulator as measured in the laboratory is shown in Figure 28. Also shown is the filter characteristic used in the calculations which consisted of a two-section low-pass filter with each section having a cut-off frequency of 1.0 MHz (simulated in the computer program by two sequential calls on the low-pass filter subroutine). The computed S-band spectrum is shown in Figure 29. To see the effects of the filter, compare Figure 29 with Figure 27 which shows the computed S-band spectrum for a wide (16 MHz) baseband signal. Note that in Figure 29 the sidebands above the subcarrier (1024 MHz) fall off more rapidly than do those in Figure 27. Also note Figure 29 shows many more spectral components scattered below the major lines, and that the components near the S-band carrier are increased about 5 dB. A photograph of the actual spectrum produced by the CCS transponder is shown in Figure 30 for comparison.

Another example of a filtered baseband spectrum of interest is that obtained by applying the transponder's telemetry bandpass filter to the square-wave modulated telemetry subcarrier. To study the

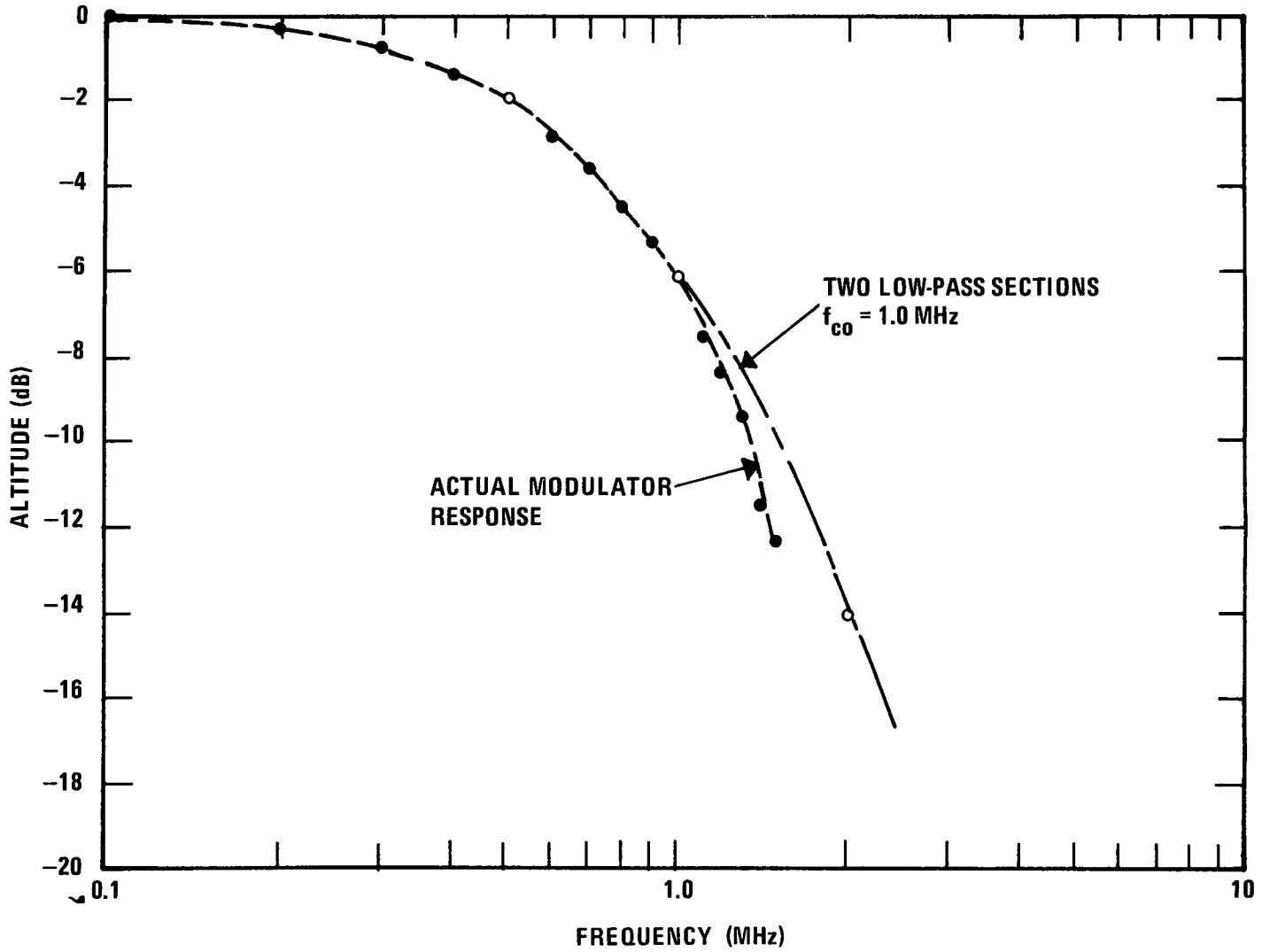

Figure 28. Frequency Response of the CCS Transponder Phase Modulator and a Two-Section R-C Low-Pass Filter with a Cutoff Frequency of 1 MHz.

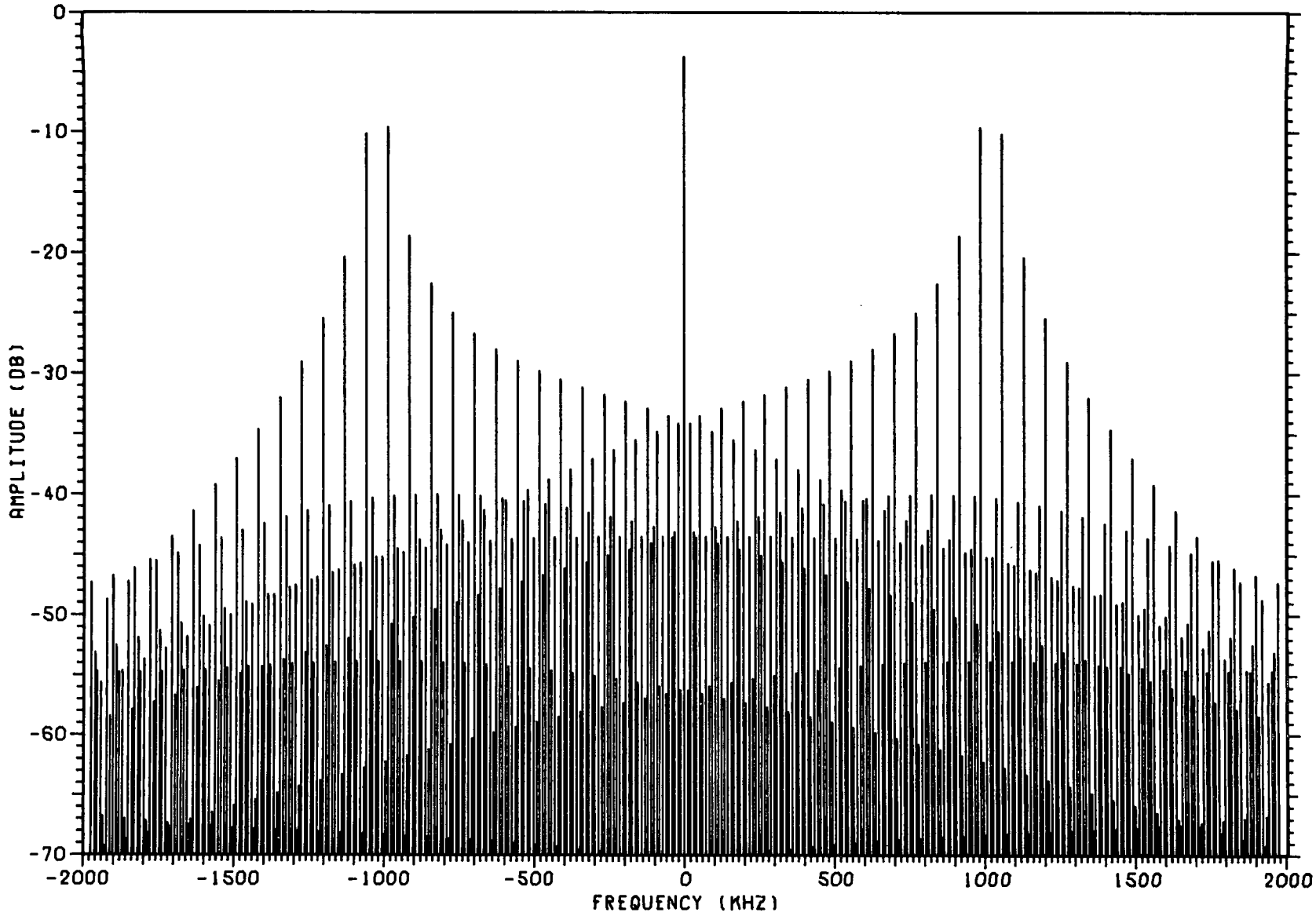

Figure 29. Computed S-Band Spectrum Obtained When a Two-Section Low-Pass Filter with a Cutoff Frequency of 1 MHz was Applied to the Wideband Baseband Signal.

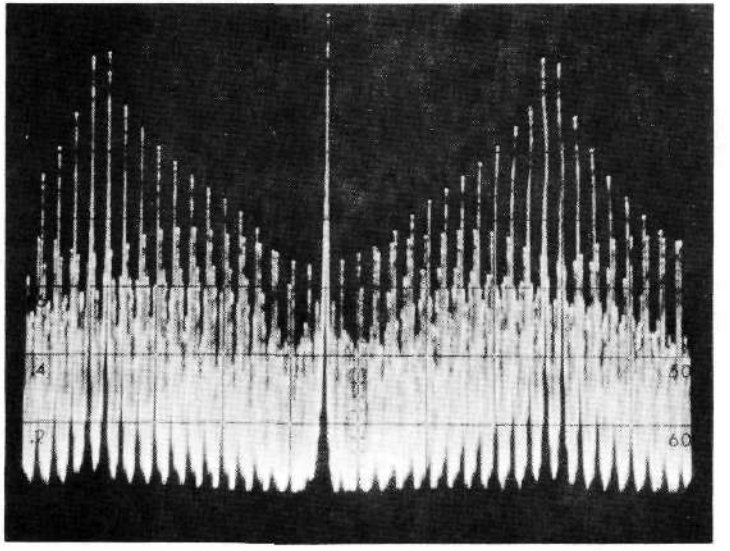

HORIZONTAL: **300kHz/cm**

VERTICAL: **10 dB/cm**

Figure 30. Measured S-Band Spectrum for Wideband Modulation of the Down-Link for Which the Computed Spectrum is Shown in Figure 29.

effect of the telemetry bandpass filter on the actual system, the down-link phase modulator characteristic was again approximated by two low-pass sections and then the CCS bandpass filter characteristic was applied. The computed S-band spectrum is shown in Figure 31.

These conditions were duplicated on the laboratory transponder and the observed spectrum is shown in Figure 32. Figures 31 and 32 show good agreement between the claculated and experimental spectra. The slight tilting of the spectral components at 988 and 1060 kHz from the S-band carrier in the computed spectrum is probably due to differences in the theoretical and actual frequency responses of the CCS bandpass filter.

D. Conclusions

Methods have been developed for the calculation of the S-band spectra produced by phase modulation of the CCS down-link carrier by various baseband signals. Two limiting cases of baseband signals were used as theoretical checks of computer programs developed. These were: (1) two-tone phase modulation of the S-band carrier representing ideal narrow band filtering of the square wave modulated telemetry subcarrier signal, and (2) a wideband telemetry subcarrier signal representing an unfiltered square wave modulated telemetry subcarrier spectrum applied to the phase modulator input. Also calculated were the S-band spectra resulting from the application of various filter functions to the wideband telemetry baseband signal. These included R-C low-pass and high-pass filters, the CCS transponder bandpass telemetry filter, and a telemetry subcarrier third harmonic notch filter. Good agreement was obtained from comparison of calculated spectral amplitudes with theoretically expected values and in some realizable cases with values obtained experimentally in the laboratory. The computer programs developed can be used to evaluate the effects of baseband filtering on radio frequency spectra in phase modulated systems such as the CCS.

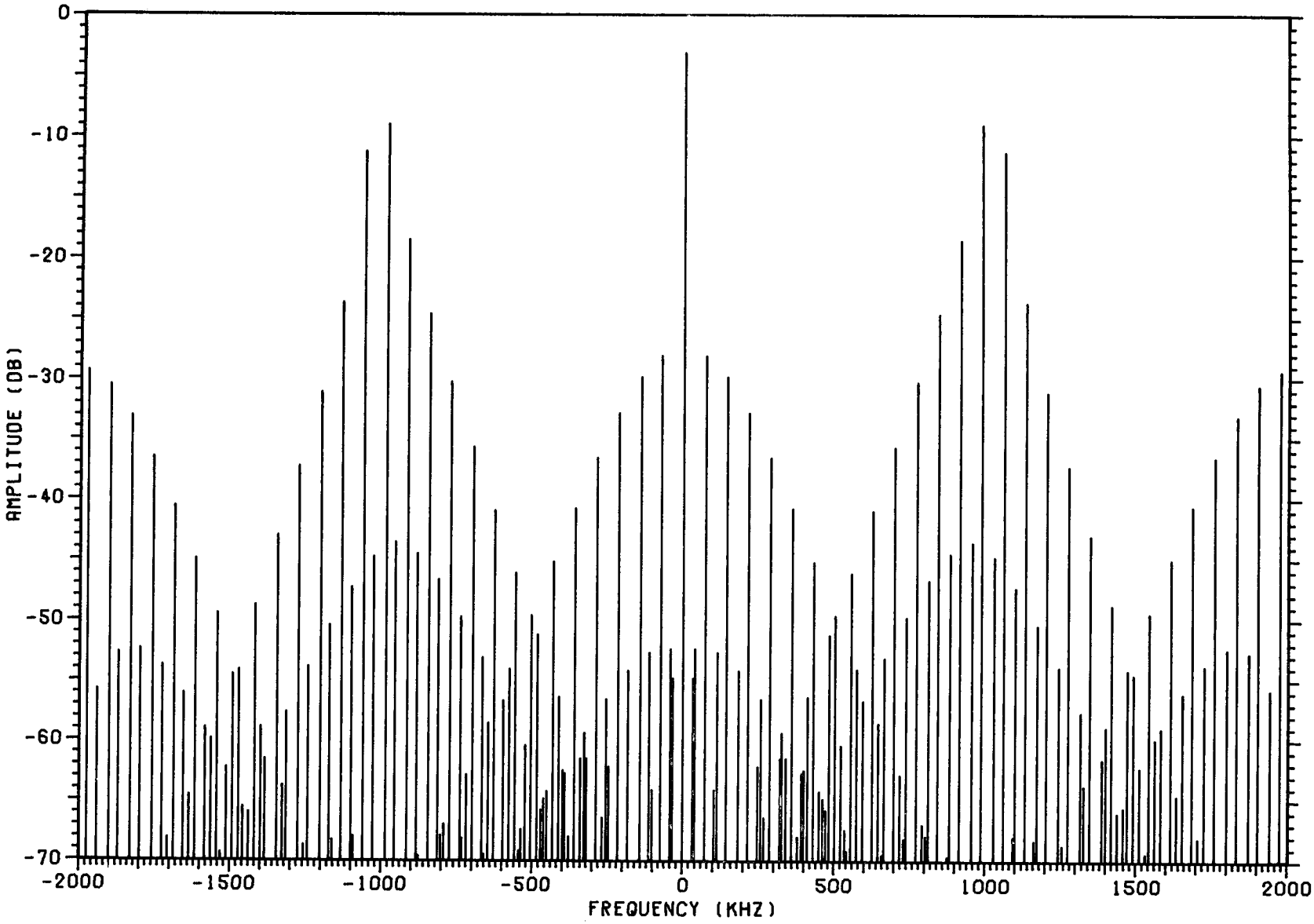

Figure 31. Computed S-Band Spectrum Obtained When the Frequency Response of the Phase Modulator was Considered and With the CCS Telemetry Bandpass Filter.

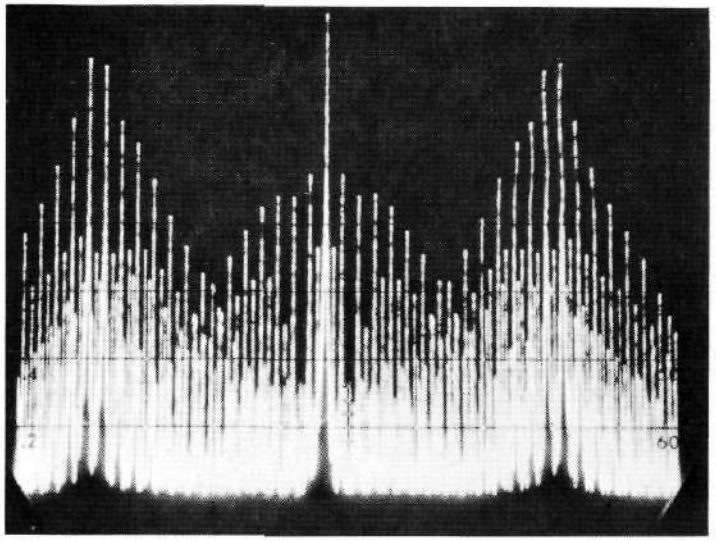

HORIZONTAL: **300 kHz/cm**

VERTICAL: **10 dB/cm**

Figure 32. Measured S-Band Spectrum Produced When the CCS Telemetry Bandpass Filter was Applied to the Wideband Subcarrier Spectrum.

For the details of the mathematical basis of the calculations, details of the filter functions, other spectral calculations, and listings of the computer programs, reference should be made to Technical Report No. 7.[19]

XII. COMMUNICATION SYSTEM MODELING INVESTIGATIONS

A. Introduction

Three aspects of communication system modeling were considered during this task phase of the contract. These were (1) modeling in the frequency domain, (2) modeling on a block basis, and (3) modeling linear circuits on a circuit detail basis using state variable techniques.

Modeling in the frequency domain was directed at an investigation of the spectral characteristics of signals present at various points in unified carrier systems such as the Command and Communications system. The investigation was directed toward future uses of such systems where modulating frequencies, signal bandwidths, and modulation indices of such systems would be varied.

Modeling on a block basis was, during this investigation, concerned with a portion of a communication system which could be analyzed using control theory. The circuitry modeled in the investigation was a sampled automatic frequency control system of an FM transmitter.

The state variable analysis of linear circuits was applied to a passive filter which represented a fairly complex circuit to model. This circuit was selected since the transfer function had already been derived in the frequency domain studies and the transient response could be readily determined for comparison purposes using FFT techniques.

Both calculated results and experimental verification are presented for the frequency domain modeling. For the automatic frequency control system analytical results were used to check a simulation approach which was then further applied to systems containing nonlinear blocks. The state variable technique for linear circuits were verified with the circuit analysis program discussed in Section XIII.

B. Frequency Domain Modeling

Techniques developed earlier in the spectral analysis studies, discussed in Sections V and XI, were further improved during this investigation. Specifically these techniques were applied in investigating the CCS down-link performance for different modulating signals and different modulation indices. Also the capability of evaluating the transfer functions of an actual system filter was developed, which permitted assessing the effect of actual filters (as well as ideal) low-pass and high-pass filters on frequency spectra. This filter transfer function evaluation capability was made compatible with the in place calculation capability of the FFT.

As an example, this technique was used to evaluate the transfer function of the bandpass telemetry filter used in the Generalized Concept Receiver (GCR) telemetry demodulator. The evaluation of this filter requires consideration of such factors as self capacitance of inductors, Q's of circuit inductances, and equivalent representations of transformers. The calculated amplitude and phase response of the filter is shown in Figure 33 and the measured amplitude response in Figure 34. The measured response was obtained using a recurrently sweeping spectrum analyzer and a constant amplitude signal generator. The generator output was slowly varied in frequency over the range of interest. The response of the filter is therefore the envelope of the repetitive spectrum analyzer responses.

In addition, the baseband and radio frequency spectra calculation capabilities of the FFT program continued to be enhanced. Plot routines for time functions have been added. Such a time waveform plot for the sum of a square wave bit pattern with an amplitude of $\pm$ 0.7 volt and a biphase modulated 1024 kHz telemetry subcarrier is shown in Figure 35. The baseband spectrum of this waveform is shown in Figure 36. The S-band spectrum for a square wave modulation index of 0.7 radians and a subcarrier modulation index of 1.0 radian is shown in Figure 37. Experimentally measured

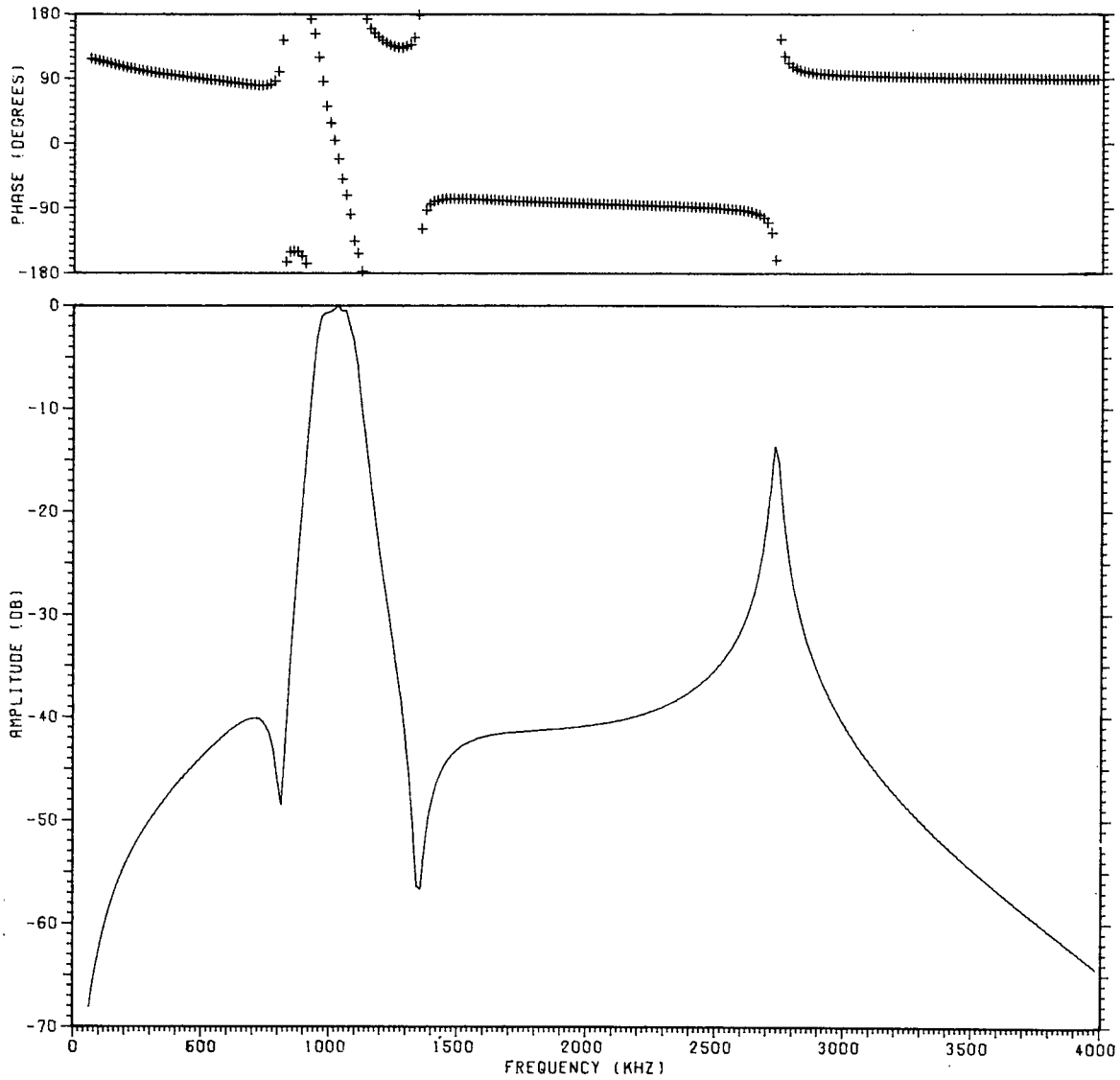

Figure 33. Frequency Response of CCS Telemetry Bandpass Filter.

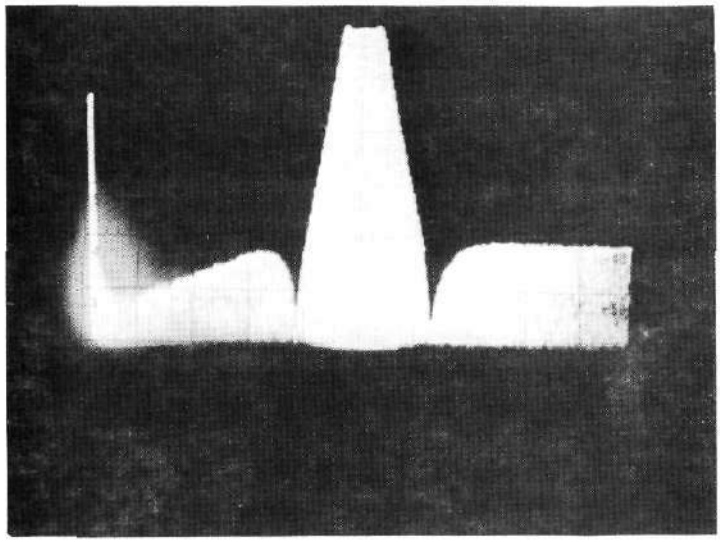

(a) HORIZONTAL CALIBRATION 200 kHz PER DIVISION.
VERTICAL CALIBRATION 10 dB PER DIVISION.

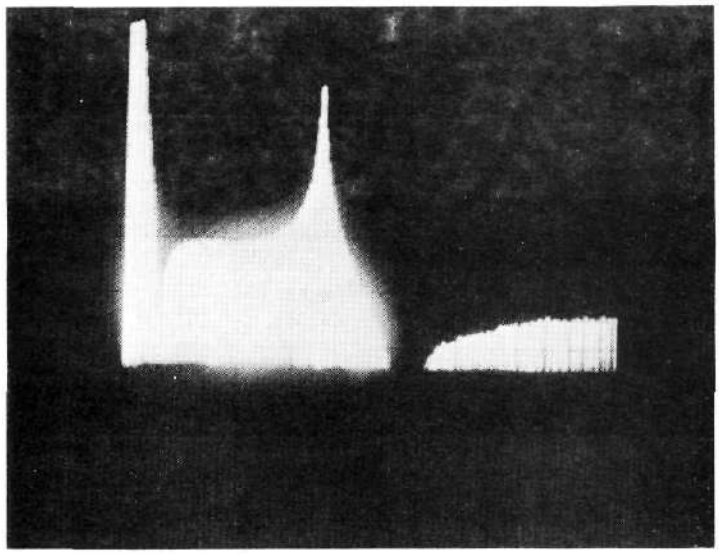

(b) HORIZONTAL CALIBRATION 0.5 MHz PER DIVISION
STARTING AT 1 MHz.
VERTICAL CALIBRATION 10 dB PER DIVISION.

Figure 34. Experimentally Determined Amplitude Response of the CCS Bandpass Telemetry Filter.

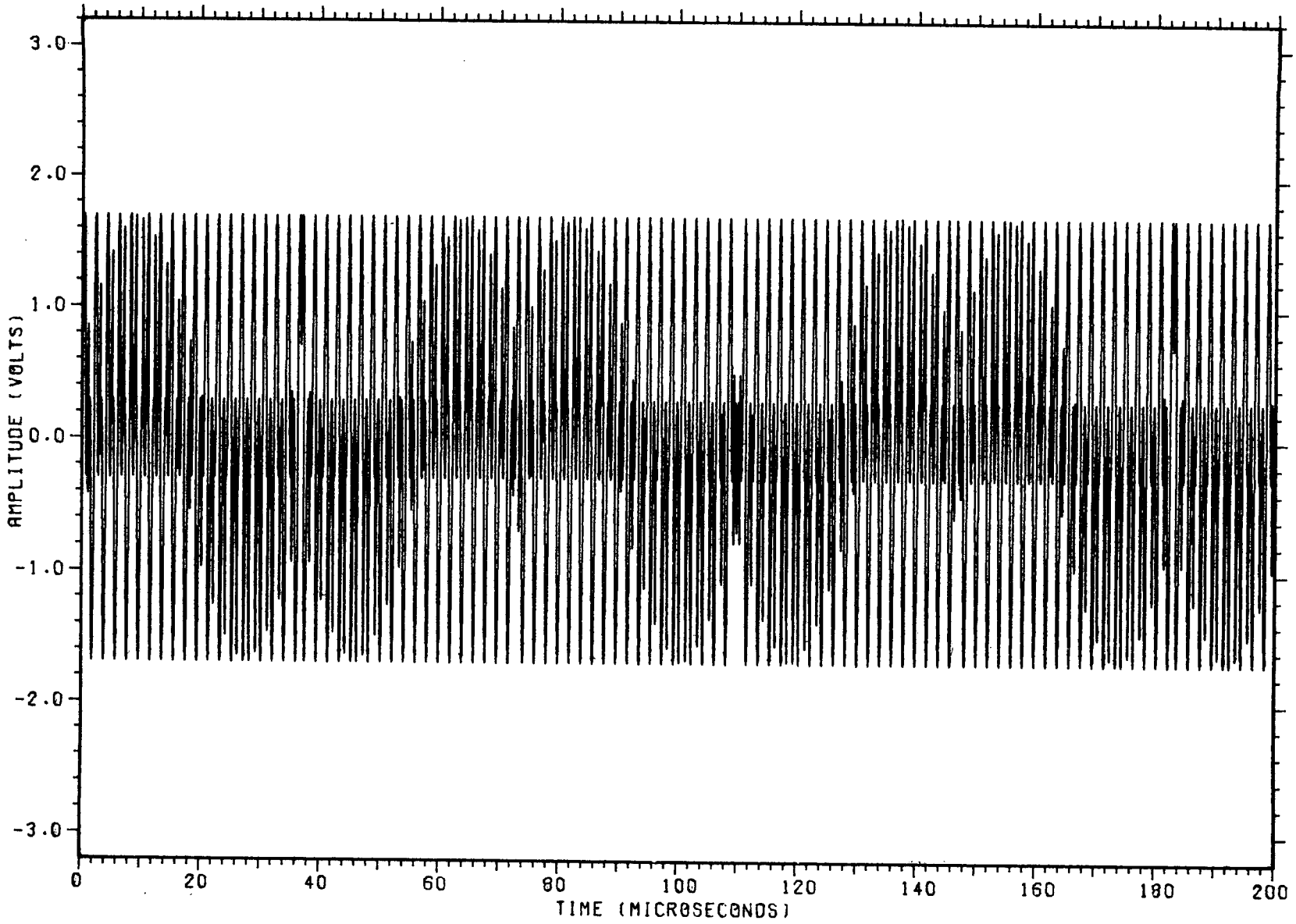

Figure 35. Time Waveform for Biphase Modulated Subcarrier Signal and PCM Signal with an Alternating Pattern of Ones and Zeros. Amplitude Relationships for $\beta_{sc} = 1.0$, $\beta_{pcm} = 0.7$.

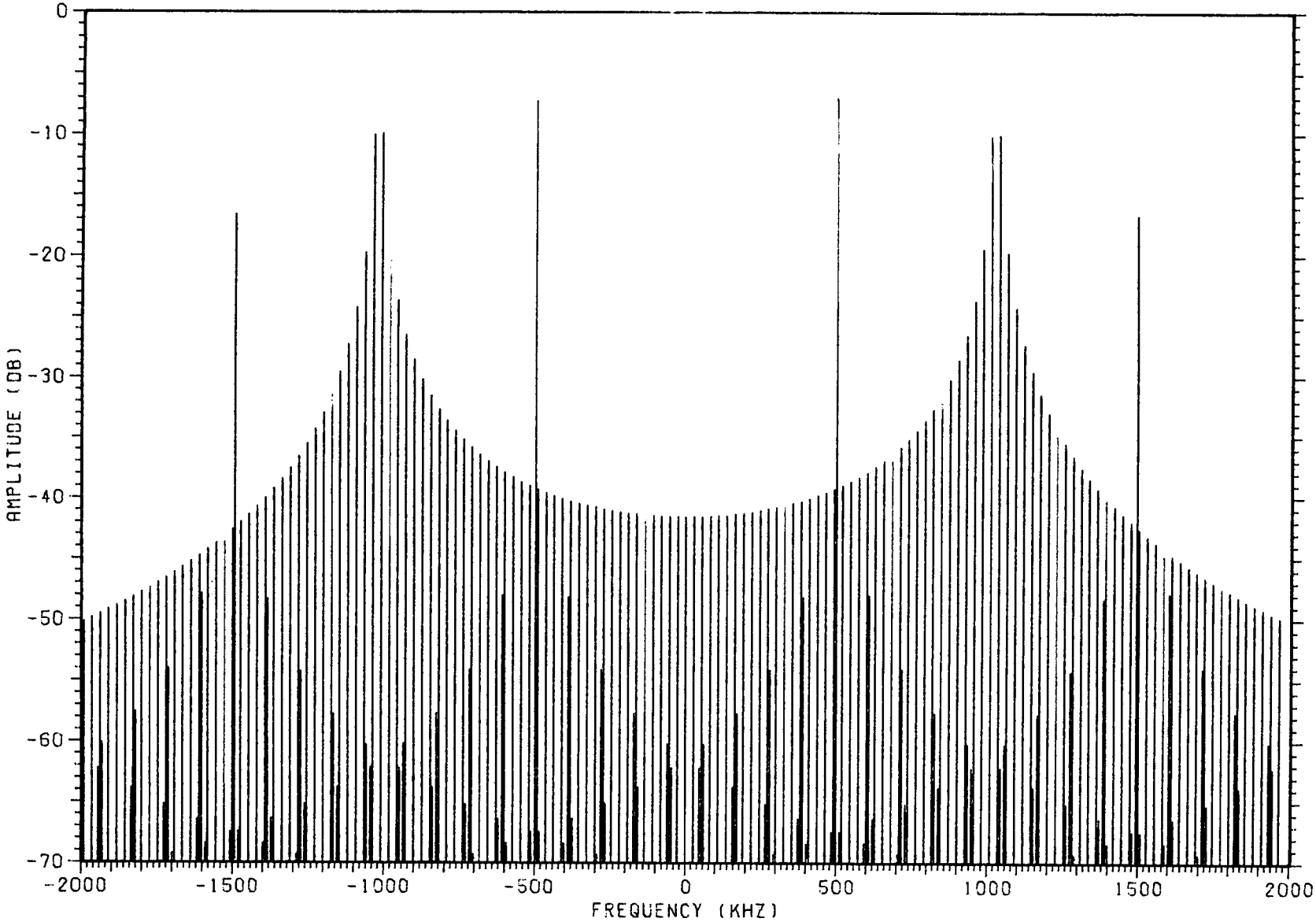

Figure 36. Baseband Frequency Spectrum of Time Waveform Shown in Figure 35.

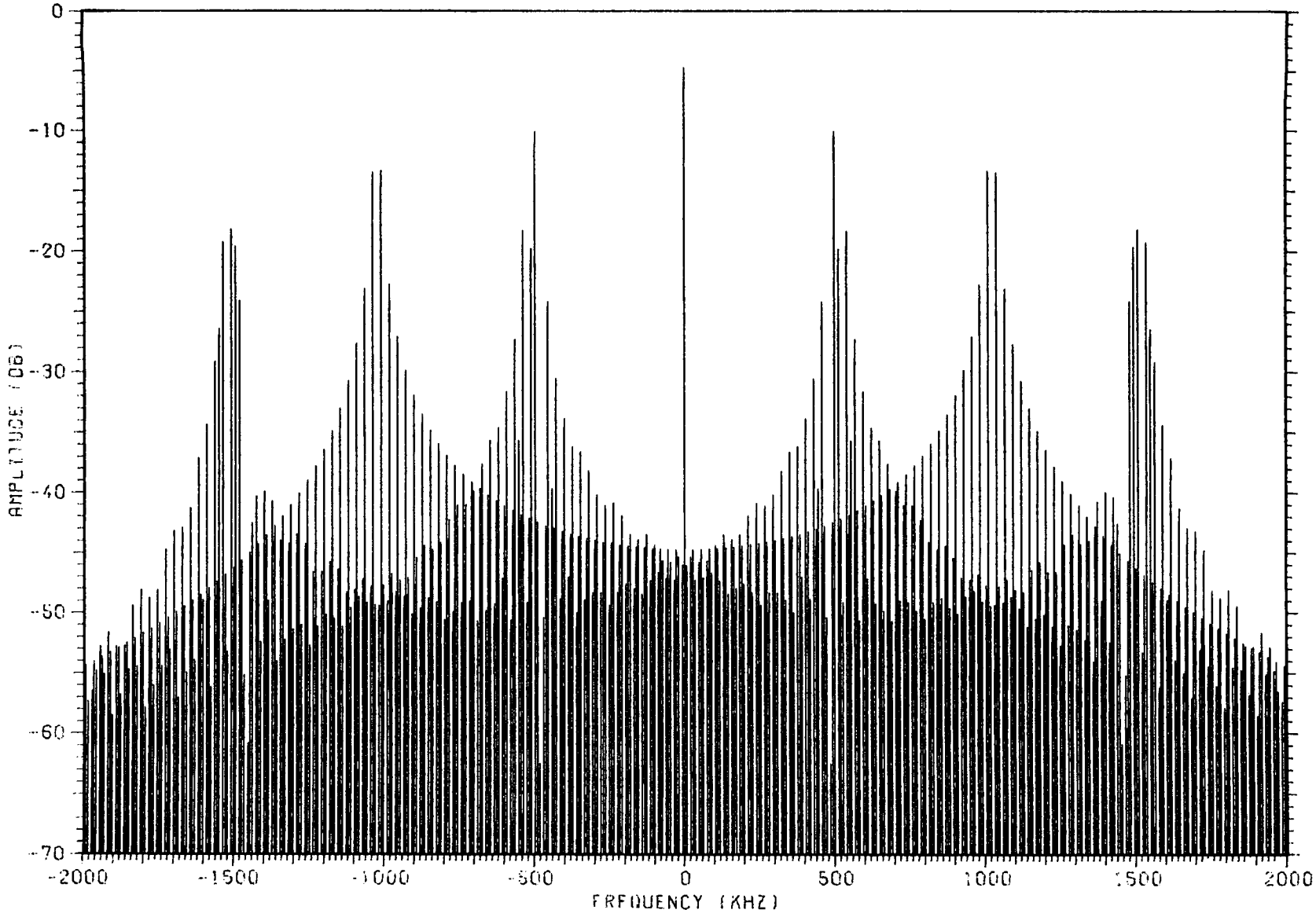

Figure 37. S-Band Spectrum of a Biphase Modulated Telemetry Subcarrier, $\beta = 1.0$, and a Manchester PCM Signal Consisting of all Ones or Zeros, $\beta = 0.7$. No Low-Pass Simulation of Phase Modulator Characteristics.

baseband and S-band spectra corresponding to these computed spectra are shown in Figure 38.

C. Block Diagram Simulation

A capability is being developed for communication systems simulation which can be used by the communication systems engineer for the analysis and design of transmitters, receivers, and other communication subsystems. Among the simulation's key features must be simplicity of specifying the input data and interpreting the output data. The development of such digital simulations had been subdivided into two areas: a block diagram simulation and a detailed circuit simulation. For the beginning of the development of the communication system simulation techniques block modeling of transmitters was selected.

The block diagram approach, where an entire unit (transmitter) or a major subsystem is simulated simultaneously, is most appropriate for modeling feedback systems. As an example of the development of the block diagram method, a transmitter with a sampled-data, Automatic Frequency Control (AFC) system was selected (see Figure 39). Choosing frequency as the variable of interest, transfer characteristics were developed for stages such as voltage controlled oscillators (VCO), frequency multipliers, FM discriminators, pulse amplifiers, and sample-and-hold circuits. Nonlinear models were also developed to represent the action of the VCO and the effect of limiting (or saturation) in the feedback path (frequency error). A digital simulation of the resulting AFC system was then developed using the state variable formulation for the dynamic systems.

An analytical solution of the AFC system for linearized stage models was developed and used to verify the linear simulation. Significant insight into the AFC system operation, including the effect of feedback gain and sampler charging time upon system stability resulted from the linearized analysis and simulation. The simulation was then updated to include nonlinear models for the

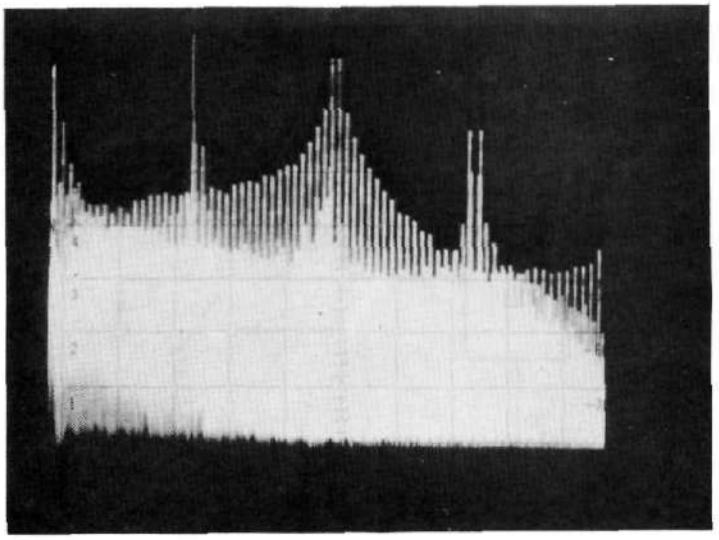

(a) BASEBAND SPECTRA

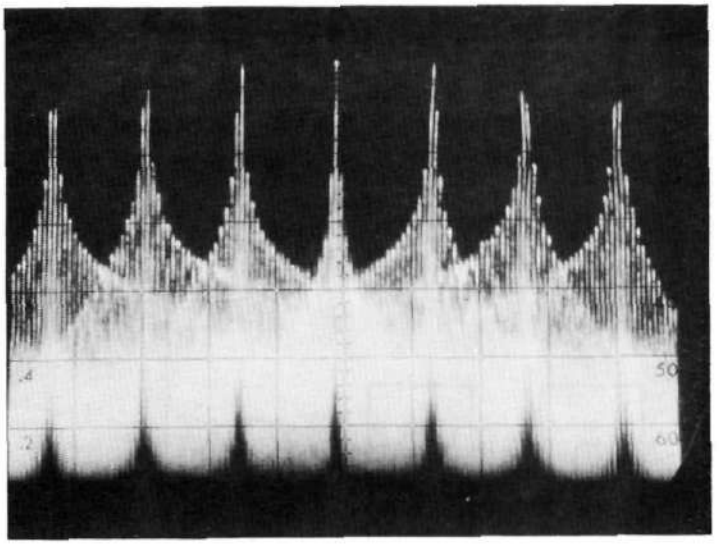

(b) S-BAND SPECTRA

Figure 38. Experimentally Determined Spectra.

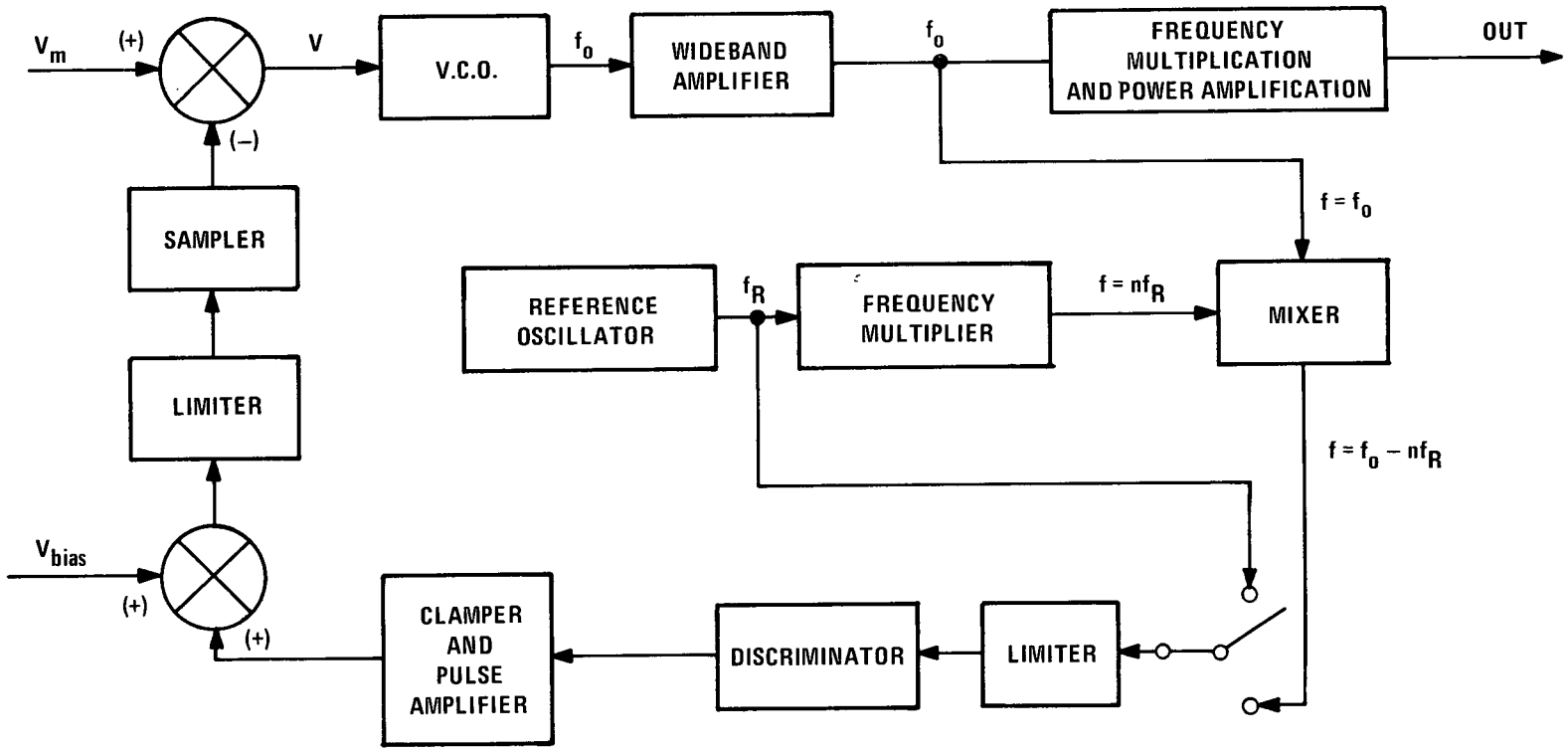

Figure 39. Block Diagram of One Possible Configuration of an AFC System of an FM Transmitter.

VCO and the feedback limiting. (Two types of sample-and-hold circuits were simulated.) Simulation results showed the AFC system to be stable and to operate satisfactorily for a wide range of gains and sampler time constants. Figure 40 shows the recovery of the VCO frequency from an initial error in the nominal (zero modulation input) frequency. The time required for recovery is seen to decrease with increasing gain, k, and the steady-state error is seen to decrease with increasing gain. Note also the effect of feedback saturation; the transient response for the highest gain (200) is no better than that for a lower gain (50) until after the error has decreased below the feedback saturation level.

The techniques developed for block diagram simulation of the transmitter AFC system are directly applicable to other communication systems where simplified models can be used to represent the stages or subsystems.

D. Development of State Variable Techniques for Linear Circuits

For a detailed circuit simulation of a communication system or subsystem, the governing differential equations, once obtained, may be solved by numerical integration. The differential equations of the detailed model will likely contain some "fast" response modes which would not be included in a simplified model for block diagram simulation, i.e., modes whose contribution to the solution are negligible, except perhaps immediately after a disturbance. The existence of such trivially fast modes introduce a difficulty into numerical integration since the integration time step size must be small with respect to the fastest mode of the system. Numerical integration of such systems, called "stiff" systems, requires an excessive amount of computer time and tends to introduce significant round-off errors.

A technique has been developed which approximates a linear, time-invariant, stiff system with a lower-order system which does not include the trivially-fast natural modes. The approximation

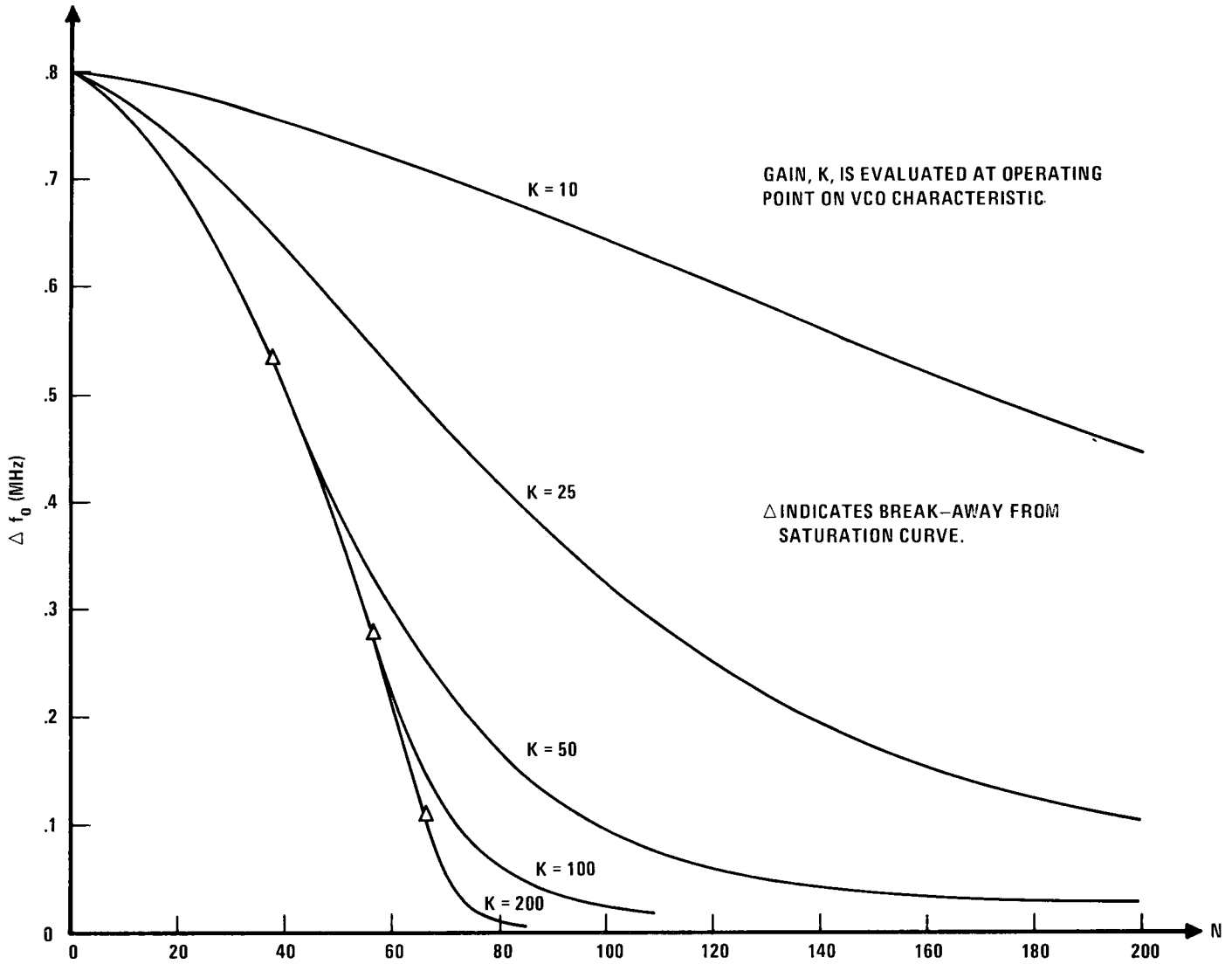

Figure 40. AFC Simulation of Transient Response with Nonlinear VCO and With ± 12 Volt Limiter.

theory has been developed and incorporated into a simulation named Approximate Linear System Analysis Program (ALSAP). The simulation accepts the system differential equations in state variable form, approximates the system by removal of the very-fast eigenvalues, and then numerically integrates the lower order system of differential equations.

A description of the development of the theory and application of ALSAP is included in Technical Report No. 9[20] where the application is to a thirteenth order RLC bandpass filter. In the report the state equations describing the filter are derived by the method of Bashkow as described by Kuo.[21]

PRECEDING PAGE BLANK NOT FILMED

XIII. TELEMETRY TRANSMITTER MODELING

A. Introduction

An investigation into the analysis of transmitter circuits by the use of models and modeling techniques was undertaken. The primary goal of this effort was to analyze the Airlock Module Transmitter, a solid-state FM transmitter operating in the VHF frequency region. A secondary goal was to develop techniques and acquire information generally applicable to analyzing transmitters with models.

The investigation was carried out on a circuit detail basis using models based on state variable techniques. The state variable analysis technique for linear circuits developed earlier on the contract was used to analyze one linear circuit in the transmitter. The ability of this model to eliminate fast circuit time constants greatly facilitated the analysis of the circuit.

Most of the transmitter circuits were nonlinear, however, and the linear analysis could not be applied. Since the time-frame of the investigation did not allow for development of complete models, an existing circuit analysis program (CIRCUS) was used to analyze the nonlinear circuits. Among these circuits was an oscillator, three frequency multipliers, and several power amplifiers. The choice of CIRCUS as the analysis program to be used was largely a matter of availability.

Many difficulties were encountered in applying CIRCUS to the transmitter circuits. As a result a complete analysis of the transmitter was not accomplished in the limited time available. However, much useful information was gained on the practical difficulties of using existing models for circuit analysis, and most of the transmitter circuits were successfully modeled and analyzed.

Using the model CIRCUS as an analysis tool presented many problems at the user-model interface. Recurring difficulties were encountered in modeling circuits and assigning parameters so that they were acceptable to the model and would run in a reasonable time

(excessive time requirements were frequently encountered). Interpretation of computed results was not always easy; if a circuit failed to perform as expected, the reason was not at all apparent. The lack of a relatively complete library of device model characteristics on solid-state devices also complicated the analysis.

B. Analysis of Transmitter Circuits

A block diagram of the Airlock Module Transmitter is shown in Figure 41. The transmitter consists of a modulation amplifier which provides the interface between the modulation input and the oscillator. The output of the modulation amplifier is applied to the voltage variable capacitor in the oscillation circuit; the variations in voltage produce frequency modulation of the transmitter. The oscillator circuit consists of a voltage controlled crystal oscillator (XVCO) operating at 19.2 MHz which provides a stable frequency source for the transmitter. The oscillator is followed by a frequency multiplier chain consisting of a tripler followed by an amplifier and two frequency doublers. The oscillator frequency is, therefore, multiplied by a factor of 12, generating an output carrier frequency of 230.4 MHz. Any modulation deviation of the crystal VCO is also multiplied by a factor of 12. Following the multipliers is a power amplifier which provides the power gain necessary to achieve an output power of approximately 15 watts. The power amplifier is followed by a coaxial bandpass filter. A voltage regulator operating from a nominal input voltage of 28 volts provides the regulated voltages needed for the transmitter circuits.

Analyses were made on all of the transmitter circuits. The modulation amplifier, an LC oscillator, the frequency tripler, and the first frequency doubler were analyzed as single stage circuits. The last times-two multiplier and the following amplifier, the three stage power amplifier, and the voltage regulator were analyzed as multistage circuits. It would have been desirable to enter the

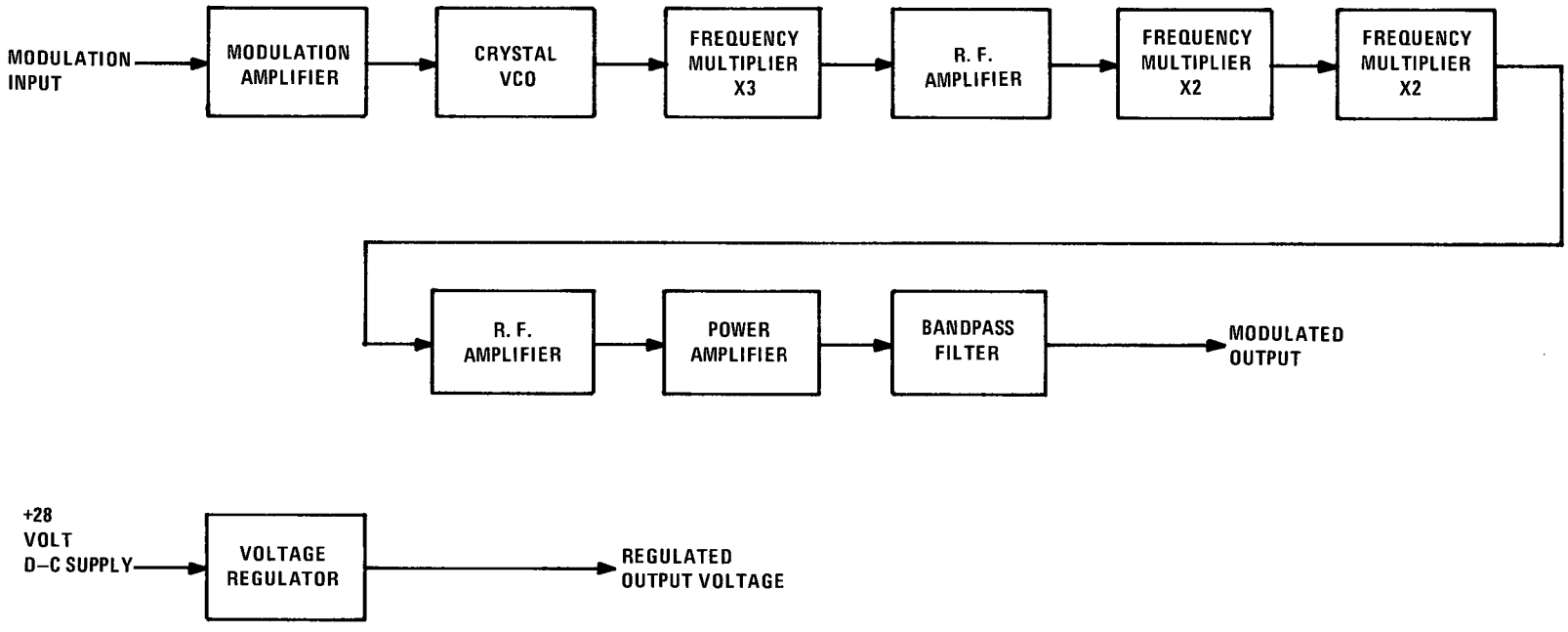

Figure 41. Block Diagram of Airlock Module Transmitter.

entire radio frequency portion of the transmitter into the analysis program at one time, but the limited time available did not permit such a run.

The modulation amplifier was analyzed using the state variable techniques developed on the contract for linear circuit analysis. This circuit was also analyzed using CIRCUS. The results of the two analyses were in good agreement.

CIRCUS was used for the analysis of the remainder of the transmitter. The next circuit encountered in the signal path through the transmitter is the crystal VCO. Difficulty was encountered immediately in an attempt to use a program like CIRCUS for the analysis of such a circuit. The integration interval required by the model for integrating the circuit equations is a function of the circuit time constants. When the circuit contains fast time constants the integration interval must be small. Fast time constants exist in the oscillator circuit, particularly those associated with the high frequency transistor needed to provide the gain necessary for oscillation. To obtain the steady state response of such a circuit, the circuit equations must be integrated for a time long enough to allow the high Q crystal resonator to build up oscillations. Thus evaluating the circuit would require integration with very small steps over a long time. Estimates indicated that the computer time required would be prohibitive.

Since the crystal oscillator could not be completely analyzed, a similar LC oscillator with a resonant Q of approximately 100 was analyzed. This LC oscillator is presented here as an example of circuit analysis using the program CIRCUS.

Data is entered into CIRCUS with data statements which name the element (R,L,C, etc.), the circuit modes between which the element is connected, and the element values. Active devices are entered in a similar manner. Figure 42 shows the circuit diagram of the LC oscillator circuit. Figure 43 shows the format of the data entered into CIRCUS for the analysis of the oscillator circuit. The output

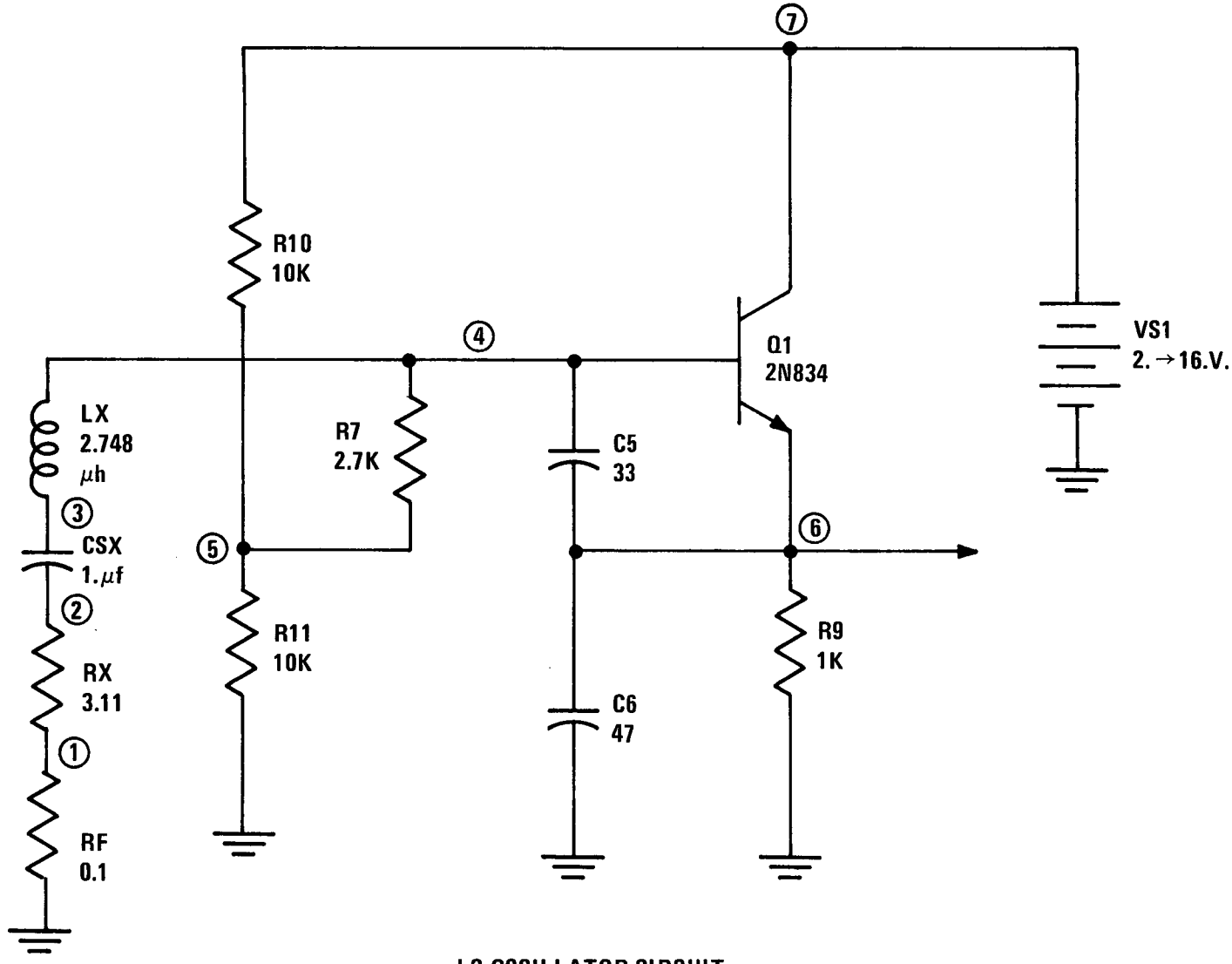

Figure 42. LC Oscillator Circuit.

```
'SIMPLE OSCILLATOR CIRCUIT'
R7, 5, 4, 2.7E3
R9, 0, 6, 1.E3
R10, 5, 7, 1.E4
R11, 0, 5, 1.E4
RX, 1, 2, 3.11
RF, 0, 1, 0.1
CSX, 2, 3, 1.E-6
C5, 6, 4, 33.E-12
C6, 0, 6, 47.E-12
LX, 3, 4, 2.748E-6
VS1, 7, 0,  2.
T1, 4, 7, 6, 2N834
DEVICE PARAMETERS
TRANSISTOR,2N834,NPN,
RB,10.,RC,11.,RE,.001,
A1,9.E-12,PHI1,.8,N1,.5,
A2,4.4E-12,PHI2,.9,N2,.08,
IES,1.26E-15,THETAN,41.2,
ICS,1.E-14,THETAI,37.7
TCN,.05,4.6E-10
TCI,.0007,5.6E-8
BN,
0., 1.E-5,2.E-5,4.E-5,6.E-5,
1.E-4,2.E-4,5.E-4,1.E-3,2.E-3,
5.E-3,1.E-2,2.E-2,4.E-2,
6.E-2,1.E-1,1.6E-1,
1., 2.8,4.1,6.,7.5,
9.8,14.,22.,30.1,38.8,
52.8,61.4,68.,63.5,
62.9,53.,46.5
BI,
0.,1.E-5,2.E-5,4.E-5,6.E-5,
1.E-4,2.E-4,5.E-4,1.E-3,2.E-3,
5.E-3,1.E-2,2.E-2,4.E-2,
.01,.019,.019,.026,.030,
.037,.048,.065,.078,.087,
.086,.07,.053,.044
END
INTERVALS, 1.E-9, 5.E-9
HOLD FINAL CONDITIONS
PRINT, VN4, VN1, ICPX, ILX, IBT1, VN6
EXECUTE
*VS1,16.
INTERVALS, 2.E-9, 1000.E-9
EXECUTE
END OF JOB
```

Figure 43. LC Oscillator Circuit Description for CIRCUS.

of CIRCUS is quite flexible. For printed output the user can designate any number of modes for printout of the node voltage. Similarly, the current in any number of elements can be printed. Other variables, such as power, can also be printed. Line printer plot routines are available for a quick look at results. Provision is also made for the inclusion of Calcomp plot routines, but time did not allow for their development during this investigation.

The oscillator output obtained with CIRCUS is shown in Figure 44. The output amplitude is almost equal to the supply voltage and the waveform is quite nonlinear as can be expected in a self-limiting oscillator.

The additional stages of the transmitter were analyzed in a similar manner with the output of one stage providing an estimate of the input to the following stage. Details of this work are reported in Technical Report No. 10.[22]

C. Conclusions

The analysis of the Airlock Module Transmitter has been accomplished using state variable techniques for linear circuits which were developed during the contract, and by the use of the circuit analysis program CIRCUS. CIRCUS was used both as a check of the linear analysis and as a tool for analyzing the nonlinear circuits. Although the entry of data into CIRCUS would seem to be straightforward, many practical difficulties were encountered in using the program. Some of these were (1) lack of valid active device parameters, (2) circuit time constants, (3) valid circuit descriptions, and (4) accuracy of entry of circuit data into the program. Experience indicates that an effort to improve the user model interface problems is needed. A better diagnostic system oriented toward providing the communication engineer with indications of circuit difficulties would be a great help.

The details of the transmitter circuit analysis investigation are contained in Technical Report No. 10.[22]

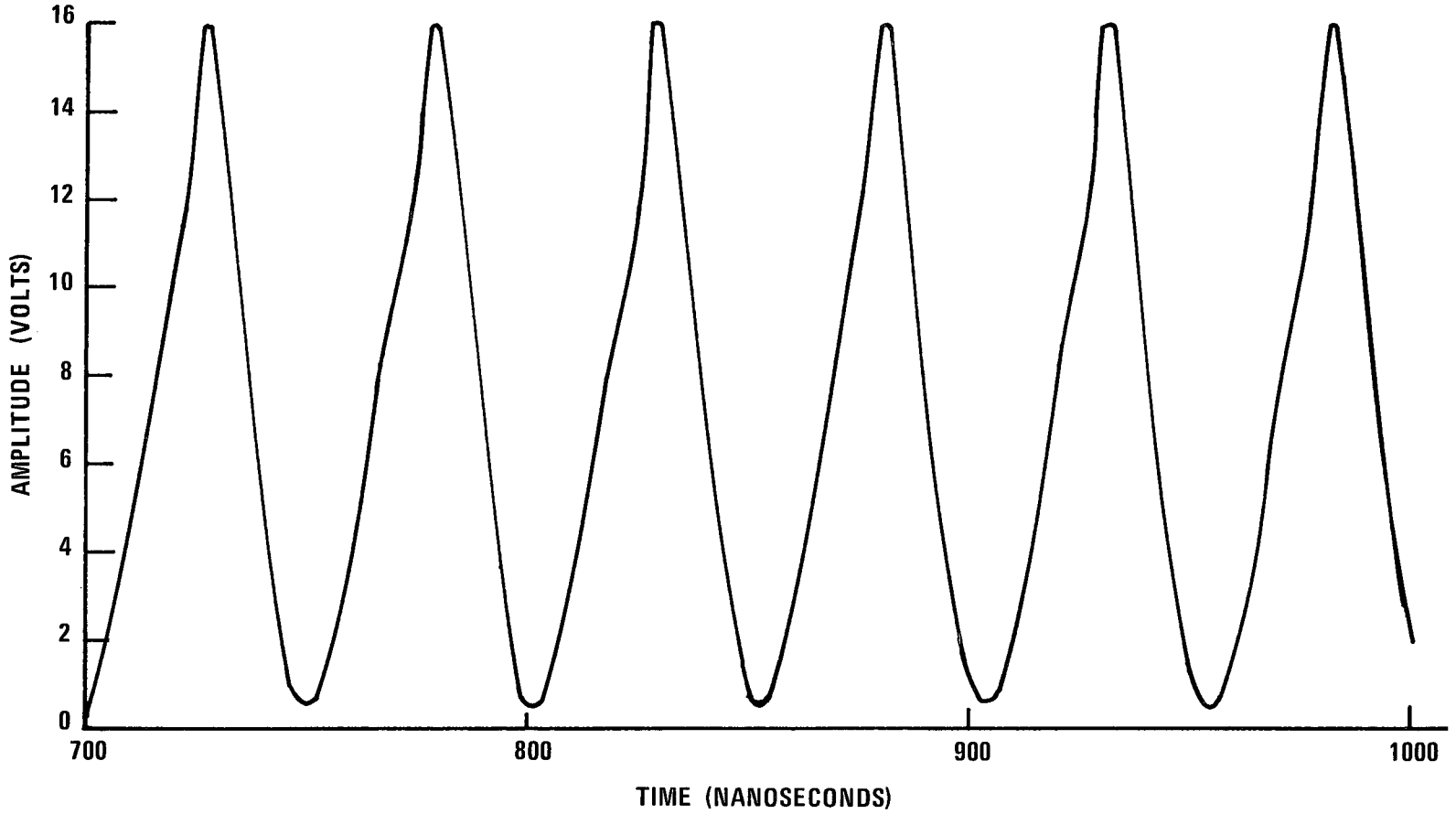

Figure 44. Computed Oscillator Output Obtained by Using Circuit Detail Analysis Techniques.

XIV. BIBLIOGRAPHY

1. Saturn I Instrumentation System Description, Volume IV, RF Systems, Chapter 6, Model 520 Saturn Radar Altimeter (Modified), George C. Marshall Space Flight Center, Astrionics Laboratory, Instrumentation and Communications Division, RF System Branch, 15 March 1964.

2. Walsh, J. R. and R. D. Wetherington, Investigation of Techniques for Improving the Operation of the Saturn Radar Altimeter, Technical Report No. 1, Project A-852, Contract NAS8-20054, Georgia Institute of Technology, Engineering Experiment Station, 18 October 1965.

3. Final Report, 890/960 Mc Transponder, Mark II, JPL Contract No. 950461, Motorola, Inc., November 1963.

4. Addendum to Final Report for 890/960 ODOP Transponder, Motorola, Inc.

5. Walsh, J. R. and R. D. Wetherington, Performance of the Phase-Lock Loop of the ODOP Transponder During Short Term Signal Fades, Technical Note No. 1, Project A-852, Contract NAS8-20054, Georgia Institute of Technology, Engineering Experiment Station, 15 February 1966.

6. Walsh, J. R., W. B. Warren, R. D. Wetherington, C. S. Wilson, H. W. Denny, and C. R. Lord, Investigation of Techniques for Improving Saturn V RF Tracking and Ranging Systems, Technical Report No. 2, Project A-852, Contract NAS8-20054, Georgia Institute of Technology, Engineering Experiment Station, 18 October 1966.

7. Wetherington, R. D. and J. R. Walsh, Spectral Studies of Signals Present in the Command and Communications System Up-Link Transmitter, Technical Report No. 3, Project A-852, Contract NAS8-20054, Georgia Institute of Technology, Engineering Experiment Station, 1 July 1967.

8. Lowery, H. R., Saturn Instrument Unit Command System, NASA Technical Memorandum NASA TM X-53350, 22 October 1965.

9. Final Report, Generalized Concept Receiver System, Interstate Electronics Corporation, Anaheim, California, Contract NAS8-11650.

10. Birchfield, J. L. and J. R. Walsh, Some Intermodulation Considerations in the Command and Communications System Down-Link Data Demodulators, Technical Note No. 2, Project A-852, Contract NAS8-20054, Georgia Institute of Technology, Engineering Experiment Station, 1 September 1968.

11. Birchfield, J. L. and J. R. Walsh, An Investigation of the Error-Rate Performance of the CCS Command Data Demodulator, Technical Report No. 5, Project A-852, Contract NAS8-20054, Georgia Institute of Technology, Engineering Experiment Station, 10 March 1970.

12. Frutiger, P., "Noise in FM Receivers with Negative Frequency Feedback," Proceedings of the IEEE, Vol. 54, No. 11, November 1966, pp. 1506-1520.

13. "Rice, S. O., "Noise in FM Receivers," Time Series Analysis, ed. by M. Rosenblatt, John Wiley and Sons, Inc., 1963, Ch. 25, pp 395-442.

14. Malone, M. J., "On the Threshold Effects in FM Data Systems," IEEE Transactions on Communications Technology, Vol. COM-14, No. 5, October 1966, pp 625-631.

15. "Baghdady, E. J. and O. P. Ely, "Effects of Exhaust Plasmas upon Signal Transmission to and from Rocket-Powered Vehicles," Proceedings of the IEEE, Vol. 54, No. 9, September 1966.

16. "Wetherington, R. D. and J. R. Walsh, A Study of Flame Attenuation of Telemetry Transmissions from Saturn Vehicles, Technical Report No. 4, Project A-852, Contract NAS8-20054, Georgia Institute of Technology, 2 February 1970.

17. Walsh, J. R. and R. D. Wetherington, Design of a Slow Scan Digital Television System, Technical Report No. 8, Project A-852, Contract NAS8-20054, Georgia Institute of Technology, Engineering Experiment Station, 1970.

18. Birchfield, J. L. and J. R. Walsh, An Investigation of Some Problems Involved in Adding an Additional Subcarrier to the CCS Down-Link, Technical Report No. 6, Project A-852, Contract NAS8-20054, Georgia Institute of Technology, Engineering Experiment Station, 20 March 1970.

19. Walsh, J. R. and R. D. Wetherington, CCS Down-Link Spectral Studies, Technical Report No. 7, Project A-852, Contract NAS8-20054, Georgia Institute of Technology, Engineering Experiment Station, May 1970.

20. Holland, L. D., J. R. Walsh and R. D. Wetherington, Communication System Modeling, Technical Report No. 9, Project A-852, Contract NAS8-20054, Georgia Institute of Technology, Engineering Experiment Station, 19 November 1971.

21. Kuo, F. F., Linear Networks and Systems, John Wiley and Sons, 1967, Chapter 6.

22. Walsh, J. R., R. D. Wetherington and L. D. Holland, Circuit Detail Modeling of the Airlock Module Transmitter, Technical Report No. 10, Project A-852, Contract NAS8-20054, Georgia Institute of Technology, Engineering Experiment Station, 19 November 1971.